ISSN 1881-7815 Online ISSN 1881-7823

BST BioScience Trends

Volume 15, Number 1
February, 2021

IRCA BSSA

IACMHR

www.biosciencetrends.com

BST
BioScience Trends

ISSN: 1881-7815
Online ISSN: 1881-7823
CODEN: BTIRCZ
Issues/Year: 6
Language: English
Publisher: IACMHR Co., Ltd.

BioScience Trends is one of a series of peer-reviewed journals of the International Research and Cooperation Association for Bio & Socio-Sciences Advancement (IRCA-BSSA) Group. It is published bimonthly by the International Advancement Center for Medicine & Health Research Co., Ltd. (IACMHR Co., Ltd.) and supported by the IRCA-BSSA.

BioScience Trends devotes to publishing the latest and most exciting advances in scientific research. Articles cover fields of life science such as biochemistry, molecular biology, clinical research, public health, medical care system, and social science in order to encourage cooperation and exchange among scientists and clinical researchers.

BioScience Trends publishes Original Articles, Brief Reports, Reviews, Policy Forum articles, Communications, Editorials, News, and Letters on all aspects of the field of life science. All contributions should seek to promote international collaboration.

Editorial Board

Editorial and Head Office

Pearl City Koishikawa 603,
2-4-5 Kasuga, Bunkyo-ku, Tokyo 112-0003, Japan
E-mail: office@biosciencetrends.com

BioScience Trends

Editorial and Head Office

Pearl City Koishikawa 603, 2-4-5 Kasuga, Bunkyo-ku,
Tokyo 112-0003, Japan

E-mail: office@biosciencetrends.com
URL: www.biosciencetrends.com

Editorial Board Members

CONTENTS

Volume 15, Number 1, 2021

Review

Original Article

Brief Report

Communication

Letter

Review

DOI: 10.5582/bst.2021.01019

Overview of the characteristics of and responses to the three waves of COVID-19 in Japan during 2020-2021

Kenji Karako[1], Peipei Song[2,*], Yu Chen[1,*], Wei Tang[2], Norihiro Kokudo[2]

[1] Department of Human and Engineered Environmental Studies, Graduate School of Frontier Sciences, The University of Tokyo, Chiba, Japan; [2] National Center for Global Health and Medicine, Tokyo, Japan.

SUMMARY The first case of COVID-19 in Japan was reported on 16 January 2020. The total number of the infected has reached 313,844 and the number of deaths has reached 4,379 as of 16 January 2021. This article reviews the characteristics of and responses to the three waves of COVID-19 in Japan during 2020-2021 in order to provide a reference for the next step in epidemic prevention and control. The Japanese Government declared a state of emergency on 7 April 2020, which suppressed the increase in the number of the infected by curtailing economic activity. The first wave peaked at 701 new cases a day and it decreased to 21 new cases on May 25 when the state of emergency was lifted. However, the number of the infected increased again due to the resumption of economic activity, with a peak of 1,762 new cases a day during the second wave. Although the situation was worse than that during the first wave, the government succeeded in limiting the increase without declaring a state of emergency again, and that may be attributed to a decrease in crowd activities and an increase in the number of inspections. During the third wave, the number of the infected continued to exceed the peak during previous waves for two months. Major factors for this rise include the government's implementation of further policies to encourage certain activities, relaxed immigration restrictions, and people not reducing their level of activity. An even more serious problem is the bed usage for patients with COVID-19; bed usage exceeds 50% not only in major cities but also in various areas. On 7 January 2021, 5,953 new cases were reported a day; this greatly exceeded the previous peak, and the state of emergency was declared again. Although Japan has been preparing its medical system since the first wave, maintaining that system has imposed a large economic burden on medical facilities, hence stronger measures and additional support are urgently needed to combat COVID-19 in the coming few months.

Keywords COVID-19, pandemic, epidemic, wave, Japan

1. Introduction

The COVID-19 outbreak is characterized as a global pandemic. According to the weekly epidemiological update released by the World Health Organization (WHO) on 29 December 2020, the total number of the infected had reached 79,231,893 and the death toll had increased to 1,754,754 globally (*1*). Every country is implementing its own measures to control the number of the infected (*2-8*). Although the number can be limited by temporary lockdowns or prohibitions on going out, the number of the infected has increased again as control measures are lifted.

Japan is one of the countries where the number of deaths per capita has remained low, but like in other countries there are signs of an increase in the infected as economic activity increases after restrictions are lifted. The first case of COVID-19 in Japan was reported on 16 January 2020. The number of the infected was almost 0 for one month, but that number gradually increased and it rose substantially starting in the middle of February. Afterwards, the number of the infected reached three peaks. On 31 December 2020, Japan reported 3,851 new cases (*9*), the highest daily tally over the past year. On 7 January 2021, 5,953 new cases were reported (*10*); this greatly exceeded the previous peak, and Japan issued a state of emergency again for the next 31 days (from 8 January to 7 February 2021) (*11*). The total number of the infected has reached 313,844 and the number of deaths has reached 4,379 as of 16 January 2021 (*12*).

Figure 1 shows the number of the infected in Japan from 16 January 2020 to 16 January 2021. There have been three waves of substantial increases in the number of the infected so far, and the national government and

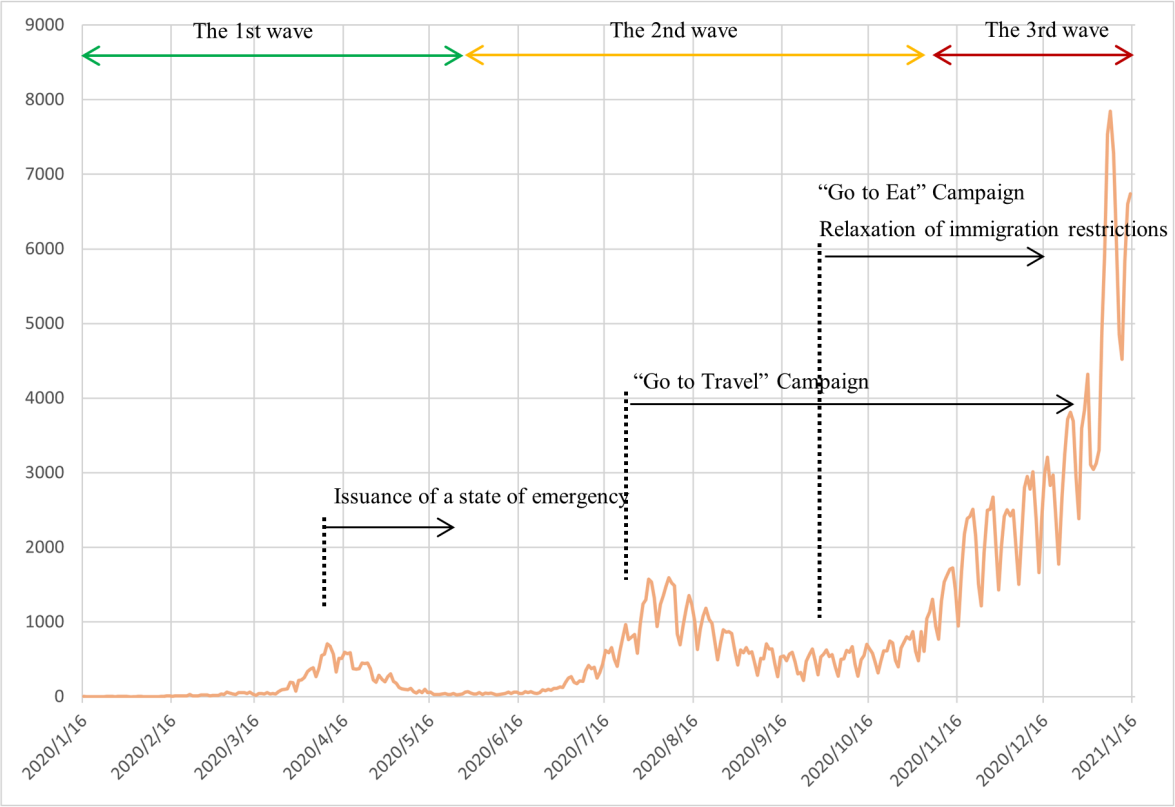

Figure 1. Number of people reported with COVID-19 from 16 January 2020 to 16 January 2021 in Japan. The first case of COVID-19 in Japan was reported on 16 January 2020. The total number of the infected reached 313,844 and the number of deaths reached 4,379 by 16 January 2021. On 7 April 2020, the Japanese Government declared a state of emergency; on 7 January 2021, the Japanese Government declared a state of emergency again. Data source: *https://www.mhlw.go.jp/stf/covid-19/kokunainohasseijoukyou.html#h2_1*

local governments have implemented different infection control measures during each phase. Japan has also implemented policies to mitigate the impact of those infection control measures on the Japanese economy. The current article summarizes the epidemic in Japan and measures implemented from 2020 to the present to provide a reference for the next step of epidemic prevention and control. Sections 2-4 summarize the countermeasures and economic measures implemented during each of the three waves of COVID-19 in Japan. Section 5 summarizes the usage of the medical system that Japan has built to combat COVID-19 and the impact of the disease.

2. The 1st wave of the outbreak in Japan

The first COVID-19 epidemic in Japan began in mid-February. At the time, there were fewer than 30 infected per day, and there were only local outbreaks of the disease. Because of the limited number of the infected, the main measures implemented were investigation of potentially infected individuals, PCR testing, and segregation. COVID-19 poses a high risk to the elderly, and Japan, which has an aging society, focused on avoiding a shortage of medical resources and reducing deaths due to COVID-19.

Specific measures were the establishment of criteria for medical consultations and PCR testing if an individual had a fever (*13,14*). In addition, the decision was made to close schools in late February (*15*). Japan also called on the public to wear masks, telework, shift work hours, refrain from holding events, and avoid contact with other people in order to reduce transmission (*16*). After the government's announcement, some companies switched to telework. As a result, the number of subway passengers during commuting hours in March in Tokyo decreased by up to 24% compared to January (*17*). Figure 2 shows changes in the percentage of commuters during commuting hours in Tokyo. In addition, immigration restrictions were imposed to prevent an influx of infected people from overseas.

Although these measures were implemented, the number of the infected per day exceeded three digits in early April. Therefore, the Japanese Government declared a state of emergency on 7 April (*18*). Many restaurants and companies complied with this order, reducing the time people spent outside their homes by reducing business hours and shifting to teleworking. A reduction of up to 68% in the number of subway passenger during commuting hours in April and May indicates that many people have complied with the state of emergency (*17*). The state of emergency limited the increase in the number of the infected from May, and on 25 May the number of new reported cases decreased

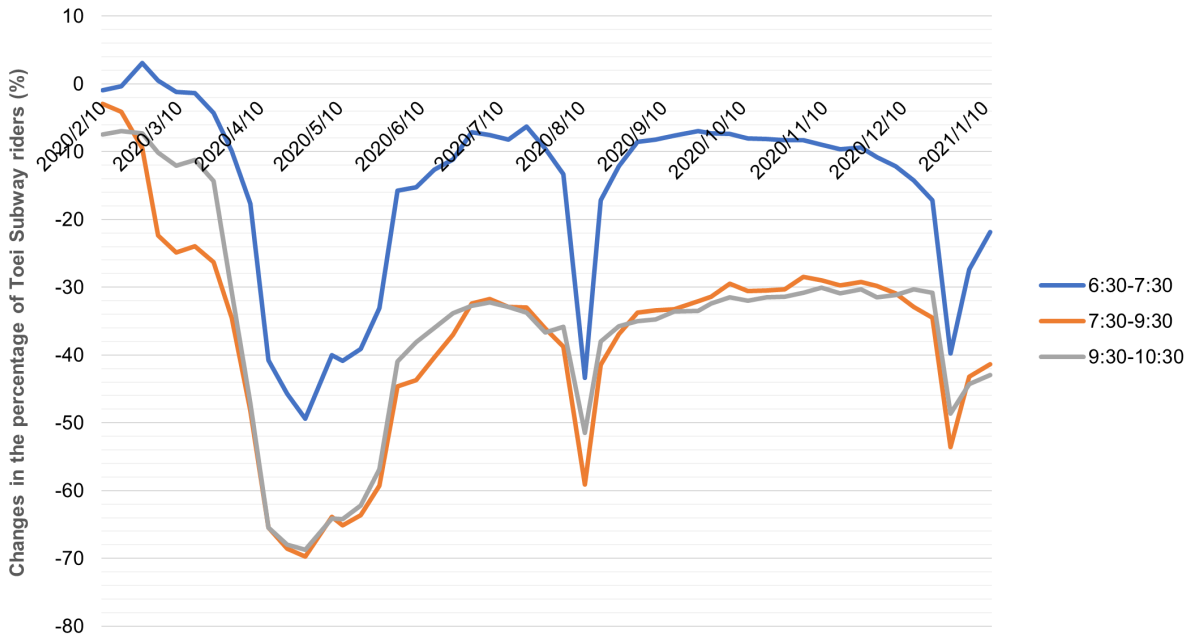

Figure 2. Changes in the percentage of Toei Subway riders during commuting hours based on the average number of riders from 10 February 2020 to 14 January 2021 in Tokyo. The number of subway passengers during commuting hours decreased significantly during the first wave. The number of commuters decreased in response to the rapid increase in the number of infected during the second wave. However, there was no decrease in the number of commuters during the third wave. Data source: *https://stopcovid19.metro.tokyo.lg.jp/cards/predicted-number-of-toei-subway-passengers*

to 21. In response to this calm, the government lifted the state of emergency (*19*) and people resumed their activities to dispel the economic consequences of the state of emergency.

3. The 2nd wave of the outbreak in Japan

The second wave was a very characteristic phase compared to the first wave, and although the peak in the number of the infected was larger than that during the first wave, it subsided without measures such as a state of emergency. The state of emergency was lifted on 25 May, and the national and local governments began to resume full-scale economic activity in order to recover from the effects of the decline in economic activity due to restrictions. Schools, which had been closed, were reopened (*20*) and the restrictions on nighttime business by restaurants were lifted in Tokyo (*21,22*). As these activities resumed, the number of people during commuting hours in Tokyo increased and reached the usual level for March. Many of the people were shifting from activities at home to going out.

There were fewer than 100 infected per day for one month after the state of emergency was lifted. As predicted by several simulations based on SIR models (*23-25*), the number of the infected increased at a stretch from the end of June once activities resumed, and the number of the infected per day exceeded 1,000 in late July. The number of the infected per day peaked during the second wave at 1,762, a number greatly exceeded the peak of 701 during the first wave. Although the situation was worse than that during the first wave, the government did not issue a state of emergency again, and some municipalities only called for restaurants to reduce their business hours starting in August in response to local outbreaks (*26,27*). Although major measures to control COVID-19 were not implemented, the number of the infected per day gradually decreased from mid-August. This is a major feature of the second wave. Observing the changes in the number of people commuting during commuting hours (Figure 2) indicates that the number of people commuting peaked from early July to mid-July and gradually decreased starting in late July. However, the decrease was slight, and by early August the number of people commuting decreased to the level in mid-June. In mid-August, however, the number of commuters decreased. This was because many companies closed during the Obon festival, which is a long holiday in Japan. Observing the decrease in the number of the infected in terms of changes in activity indicates that some people refrained from leaving their homes in mid-July, when the number of the infected per day reached about 700. As of the beginning of August, the increase in the infected began to decrease. In addition, the number of the infected decreased significantly because of the Obon festival since many people were less active.

The second wave subsided by early September, and the number of the infected per day had decreased to about 500. The number of commuters increased to the same level as in early July, when the number of the infected during the second wave began to increase. Unlike the second wave, however, the number of the infected did not

increase sharply again. There was no significant change until the end of October, and the number of the infected per day was constant. The reason why there was no increase like that during the second wave is presumably because of increased PCR testing. As of June, about 2,000 people per day were tested in Tokyo, but in July, when the number of the infected increased, 4,000 people per day were tested; since August, 6,000 people have been tested per day (*28*). The extensive testing at that time – when the infected decreased because of the temporary drop in activity caused by the Obon festival – was able to detect the infected early and to eliminate the chance of them transmitting SARS-CoV-2 to others. As a result, the increase in the number of the infected was kept to a certain level, and that was maintained until the end of October.

4. The 3rd wave of the outbreak in Japan

During the third wave, the number of the infected has increased since early November 2020, and as many as 3,000 new cases were reported on 16 December. During this wave, the number of the infected increased for some reason, as it did during the early stage of the second wave. Unlike during the second wave, there are no signs that the increase in the number of the infected during this third wave will decrease in December, which is more than a month after the increase in the number of the infected. The government did not declare a state of emergency, and local governments only called for reduced business hours and limited activities (*29,30*). These orders to reduce business hours were implemented starting in December, one month after the infection began to increase, as occurred during the second wave. The order had no significant effects, and the number of the infected increased.

One of the major factors behind the continuous increase in the number of the infected during the third wave is that people had not reduced their level of activity. During the second wave, the number of commuters decreased in response to the rapid increase in the number of the infected, but there was no decrease in the number of commuters during the third wave, as shown in Figure 2. The number of commuters remained about the same as the number of commuters in October even though the number of the infected increased sharply. In September and October, about 500 infected were reported every day, so people seemed inured and they continued their activities even though the number of the infected increased rapidly. In addition, there was no opportunity for a temporary decrease in activity because of no long holidays like the Obon festival. In Tokyo, about 8,000 people per day were tested starting in November. Testing is increasing, but it is not sufficient to limit the increase in the number of the infected, and a larger number of people might be infected than during the second wave. That said, increased testing does not appear to be sufficient if it is not effective in reducing crowd activities.

There are several possible causes for the increase in the number of the infected in Japan. One possible cause is "Go To" campaign, which encourages travel and dining out to encourage economic activity (*31*). As part of this campaign, the government will bear some of the costs when traveling or dining out. The travel campaign started on 22 July 2020. Travel to Tokyo was initially excluded from the campaign but it was included starting in October. The dining out campaign also started in October. As of October, when the campaign started in earnest, the number of the infected per day was constant, but the number of the infected per day started to increase in early November. Another possible cause is that Japan gradually relaxed immigration restrictions starting on 1 October 2020 (*32*). As of 1 October, 215,599 people had undergone PCR testing in airport quarantine; of those, a total of 951 tested positive (*33*). As of 31 December, a total of 403,864 people had been tested, and a total of 1,871 tested positive (*34*). As of 1 July, 76,268 people had undergone PCR testing in airport quarantine; of those, a total of 314 tested positive (*35*). In the 3 months before relaxed immigration restrictions (1 July – 1 October), positivity for SARS-CoV-2 was 0.46%; in the 3 months after relaxed immigration restrictions (1 October – 31 December), positivity for SARS-CoV-2 was 0.49%. Thus, there was little difference in positivity. The aforementioned factors cannot be definitively identified as the cause of the sharp increase in the number of the infected. However, policies to encourage activities may have disturbed the calm after the second wave subsided.

5. The impact of COVID-19 on medical facilities

The Japanese Government has implemented measures mainly intended to reduce the number of deaths. This section summarizes the medical system that Japan has built to fight COVID-19 and the impact of COVID-19 on medical facilities and workers. The Japanese Government began to prepare its medical system in March, when COVID-19 began to spread, in case the number of the infected peaked in the future. In order to prevent the transmission of COVID-19, Japan created dedicated wards for patients with the disease while securing dedicated accommodations for asymptomatic patients. As of 27 May, Japan had about 18,000 beds and about 19,000 rooms available nationwide for patients with COVID-19.

Figures 3 and 4 summarize bed usage for patients with COVID-19 and severe COVID-19 in Hokkaido, Kanto, and Kansai (*36*). Since peaks during the first and second waves were small and the waves were brief, the medical system had breathing room. During the third wave, however, the medical system was in crisis. During the third wave, there were more infected than

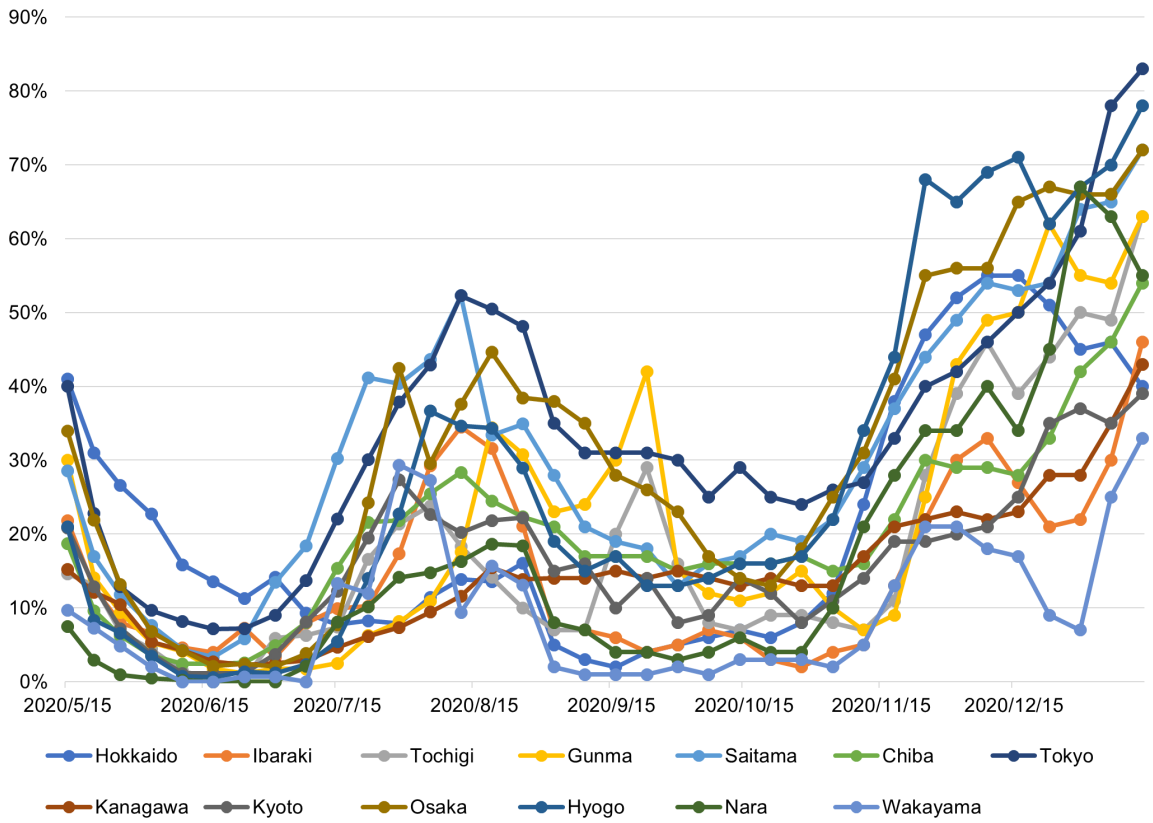

Figure 3. Bed usage rate in each region with respect to the number of beds allocated to patients with COVID-19. Data source: *https://www.mhlw.go.jp/stf/seisakunitsuite/newpage_00023.html*

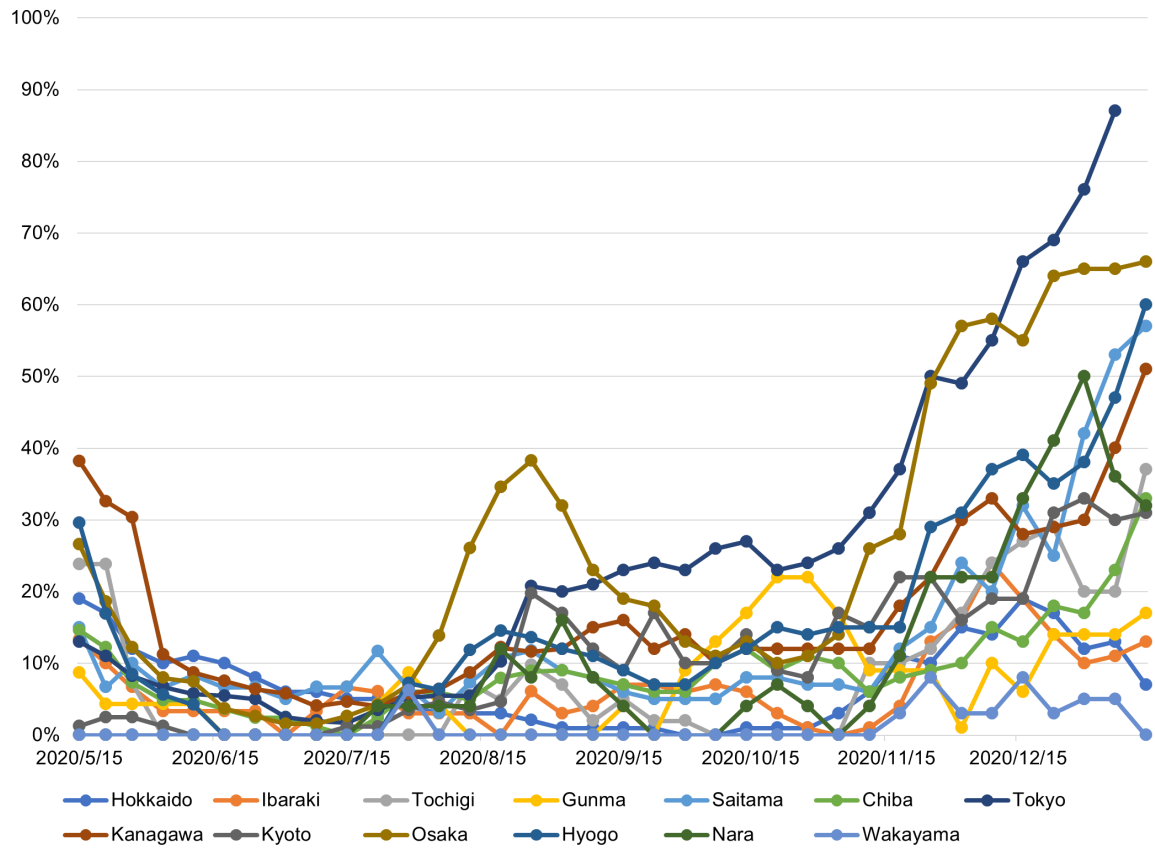

Figure 4. Bed usage rate in each region with respect to the number of beds allocated to patients with severe COVID-19. Data source: *https://www.mhlw.go.jp/stf/seisakunitsuite/newpage_00023.html*

Table 1. Average monthly number of patients, amount of profit and loss for medical facilities that responded to a survey on the fiscal status of hospitals during COVID-19 pandemic (profit and loss is in units of 1,000 yen)

Items	April		May		June		July		August		September	
	2019	2020	2019	2020	2019	2020	2019	2020	2019	2020	2019	2020
Total number of outpatients	9,181	7,418	8,994	6,801	8,934	8,287	9,941	8,797	9,424	8,289	9,049	8,587
Total number of inpatients	6,684	6,005	6,761	5,799	6,640	5,922	6,985	6,398	7,030	6,460	6,707	6,259
Profit and Loss (all hospitals with valid responses to the survey)	7,374	-42,279	20,102	-36,488	-32,745	-59,514	15,168	-7,691	24,207	2,400	-18,726	-10,646
Profit and Loss (hospitals not accepting patients with COVID-19)	6,159	-11,870	11,284	-8,553	-11,848	-21,435	7,120	-2,308	10,993	2,848	-7,221	-1,502
Profit and Loss (hospitals accepting patients with COVID-19)	9,685	-100,088	36,656	-88,932	-75,905	-138,161	35,299	-21,157	50,364	1,513	-43,816	-30,586

Data source: *https://ajhc.or.jp/siryo/20200806_covid19ank.pdf; https://ajhc.or.jp/siryo/20201112_covid19ank.pdf*

the peak number reported during the second wave. As of 16 December 2020, bed usage by patients with COVID-19 exceeded 50% in major regions such as Hokkaido, Gunma, Saitama, Tokyo, Osaka, and Hyogo. Even in late December, bed usage was on the rise in areas other than Hokkaido, and it is also increasing in other areas. If this continues, it will have a major impact on the medical system. Not only are usage rates rising in large cities such as Tokyo and Osaka but also in rural prefectures where many beds cannot be prepared. Despite its aim of reducing the number of deaths, Japan did not implement strong COVID-19 countermeasures during the third wave, leading to the current crisis. Stronger control measures need to be urgently implemented.

While medical facilities and staff have doing their utmost to combat COVID-19, they have also suffered financially and from fatigue. According to a survey of the fiscal status of hospitals (*37,38*) as shown in Table 1, the average number of outpatients and inpatients at responding medical facilities decreased by more than 10% in April and May, when the state of emergency was declared, compared to 2019. Although some outpatients returned in June after the state of emergency was lifted, the number of inpatients did not change significantly, and the number of outpatients decreased again in July and August during the second wave. The fiscal state of medical facilities has also deteriorated compared to the previous year, and medical facilities that accept patients with COVID-19 are losing significantly compared to medical facilities that do not. Hospitals that allocate beds to patients with COVID-19 had higher labor costs and higher medical costs compared to the same period last year. As with the number of outpatients, significant losses occurred in April and May during the state of emergency. The government has been providing assistance to medical facilities that accept patients with COVID-19 and healthcare that treat them since June (*39,40*). If, however, increased bed usage continues for a long time like it did in April and May, then it seriously impact medical facilities.

6. Conclusion

In Japan, peaks in COVID-19 infection were suppressed immediately during the first and second waves, but the number of the infected has exceeded the previous peaks for two months during the third wave. In addition, bed usage by patients with COVID-19 exceeds 50% not only in major cities but also in various areas. During the first wave, Japan implemented a major measure by declaring the state of emergency. Due to the large economic impact, Japanese government was not able to implement measures to significantly reduce people's activities subsequently, instead, the government initiated a campaign to support economic activity. During the third wave, bed usage by patients with COVID-19 is a pressing problem because of the unprecedented number of the infected. Although Japan has been preparing its medical system since the first wave, maintaining that system has imposed a large economic burden on medical facilities, hence stronger measures and additional assistance are urgently needed to combat COVID-19 in the coming few months.

Funding: None.

Conflict of Interest: The authors have no conflict of interest to disclose.

References

1. World Health Organization. Weekly epidemiological update - 29 December 2020. *https://www.who.int/publications/m/item/weekly-epidemiological-update---29-december-2020* (accessed January17, 2021).
2. Mitsuya H, Kokudo N. Sustaining containment of COVID-19: Global sharing for pandemic response. Glob Health Med. 2020; 2:53-55.
3. Song P, Karako T. Scientific solidarity in the face of the COVID-19 pandemic: researchers, publishers, and medical associations. Glob Health Med. 2020; 2:56-59.
4. Wang H, Song P, Gu Y, Schroeder E, Jin C. Rapid health systems change: Online medical consultations to fight COVID-19. Ann Transl Med. 2020; 8:726.
5. Xu YY, Chen YZ, Tang XY. Guidelines for the diagnosis and treatment of coronavirus disease 2019 (COVID-19) in China. Glob Health Med. 2020; 2:66-72.
6. Wang X, Wu W, Song P, He J. An international comparison analysis of reserve and supply system for emergency medical supplies between China, the United States, Australia, and Canada. Biosci Trends. 2020; 14:231-240.
7. Villa S, Lombardi A, Mangioni D, Bozzi G, Bandera A, Gori A, Raviglione MC. The COVID-19 pandemic preparedness ... or lack thereof: from China to Italy. Glob Health Med. 2020; 2:73-77.
8. Kariya T. Rapid spread of COVID-19 in New York and the response of the community. Glob Health Med. 2020; 2:123-126.
9. Ministry of Health, Labor, and Welfare. The current status of COVID-19 and the response by the Ministry of Health, Labor, and Welfare (December 31, 2020). *https://www.mhlw.go.jp/stf/newpage_15828.html* (accessed January 17, 2021). (in Japanese)
10. Ministry of Health, Labor, and Welfare. The current status of COVID-19 and the response by the Ministry of Health, Labor and Welfare (January 7, 2021). *https://www.mhlw.go.jp/stf/newpage_15916.html* (accessed January 17, 2021). (in Japanese)
11. Cabinet Secretariat. Declaration of a State of Emergency in response to the Novel Coronavirus Disease (January 7). *https://japan.kantei.go.jp/ongoingtopics/_00038.html* (accessed January 8, 2021).
12. Ministry of Health, Labor, and Welfare. The current status of COVID-19 and the response by the Ministry of Health, Labor and Welfare (January 16, 2021). *https://www.mhlw.go.jp/stf/newpage_16124.html* (accessed January 17, 2021). (in Japanese)
13. Ministry of Health, Labor, and Welfare. Number of people undergoing PCR testing [for SARS-CoV-2] daily. *https://www.mhlw.go.jp/content/pcr_tested_daily.csv* (accessed January17, 2021). (in Japanese)
14. Ministry of Health, Labor, and Welfare. Mandatory testing for SARS-CoV-2 [based on the Infectious Diseases Act]. *https://www.mhlw.go.jp/content/000601420.pdf* (accessed January 17, 2021). (in Japanese)
15. Ministry of Education, Culture, Sports, Science, and Technology. Temporary closure of elementary schools, junior high schools, high schools, and special needs schools, to combat COVID-19. *https://www.mext.go.jp/content/202002228-mxt_kouhou01-000004520_1.pdf* (accessed January 17, 2021). (in Japanese)
16. Ministry of Health, Labor, and Welfare. Basic policies to combat COVID-19. *https://www.mhlw.go.jp/content/10900000/000599698.pdf* (accessed January 17, 2021). (in Japanese)
17. Tokyo Metropolitan Government. Changes in the number of Toei Subway riders. *https://stopcovid19.metro.tokyo.lg.jp/cards/predicted-number-of-toei-subway-passengers/* (accessed January 17, 2021). (in Japanese)
18. Prime Minister's Office of Japan. COVID-19 Control Headquarters (27th meeting). *https://www.kantei.go.jp/jp/98_abe/actions/202004/07corona.html/* (accessed January 17, 2021). (in Japanese)
19. Prime Minister's Office of Japan. COVID-19 Control Headquarters (36th meeting). *https://www.kantei.go.jp/jp/98_abe/actions/202005/25corona.html* (accessed January 17, 2021). (in Japanese)
20. Ministry of Education, Culture, Sports, Science and Technology. The status of reopening of schools in relation to COVID-19. *https://www.mext.go.jp/content/20200603-mxt_kouhou01-000004520_4.pdf* (accessed January 17, 2021). (in Japanese)
21. Tokyo Metropolitan Government. Roadmap to overcoming COVID-19. *https://www.metro.tokyo.lg.jp/tosei/hodohappyo/press/2020/05/22/documents/11_00_1.pdf* (accessed January 17, 2021). (in Japanese)
22. Tokyo Metropolitan Government. Measures to prevent the spread of COVID-19 in Step 3. *https://www.bousai.metro.tokyo.lg.jp/1007942/1008452.html* (accessed January 17, 2021). (in Japanese)
23. Kobayashi G, Sugasawa S, Tamae H, Ozu T. Predicting intervention effect for COVID-19 in Japan: State space modeling approach. BioSci Trends 2020; 14:174-181.
24. Karako K, Song P, Chen Y, Tang W. Shifting workstyle to teleworking as a new normal in face of COVID-19: Analysis with the model introducing intercity movement and behavioral pattern. Ann Transl Med. 2020; 8:1056.
25. Karako K, Song P, Chen Y, Tang W. Analysis of COVID-19 infection spread in Japan based on stochastic transition model. Biosci Trends. 2020; 14:134-138.
26. Tokyo Metropolitan Government. "Assistance fund for reduced business hours to prevent a pandemic" (Bulletin No. 626). *https://www.metro.tokyo.lg.jp/tosei/hodohappyo/press/2020/07/31/13.html* (accessed January 17, 2021). (in Japanese)
27. Osaka Prefectural Government. From 1 to 20 August 2020: "Requirements based on the response to the Yellow Stage (an alert)." *http://www.pref.osaka.lg.jp/kikaku/kinkyuzitai-yousei/index.html#0801* (accessed January 17, 2021). (in Japanese)
28. Tokyo Metropolitan Government. COVID-19 Control Website: Latest trends in Tokyo. *https://stopcovid19.metro.tokyo.lg.jp/* (accessed January 17, 2021). (in Japanese)
29. Tokyo Metropolitan Government. "Assistance fund for reduced business hours to prevent a pandemic (implemented 28 November - 17 December)" (Bulletin No.1072). *https://www.metro.tokyo.lg.jp/tosei/hodohappyo/press/2020/11/25/29.html* (accessed January 17, 2021). (in Japanese)
30. Osaka Prefectural Government. From 4 December to 15 December 2020 "Requirements based on the response

to the Red Stage (a crisis situation)" *http://www.pref.osaka.lg.jp/kikaku/kinkyuzitai-yousei/index.html#12041* (accessed January 17, 2021). (in Japanese)
31. Japan Tourism Agency, Ministry of Land, Infrastructure, Transport and Tourism. The "Take a Trip" Project. *https://www.mlit.go.jp/kankocho/content/001358665.pdf* (accessed January 17, 2021). (in Japanese)
32. Ministry of Foreign Affairs. New border control measures for COVID-19. *https://www.anzen.mofa.go.jp/info/pcwideareaspecificinfo_2020C090.html* (accessed January 17, 2021). (in Japanese)
33. Ministry of Health, Labor, and Welfare. The current status of COVID-19 and the response by the Ministry of Health, Labor, and Welfare (1 October 2020). *https://www.mhlw.go.jp/stf/newpage_13886.html* (accessed January 17, 2021). (in Japanese)
34. Ministry of Health, Labor, and Welfare. The current status of COVID-19 and the response by the Ministry of Health, Labor, and Welfare (31 December 2020). *https://www.mhlw.go.jp/stf/newpage_15828.html* (accessed January 17, 2021). (in Japanese)
35. Ministry of Health, Labor, and Welfare. The current status of COVID-19 and the response by the Ministry of Health, Labor, and Welfare (1 July 2020). *https://www.mhlw.go.jp/stf/newpage_12177.html* (accessed January 17, 2021). (in Japanese)
36. Ministry of Health, Labor, and Welfare. Survey on the status of care and the number of beds reserved for inpatients. *https://www.mhlw.go.jp/stf/seisakunitsuite/newpage_00023.html* (accessed January 17, 2021). (in Japanese)
37. Association of Japanese Healthcare Corporations. Survey of the fiscal status of hospitals due to the COVID-19 pandemic (1st quarter of 2020). *https://ajhc.or.jp/siryo/20200806_covid19ank.pdf* (accessed January 17, 2021). (in Japanese)
38. Association of Japanese Healthcare Corporations. Survey of the fiscal status of hospitals due to the COVID-19 pandemic (2nd quarter of 2020). *https://ajhc.or.jp/siryo/20201112_covid19ank.pdf* (accessed January 17, 2021). (in Japanese)
39. Ministry of Health, Labor, and Welfare. Implementation of an assistance program to prevent the spread of infection at medical facilities and pharmacies among urgent comprehensive assistance programs to combat COVID-19. *https://www.mhlw.go.jp/content/10800000/000642278.pdf* (accessed January 17, 2021). (in Japanese)
40. Ministry of Health, Labor, and Welfare. Implementation of an assistance program paying a bonus to personnel responding to COVID-19 among urgent comprehensive assistance programs to combat COVID-19. *https://www.mhlw.go.jp/content/10800000/000641418.pdf* (accessed January 17, 2021). (in Japanese)

Received December 22, 2020; Revised January 21, 2021; Accepted January 27, 2021.

**Address correspondence to:*
Peipei Song, National Center for Global Health and Medicine, 1-21-1 Toyama, Shinjuku-ku, Tokyo 162-8655, Japan.
E-mail: ppsong-tky@umin.ac.jp

Yu Chen, Department of Human and Engineered Environmental Studies, Graduate School of Frontier Sciences, The University of Tokyo, 5-1-5 Kashiwanoha, Kashiwa Chiba 227-8568, Japan.
E-mail: chen@edu.k.u-tokyo.ac.jp

Released online in J-STAGE as advance publication January 29, 2021.

Review

DOI: 10.5582/bst.2020.01039

The immunological characteristics of gallbladder carcinoma and advances in immunotherapy practices

Haihong Cheng[1], Di Zhou[2], Shouhua Wang[2], Jun Ding[3,*], Fei Ma[1,4,*]

[1] Department of Oncology, Xinhua Hospital Affiliated to Shanghai Jiao Tong University School of Medicine, Shanghai, China;
[2] Department of General Surgery, Xinhua Hospital Affiliated to Shanghai Jiao Tong University School of Medicine, Shanghai, China;
[3] Department of Biliary and Pancreatic Surgery, Shanghai Shuguang Hospital Affiliated with the Shanghai University of T.C.M., Shanghai, China;
[4] Shanghai Institute for Pediatric Research, Shanghai, China.

SUMMARY Gallbladder carcinoma (GBC) is one of the most common malignant tumors in the biliary system, ranking sixth among gastrointestinal malignancies. In addition, the incidence of GBC has recently increased in China. GBC metastasizes early and invades adjacent organs such as the liver, making patients with GBC ineligible for radical surgery and giving them a poor prognosis. What is more, GBC is more inclined to develop chemo-resistance, which requires new strategies for clinical intervention. Cancer immunotherapy has made great advances over the past few years, with improved clinical efficacy against multiple malignancies, including GBC. This review summarizes the immunological characteristics of GBC as well as current advances in immunotherapies for GBC in order to provide new insights into future treatment and prevention of GBC.

Keywords gallbladder carcinoma, immunological characteristic, immunotherapy practices, vaccine, adoptive immunotherapy, cytokine

1. Introduction

Gallbladder carcinoma (GBC) is one of the most common primary malignancies of the biliary tract, with a higher incidence in women than in men. More than 90 percent of GBC are adenocarcinomas, which are moderately or poorly differentiated in most cases (*1*). The prognosis for GBC is extremely poor, with a median overall survival (OS) of around 4-7 months (*2*). At present, surgery, radiation, and systemic chemotherapy are the main treatments for GBC depending on the tumor stage and grade. The standard first-line chemotherapy regimen for advanced GBC, gemcitabine (Gem) and cisplatin (GC), has an objective response rate (ORR) of only around 30%. The median OS is only 11.7 months (*3*) and the 5-year overall survival rate is less than 5% after chemotherapy. Hence, exploring new treatment options is crucial to improving the survival of patients.

Unlike conventional therapies targeting tumor cells directly, cancer immunotherapy modulates the host's immune responses to induce sustained anti-tumor immunity and restrict tumor growth. Comprehensive strategies for cancer immunotherapy have been formulated depending on the immunological characteristics of the tumor itself and the host. In recent years, successful examples of cancer immunotherapy include the adoptive transfer of immune cells (*4,5*) and immune checkpoint blockades (*6,7*). In addition, tumor vaccines have also been developed with apparent efficacy in pre-clinical studies. Attempts at cancer immunotherapy for GBC are promising. This review summarizes current insights into the immunological characteristics of GBC and frontiers in immunotherapeutic approaches for GBC, which will facilitate the identification of new options to improve the clinical efficacy of therapies for GBC.

2. Immunological characteristics of GBC

The immune system plays a vital role in the development and progression of tumors. It can monitor the "non-self" mutant cells in the body and eliminate them specifically through cell immune mechanisms to maintain homeostasis. However, mutant cells may evade monitoring by the immune system through various mechanisms including low levels of expression of MHC molecules and tumor antigens, blocking of tumor antigens, and release of immunosuppressive factors. With these mechanisms, mutant cells can rapidly proliferate in an uncontrolled manner (*2*). In addition, the immune system can promote processes such as angiogenesis to promote tumor progression *via* the tumor microenvironment (*2*). Thus, immune therapy

should play a vital role in the treatment of a variety of cancers. Treating malignant tumors of the biliary system by regulating the immune system has become a hot topic of recent research (*8*). Both the innate immune system and the adaptive immune system warrant study.

Malignancies with different origins have the same features. Immune cell infiltration can be found in the tumor microenvironment. Differences in the pattern of infiltration affect the prognosis for a tumor (*2*). An increasing number of studies has indicated that substantial infiltration of macrophages, neutrophils, and regulatory T cells (Tregs) predicts a poor prognosis, while substantial infiltration of cytotoxic T lymphocytes (CTL) and mast cells indicates a better prognosis. Wang *et al*. established an immune index model based on the distribution of 5 types of infiltrating immune cells in GBC tissues, and they found that patients with a lower immune index ($Macrophage^{low}$ Neu^{low} $Treg^{low}$ CTL^{high} MC^{high}) had a better survival rate (*9*) .

2.1. The innate immune system

The innate immune system recognizes tumor antigens, induces and strengthens the adaptive immune system, and can kill tumor cells directly. In the tumor microenvironment, however, these effects are suppressed. Numerous studies have attempted to manipulate innate immunity to fight tumors (*10*). The cells involved in innate immunity primarily include mono-nuclear phagocytes, neutrophils, NK cells, NKT cells, γδT cells, and mast cells. Macrophages can be divided into two different types depending on their state of activation and function: M1 macrophages and M2 macrophages, or respectively classically activated macrophages and alternatively activated macrophages. M2 macrophages are associated with a poor prognosis in many primary tumors. Recent studies have indicated that CCL18 secreted by M2 macrophages promotes the migration and invasion of GBC cells *via* the PI3K/Akt pathway (*11*), which provides a new direction for research into targeted therapy for GBC. Neutrophils have been proven to be correlated with a lower survival rate for patients with head and neck malignancies or breast cancer (*2*). The neutrophil-lymphocyte ratio (NLR) is the most studied index in GBC. An increased NLR implies a poor prognosis (*12-15*). Du *et al*. found that the derived neutrophil-to-lymphocyte ratio (dNLR), lymphocyte-to-monocyte ratio (LMR), Fib-to-pAlb ratio (FPR), and CEA are closely related to the clinical prognosis for patients with metastatic GBC (mGBC). They are both independent risk factors that affect the prognosis for patients with mGBC. Among the aforementioned indices, dNLR has the highest predictive effect (*16*). Mast cells can inhibit tumor progression by releasing cytokines such as TNF or recruiting dendritic cells (DC), CD8+ T cells and NK cells. Bo *et al*. explored the relationship between tumor-infiltrating mast cells (TIMs) and the prognosis for patients with GBC treated with Gem. Gene enrichment analysis indicated that TIMs are related to the activation and recruitment of CD8+ T cells. Patients with advanced GBC and a high number of TIMs can significantly benefit from chemotherapy and have promising outcomes (*17*). γδ+T cells can recognize antigens not restricted by MHC. Recently, a study found that γδ+T cells are the main source of IL-17, which can promote tumor angiogenesis in patients with GBC. Blocking the production of IL17 *via* this pathway may be a new way to treat the disease (*18*) .

2.2. The adaptive immune system

The adaptive immune system mainly involves DC, CD4+ T lymphocytes, CD8+ T lymphocytes, and B lymphocytes. In the process of immune regulation, CD4+Treg cells inhibit the activation and proliferation of T cells; CD8+CTL and CD4+Treg cells are crucial cells in the anti-tumor immune response (*19*). T cell infiltration in human cancers determines the clinical outcomes of tumor to a certain extent. Antigen recognition in the tumor microenvironment plays a significant role in the function of T cells. Identifying therapeutic targets that could simultaneously improve T cell function is warranted.

Numerous studies on GBC also have focused on the adaptive immune system. Foxp3 is one of the vital transcription factors that control the development and function of CD4+ Treg cells. An immunohistochemical analysis of 80 patients with GBC found that CD8+ T cells were related to the improved survival time of patients with advanced GBC while Foxp 3+ T cells indicated a poorer prognosis (*20*). Oguro *et al*. recently discovered a co-inhibitory receptor, B and T lymphocyte attenuator (BTLA), that is structurally and functionally similar to cytotoxic T lymphocyte-associated antigen 4 (CTLA-4) and programmed death receptor 1(PD-1) and that is expressed on most lymphocytes. BTLA should be a novel therapeutic target by reversing the immune escape of tumors and enhancing anti-tumor immune function (*21*). In addition, a high platelet to lymphocyte ratio (PLR) is also independently associated with a poor prognosis in patients with GBC (*22*).

3. Cancer Immunotherapy for GBC

Thanks to the rapid advances in cancer immunology and immunotherapy, GBC immunotherapy has become a viable option in clinical trials and clinical practice. Current mainstream immunotherapies include therapeutic vaccines, adoptive immunotherapy, immune checkpoint inhibitors, and cytokines. Table 1 summarizes the completed clinical trials and Table 2 summarizes the ongoing clinical trials on immunotherapies for GBC. Due to the low incidence

Table 1. Clinical studies of immunotherapies for GBC

Immunotherapy	Treatment regimens	Phase	Targeted disease	OS (mo)	PFS (mo)	*Ref.*
Peptide-based vaccine (WT1)	Peptide vaccine+ gemcitabine	I	Pancreatic, GBC, ICC, ECC	9.3	–	(*8*)
CAR-T	CAR-T+ CTX+ nab-P	I	CC, GC	–	4	(*23*)
INF-α	5-FU+INF-α	–	BTC	11.9	6.2	(*24*)

BTC: biliary tract carcinoma.; CC: cholangiocarcinoma; CTX: cyclophosphamide; ECC: extrahepatic cholangiocarcinoma; GBC: gallbladder cancer; ICC: intrahepatic cholangiocarcinoma; INF-α: interferon-α; nab-P: nab-paclitaxel; OS: overall survival; PFS: progression-free survival.

Table 2. Ongoing clinical trials of immunotherapies for GBC

Treatment regimen	Phase	Estimated date of completion	Targeted disease	Identification number
Afatinib + Nivolumab	–	December 31, 2020	GBC	ChiCTR1800018149
Camrelizumab + Cap + radiotherapy	II	June 2024	BTC, ECC, GBC	NCT04333927
Atezolizumab + Cobimetinib	II	June 30, 2021	GBC, ICC, CC	NCT03201458
Bintrafusp alfa + Gem + Cis	II/III	July 24, 2023	BTC, CC, GBC	NCT04066491
Durvalumab + Gem/Cis	II	December 30, 2022	BTC, GBC, CC	NCT04308174
Avelumab + Peposertib + Radiotherapy	I/II	December 3, 2022	GBC, Solid Neoplasm, (and 26 more...)	NCT04068194
Tumor-infiltrating Lymphocytes	I/II	October 2022	Gastrointestinal Cancer, Pancreatic Cancer, GBC, (and 8 more...)	NCT04426669
Ipilimumab + Nivolumab	II	August 1, 2021	GBC, Acinar Cell Carcinoma, Adenoid Cystic Carcinoma, (and 91 more...)	NCT02834013
Pembrolizumab + Gem + Cis	III	August 31, 2023	BTC	NCT04003636
Manganese Chloride + nab-P + Gem + anti-PD-1 antibody	I/II	August 31, 2021	BTC	NCT04004234
AZD6738 + Durvalumab	II	March 31, 2022	BTC	NCT04298008
Durvalumab + Tremelimumab	II	December 2023	ICC	NCT04238637
Pembrolizumab	II	August 2021	BTC	NCT03110328

BTC: biliary tract carcinoma; CC: cholangiocarcinoma; CTX: cyclophosphamide; ECC: extrahepatic cholangiocarcinoma; GBC: gallbladder cancer; Gem: gemcitabine; ICC: intrahepatic cholangiocarcinoma; INF-α: interferon-α; nab-P: nab-paclitaxel OS: overall survival; PFS: progression-free survival.

of GBC, patients with that disease have mostly been included in clinical trials on BTC. The information about ongoing clinical trials was obtained from the Chinese Clinical Trial Registry and ClinicalTrials.gov.

3.1. Tumor vaccines

Current research on immunotherapy for GBC is mainly focused on peptide vaccines and DC vaccines (*25*). mRNA vaccines and DNA vaccines may also be promising areas of research in the future. Wilm's tumor 1 (WT1) and Mucin 1 (MUC1) are currently two antigens studied mostly in BTC. According to recent studies, both have been found to be associated with a poor prognosis in patients with cancer (*26*). A combination of Gem and WT1 vaccine was investigated in a Phase I study to treat unresectable GBC, cholangiocarcinoma, and pancreatic cancer (*8*). An increase in WT1-specific lymphocytes was observed. Moreover, the toxicity of the vaccine was negligible. In 2017, long-term remission was achieved in a patient with stage IV GBC who was treated with a combination of chemotherapy (Gem and titanium silicate-1) and an autologous formalin-fixed tumor vaccine containing autologous tumor fragments (*27*), suggesting the prospective clinical use of vaccines to treat GBC.

Traditional peptide vaccines have the disadvantage of low immunogenicity and MHC restriction. In contrast, DC vaccines can activate stronger immune responses by presenting specific antigens or tumor lysates. Since the first use of DCs loaded with melanoma-associated antigen (MAGE-1) to treat malignant melanoma *in vitro* in 1995, more than 400 clinical trials based on DC vaccines for the treatment of various malignant tumors have been conducted or completed worldwide (*28*). As early as 2005, researchers utilized tumor lysate antigens to produce 10 doses of autologous dendritic cell vaccines and successfully used them to treat a patient with stage III (T2, N1, M0) GBC; long-term remission (> 12 months) was achieved without metastasis (*29*). In a study in 2018, Rojas-Sepúlveda *et al*. selected GBC cell lines expressing tumor-associated antigens to prepare lysates (*25*). When subjected to heat shock, DCs become mature and capable of activating antigen-specific T cells. The study used allogeneic cancer cell lysates to prepare DC vaccines. This enhanced their efficacy, providing an alternative treatment for unresectable advanced GBC. The use of cell lysates

has many incomparable advantages. DCs can present a variety of antigens concurrently, and the damage-associated molecular patterns (DAMPs) produced by GBC cells under conditions such as heat shock can also promote the maturation and activation of DCs (*30*). The vaccine production process, such as the selection of DCs, optimization of DC maturation, and transportation should be optimized in order to maximize the efficacy of vaccines in the future (*31*). Zhang *et al*. screened six MHC I candidate tumor antigens in mouse lung cancer cell lines to prepare neoantigen adjuvant vaccines and neoantigen-sensitized DC vaccines, and they concluded that DC vaccines can produce a stronger immune response in mouse models of tumors (*28*).

Therapeutic mRNA vaccines can provide complete antigens, which is an advantage over peptide-based vaccines. Choosing a suitable ionizable lipid material as a carrier can promote the delivery of mRNA and result in stronger and more specific immune activation (*32*). Currently, mRNA vaccines are being investigated in a series of phase I and II clinical trials involving malignant melanoma, prostate cancer, glioblastoma, colorectal cancer, breast cancer, and non-small cell lung cancer (*33*). Although mRNA-based vaccines seem to offer promise and have advantages according to preclinical research, clinical trials are currently limited to phase I and phase II trials. Therefore, there is a long way to go before using those vaccines in the clinical treatment of GBC, though they are certainly worth exploring further.

A DNA vaccine refers to a plasmid designed to deliver genes encoding tumor antigens (TA) to stimulate or enhance the immune response to tumor cells expressing TA. A slew of completed clinical trials tested the efficacy of DNA vaccines against breast cancer, cervical cancer, pancreatic cancer, prostate cancer, multiple myeloma, and malignant melanoma. To date, DNA vaccines have not been investigated in GBC. One of their disadvantages, such vaccines might not be able to overcome the immune escape given the lack of relevant antigens in some tumor cells. This problem may be overcome through the combined use of antigens or selection of optimal antigens (*34*).

As precision medicine continues to develop, personalized tumor vaccines have also become a hot topic of research. Tumor neoantigens expressed as a result of mutations in tumor cell-related genes have high immunogenicity, and personalized tumor vaccines are likely to be highly efficacious (*35*). However, the heterogeneity of tumor cells hampers the selection of the mutation with the best immunogenicity. Moreover, manufacturing personalized vaccines is time-consuming, laborious, and costly (*36*).

3.2. Adoptive immunotherapy

Adoptive immunotherapy means the infusion of peripheral blood or tumor-infiltrating immune cells that have been modified and expanded *in vitro* in order to facilitate tumor suppression. As early as 1998, there was a case report about the combination of anticancer drugs and adoptive immunotherapy (infused TILs and CTLs obtained by co-cultivation of peripheral immune cells and autologous tumor cells) to treat advanced GBC, and that combination was efficacious to a certain extent (*37*). The patient's quality of life was improved remarkably and there was no biliary drainage due to the effects of immunochemotherapy. In another case in 2014, infusion of autologous NK cells and activated T cells (extracting peripheral blood NK cells and T cells to activate and expand those cells *in vitro*) sustained remission for more than 6 months in a patient with stage IV GBC who had not benefited from surgery or chemotherapy (*5*). A case in Japan in 2018 indicated that a combination of chemotherapy and adoptive immunotherapy (starting with cytokine-induced killer cells (CIK) and later changing to DC-induced killer cells (DIK)) achieved a long-term survival of almost 10 years in a patient (*4*). In this case, the only reported immunotherapy-related adverse event was a mild fever that did not noticeably affect the patient's quality of life. In a newly completed phase I clinical trial of 19 patients with EGFR-positive advanced biliary system malignancies (14 patients with cholangiocarcinoma and 5 with GBC), patients received autologous T cell therapy with chimeric EGFR antigen receptors. Among the 17 patients who were ultimately evaluable, 1 had complete remission, 10 had stable disease, and median progression-free survival was 4 months (2.5-22 months). Notwithstanding some reactions like mucosal/cutaneous toxicities and acute pulmonary edema, the T cell infusion was tolerated (*23*). A phase I/II clinical trial using TILs to treat GBC and other solid tumors will finish in 2022 (NCT04426669).

3.3. Immune checkpoint inhibitors

Immune checkpoint molecules (Checkpoints) play an inhibitory role in immune regulation. Currently, the most studied targets include PD-1/programed cell death ligand 1 (PD-L1) and CTLA-4. A recent study found that PD-L1 expressed on DCs interacts with PD-1 on T cells, resulting in inhibition of the anti-tumor response after DCs present tumor antigens to T cells. The down-regulation of PD-L1 in DCs and the silencing of PD-1 on T cells may lead to enhanced T cell activation of DCs, thereby producing effective anti-tumor T cell responses (*38*). Mayoux *et al*. posited a new mechanism: since PD-L1 can bind to PD-1 and B7.1 (CD80), a PD-L1 blockade can reduce PD-L1 binding to B7.1 on DCs; increasing the interaction of B7.1 and CD 28 can enhance the activation of T cells (*7*). The above studies all noted the significant role of DCs in anti-PD-L1 therapy, suggesting that the combination of DC vaccines and Checkpoints has a huge potential.

Given the remarkable efficacy of monoclonal antibodies (MAb) against the PD-1/PD-L1 pathway in non-small cell lung cancer, renal cell carcinoma, malignant melanoma, and urothelial carcinoma (*39*), the US Food and Drug Administration (FDA) has approved its use to treat a number of solid tumors. The expression of PD-L1 in 174 patients with GBC was measured using tissue microarray technology (*39*). PD-L1 expression was found in 23% of cancer tissues, suggesting the potential to use anti-PD-L1 therapy in GBC. Recently, a patient with recurrent and metastatic GBC with a high level of PD-L1 expression (≥ 50%) significantly benefited from radiotherapy combined with nivolumab with no adverse events (*6*). A point worth highlighting is that the FDA has recently approved durvalumab for the treatment of BTC. A clinical trial (NCT03110328) is currently underway to evaluate the feasibility and efficacy of pembrolizumab in the treatment of BTC.

CTLA-4 is a homolog of CD28 that sends an inhibitory signal to T cells. Combined therapy with PD-1 and CTLA-4 antibodies has been effectively used to treat multiple tumors (*40*). More clinical trials are investigating double checkpoint inhibitors for the treatment of GBC. A phase II study indicated that durvalumab and tremelimumab combined with a GP chemo-regimen resulted in an OS of 20.7 months in 121 patients with BTC, as was reported at ASCO this year. More trials using these two drugs or other immunotherapy combinations are recruiting subjects or preparing final results, as shown in Table 2. In addition to double checkpoint inhibition, clinical trials are also examining combinations with chemotherapy, target therapy or radiotherapy, including NCT04333927, NCT03201458, NCT04003636, NCT04003636, and NCT04066491 (Table 2).

The BTLA described above, which is widely expressed in human T cells, is a promising target as well. Antibodies that block such molecules can enhance human T cell responses as monotherapy or in combination with anti-PD-1 treatment (*41*).

3.4. Cytokines

IL-2 is a key factor in maintaining the activation of T cells, and its clinical use in metastatic malignant melanoma and metastatic renal cell carcinoma has been approved by the FDA (*34*). The synergistic use of IL-2 and PD-1/PD-L1 blockers has been used in clinical trials on non-small cell lung cancer, bladder cancer, and malignant melanoma (*42*). Studies have found that IFN-γ can inhibit the differentiation of monocytes into M2 macrophages and promote the transformation of M2 macrophages into M1 macrophages. Sun *et al*. subcutaneously inoculated BALB/C nude mice with a human GBC cell line (GBC-SD) to create an animal model. After intratumor injection of recombinant mouse IFN-γ, levels of vascular endothelial growth factor and the extent of angiogenesis in tumor tissues decreased significantly (*43*). IFN-α can activate anti-tumor immunity by promoting T cells, NK cells, and DCs while inhibiting the activity of Treg cells (*24,44*). In one study, about 23 patients with ICC and 2 patients with GBC received combined therapy with 5-fluorouracil and IFN-α (*24*). The overall response rate was 24% (6 of 25 patients had partial remission). Only one patient developed Grade 4 anemia and received a blood transfusion. However, no adverse reactions resulted in the discontinuation of treatment. Both IL-24 and IL-37 have pro-apoptotic or inhibitory effects on GBC cells, and they are also expected to become one of the approaches to the treatment of GBC (*45,46*).

4. Conclusion

Thus far, great efforts have been made to devise the therapeutic strategies for and to improve the efficacy of non-surgical treatments of GBC, including devising new therapeutic approaches such as targeted drugs and vaccines. The results of numerous clinical trials that have examined the efficacy of immunotherapy, as mentioned earlier, are particularly encouraging. Moreover, numerous clinical studies of treatments for GBC are underway. A point of paramount importance is to capitalize on combined therapies such as combined use of chemotherapy and immunotherapy or use of immunotherapies targeting different pathways. These approaches should have a synergistic effect with minimal toxicity.

Given the relatively low incidence of GBC, few patients with GBC are admitted to any hospital. Thus, large-scale multi-center clinical studies are crucial to achieving expected breakthroughs.

Funding:This work was supported by the National Natural Science Foundation of China (grant no. 81802337), Shanghai Jiao Tong University (grant no. YG2017MS74), and the Shanghai Health Committee (grant no. 2020404447).

Conflict of Interest: The authors have no conflicts of interest to disclose.

References

1. Lazcano-Ponce EC, Miquel JF, Muñoz N, Herrero R, Ferrecio C, Wistuba II, de Ruiz PA, Urista GA, Nervi F. Epidemiology and molecular pathology of gallbladder cancer. CA Cancer J Clin. 2001; 51:349-364.
2. Palucka AK, Coussens LM. The basis of oncoimmunology. Cell. 2016; 164:1233-1247.
3. Park K, Kim KP, Park S, Chang HM. Comparison of gemcitabine plus cisplatin versus capecitabine plus cisplatin as first-line chemotherapy for advanced biliary tract cancer. Asia Pac J Clin Oncol. 2017; 13:13-20.
4. Kawamoto M, Wada Y, Koya N, Takami Y, Saitsu H,

Ishizaki N, Tabata M, Onishi H, Nakamura M, Morisaki T. Long-term survival of a patient with recurrent gallbladder carcinoma, treated with chemotherapy, immunotherapy, and surgery: A case report. Surg Case Rep. 2018; 4:115.
5. Bhamare S, Prabhakar P, Dharmadhikari A, Dedeepiya VD, Terunuma H, Senthilkumar R, Srinivasan T, Reena HC, Preethy S, Abraham SJ. Autologous immune enhancement therapy in a case of gall bladder cancer stage IV after surgical resection and chemotherapy yielding a stable non-progressive disease. J Cancer Res Ther. 2014; 10:752-754.
6. Kong W, Wei J, Liu J, Qiu Y, Shi J, He J, Su M, Xiao M, Liu B. Significant benefit of nivolumab combining radiotherapy in metastatic gallbladder cancer patient with strong PD-L1 expression: A case report. Onco Targets Ther. 2019; 12:5389-5393.
7. Mayoux M, Roller A, Pulko V, *et al*. Dendritic cells dictate responses to PD-L1 blockade cancer immunotherapy. Sci Transl Med. 2020; 12.
8. Marks EI, Yee NS. Immunotherapeutic approaches in biliary tract carcinoma: Current status and emerging strategies. World J Gastrointest Oncol. 2015; 7:338-346.
9. Wang J, Bo X, Wang C, *et al*. Low immune index correlates with favorable prognosis but with reduced benefit from chemotherapy in gallbladder cancer. Cancer Sci. 2020; 111:219-228.
10. Demaria O, Cornen S, Daëron M, Morel Y, Medzhitov R, Vivier E. Harnessing innate immunity in cancer therapy. Nature. 2019; 574:45-56.
11. Zhou Z, Peng Y, Wu X, Meng S, Yu W, Zhao J, Zhang H, Wang J, Li W. CCL18 secreted from M2 macrophages promotes migration and invasion *via* the PI3K/Akt pathway in gallbladder cancer. Cell Oncol (Dordr). 2019; 42:81-92.
12. Beal EW, Wei L, Ethun CG, *et al*. Elevated NLR in gallbladder cancer and cholangiocarcinoma - making bad cancers even worse: Results from the US Extrahepatic Biliary Malignancy Consortium. HPB (Oxford). 2016; 18:950-957.
13. Liu F, Hu HJ, Ma WJ, Yang Q, Wang JK, Li FY. Prognostic significance of neutrophil-lymphocyte ratio and carbohydrate antigen 19-9 in patients with gallbladder carcinoma. Medicine (Baltimore). 2019; 98:e14550.
14. Zhang L, Wang R, Chen W, Xu X, Dong S, Fan H, Liu C. Prognostic significance of neutrophil to lymphocyte ratio in patients with gallbladder carcinoma. HPB (Oxford). 2016; 18:600-607.
15. Zhang Y, Jiang C, Li J, Sun J, Qu X. Prognostic significance of preoperative neutrophil/lymphocyte ratio and platelet/lymphocyte ratio in patients with gallbladder carcinoma. Clin Transl Oncol. 2015; 17:810-818.
16. Du JH, Lu J. Circulating CEA-dNLR score predicts clinical outcome of metastatic gallbladder cancer patient. J Clin Lab Anal. 2019; 33:e22684.
17. Bo X, Wang J, Wang C, *et al*. High infiltration of mast cells is associated with improved response to adjuvant chemotherapy in gallbladder cancer. Cancer Sci. 2020; 111:817-825.
18. Patil RS, Shah SU, Shrikhande SV, Goel M, Dikshit RP, Chiplunkar SV. IL17 producing gammadeltaT cells induce angiogenesis and are associated with poor survival in gallbladder cancer patients. Int J Cancer. 2016; 139:869-881.
19. Lin J, Long J, Wan X, Chen J, Bai Y, Wang A, Yang X, Wu Y, Robson SC, Sang X, Zhao H. Classification of gallbladder cancer by assessment of CD8(+) TIL and PD-L1 expression. BMC Cancer. 2018; 18:766.
20. Fluxa P, Rojas-Sepulveda D, Gleisner MA, Tittarelli A, Villegas P, Tapia L, Rivera MT, Lopez MN, Catan F, Uribe M, Salazar-Onfray F. High CD8(+) and absence of Foxp3(+) T lymphocytes infiltration in gallbladder tumors correlate with prolonged patients survival. BMC Cancer. 2018; 18:243.
21. Oguro S, Ino Y, Shimada K, Hatanaka Y, Matsuno Y, Esaki M, Nara S, Kishi Y, Kosuge T, Hiraoka N. Clinical significance of tumor-infiltrating immune cells focusing on BTLA and Cbl-b in patients with gallbladder cancer. Cancer Sci. 2015; 106:1750-1760.
22. Pang Q, Zhang LQ, Wang RT, Bi JB, Zhang JY, Qu K, Liu SS, Song SD, Xu XS, Wang ZX, Liu C. Platelet to lymphocyte ratio as a novel prognostic tool for gallbladder carcinoma. World J Gastroenterol. 2015; 21:6675-6683.
23. Guo Y, Feng K, Liu Y, Wu Z, Dai H, Yang Q, Wang Y, Jia H, Han W. Phase I study of chimeric antigen receptor-modified T cells in patients with EGFR-positive advanced biliary tract cancers. Clin Cancer Res. 2018; 24:1277-1286.
24. Yashima Y, Sato S, Kawai T, Sugimoto T, Sato T, Kanda M, Obi S. Intraarterial 5-fluorouracil and interferon therapy is safe and effective for nonresectable biliary tract adenocarcinoma. Hepatol Int. 2015; 9:142-148.
25. Rojas-Sepulveda D, Tittarelli A, Gleisner MA, Avalos I, Pereda C, Gallegos I, Gonzalez FE, Lopez MN, Butte JM, Roa JC, Fluxa P, Salazar-Onfray F. Tumor lysate-based vaccines: On the road to immunotherapy for gallbladder cancer. Cancer Immunol Immunother. 2018; 67:1897-1910.
26. Zhao L, Zhong L, Xu S, Li B. Immunotherapeutic approaches in cancer treatment. Anticancer Agents Med Chem. 2019; 19:204-205.
27. Imaoka Y, Kuranishi F, Miyazaki T, Yasuda H, Ohno T. Long-lasting complete response status of advanced stage IV gall bladder cancer and colon cancer after combined treatment including autologous formalin-fixed tumor vaccine: Two case reports. World J Surg Oncol. 2017; 15:170.
28. Zhang R, Yuan F, Shu Y, Tian Y, Zhou B, Yi L, Zhang X, Ding Z, Xu H, Yang L. Personalized neoantigen-pulsed dendritic cell vaccines show superior immunogenicity to neoantigen-adjuvant vaccines in mouse tumor models. Cancer Immunol Immunother. 2020; 69:135-145.
29. Khan JA, Yaqin S. Successful immunological treatment of gallbladder cancer in India--Case report. J Zhejiang Univ Sci B. 2006; 7:719-724.
30. Nigro A, Montico B, Casolaro V, Dal Col J. A novel dendritic cell-based vaccination protocol to stimulate immunosurveillance of aggressive cancers. Methods Mol Biol. 2019; 1884:317-333.
31. Perez CR, De Palma M. Engineering dendritic cell vaccines to improve cancer immunotherapy. Nat Commun. 2019; 10:5408.
32. Miao L, Li L, Huang Y, Delcassian D, Chahal J, Han J, Shi Y, Sadtler K, Gao W, Lin J, Doloff JC, Langer R, Anderson DG. Delivery of mRNA vaccines with heterocyclic lipids increases anti-tumor efficacy by STING-mediated immune cell activation. Nat Biotechnol. 2019; 37:1174-1185.
33. Pardi N, Hogan MJ, Porter FW, Weissman D. mRNA vaccines - A new era in vaccinology. Nat Rev Drug

Discov. 2018; 17:261-279.
34. Lopes A, Vandermeulen G, Preat V. Cancer DNA vaccines: Current preclinical and clinical developments and future perspectives. J Exp Clin Cancer Res. 2019; 38:146.
35. Vormehr M, Diken M, Tureci O, Sahin U, Kreiter S. Personalized neo-epitope vaccines for cancer treatment. Recent Results Cancer Res. 2020; 214:153-167.
36. Schlom J, Gulley JL. Vaccines as an integral component of cancer immunotherapy. JAMA. 2018; 320:2195-2196.
37. Murakami K, Tanimura H, Yamaue H, Mizobata S, Noguchi K, Nakamori M, Shimamoto T. Clinical effect of immunochemotherapy for a patient with advanced gallbladder cancer: Report of a case. Surg Today. 1998; 28:923-928.
38. Hassannia H, Ghasemi Chaleshtari M, Atyabi F, Nosouhian M, Masjedi A, Hojjat-Farsangi M, Namdar A, Azizi G, Mohammadi H, Ghalamfarsa G, Sabz G, Hasanzadeh S, Yousefi M, Jadidi-Niaragh F. Blockage of immune checkpoint molecules increases T-cell priming potential of dendritic cell vaccine. Immunology. 2020; 159:75-87.
39. Neyaz A, Husain N, Kumari S, Gupta S, Shukla S, Arshad S, Anand N, Chaturvedi A. Clinical relevance of PD-L1 expression in gallbladder cancer: A potential target for therapy. Histopathology. 2018; 73:622-633.
40. Zhang E, Gu J, Xu H. Prospects for chimeric antigen receptor-modified T cell therapy for solid tumors. Mol Cancer. 2018; 17:7.
41. Rosskopf S, Leitner J, Zlabinger GJ, Steinberger P. CTLA-4 antibody ipilimumab negatively affects $CD4^+$ T-cell responses *in vitro*. Cancer Immunol Immunother. 2019; 68:1359-1368.
42. Barroso-Sousa R, Ott PA. Transformation of old concepts for a new era of cancer immunotherapy: Cytokine therapy and cancer vaccines as combination partners of PD1/PD-L1 inhibitors. Curr Oncol Rep. 2018; 21:1.
43. Sun T, Yang Y, Luo X, Cheng Y, Zhang M, Wang K, Ge C. Inhibition of tumor angiogenesis by interferon-gamma by suppression of tumor-associated macrophage differentiation. Oncol Res. 2014; 21:227-235.
44. Ma H, Jin S, Yang W, Zhou G, Zhao M, Fang S, Zhang Z, Hu J. Interferon-alpha enhances the antitumour activity of EGFR-targeted therapies by upregulating RIG-I in head and neck squamous cell carcinoma. Br J Cancer. 2018; 118:509-521.
45. Jia J, Li S, Gong W, Ding J, Fang C, Quan Z. mda-7/IL-24 induces apoptosis in human GBC-SD gallbladder carcinoma cells *via* mitochondrial apoptotic pathway. Oncol Rep. 2011; 25:195-201.
46. Wu TJ, Xu B, Zhao GH, Luo J, Luo C. IL-37 suppresses migration and invasion of gallbladder cancer cells through inhibition of HIF-1alpha induced epithelial-mesenchymal transition. Eur Rev Med Pharmacol Sci. 2018; 22:8179-8185.

Received December 5, 2020; Revised January 21, 2021; Accepted January 29, 2021.

**Address correspondence to:*
Fei Ma, Department of Oncology, Xinhua Hospital Affiliated to Shanghai Jiao Tong University School of Medicine, No. 1665 Kongjiang Road, Shanghai 200092, China.
E-mail: mafei@xinhuamed.com.cn

Jun Ding, Department of Biliary and Pancreatic Surgery, Shanghai Shuguang Hospital Affifiliated to Shanghai University of T.C.M., Shanghai,201203, China.
E-mail: doctording0916@126.com

Released online in J-STAGE as advance publication February 7, 2021.

Original Article

DOI: 10.5582/bst.2020.03317

Role of key amino acids in the transmembrane domain of the Newcastle disease virus fusion protein

Yanan Huang[1], Yaqing Liu[1], Yanguo Li[2], Ying Liu[1], Chi Zhang[1], Hongling Wen[1], Li Zhao[1], Yanyan Song[1], Liyang Wang[3,*], Zhiyu Wang[1,*]

[1] Department of Virology, School of Public Health, Cheeloo College of Medicine, Shandong University, Ji'nan, Shandong, China;
[2] Department of Health Management and Services, Cangzhou Medical College, Cangzhou, Hebei, China;
[3] Department of Clinical Laboratory, Qilu Hospital, Cheeloo College of Medicine, Shandong University, Ji'nan, Shandong, China.

SUMMARY Newcastle disease (ND), caused by the Newcastle disease virus (NDV), is transmitted by poultry with severe infectivity and a high fatality rate. The fusion (F) protein on the NDV envelope facilitates the merger of the viral and host cell membranes with the help of the homologous hemagglutinin-neuraminidase protein (HN). The transmembrane (TM) domains of viral fusion proteins are typically required for fusion, but the key amino acids in NDV F TM domains have not been identified. Site-directed mutagenesis was utilized to change the conserved amino acids at 500, 501, 502, 505, 510, 513, 516, 519, and 520 to alanine. It was found that mutants L519 and V520 had an interrupted protein expression, decreased to below 10%, and mutants A500, I505, V513, and V516 had a hypoactive impact on fusion activity, decreased to 85.38%, 67.05%, 55.38% and 51.13% of wt F, respectively. The results indicated that the TM domain plays a vital part in the fusion activity of the NDV F protein.

Keywords NDV, fusion protein, transmembrane domain, cell fusion

1. Introduction

Newcastle disease (ND), caused by the virulent Newcastle disease virus (NDV) and resulting in high mortality in the avian industry, causes devastating economic effects on a wide range of domestic and wild bird production worldwide. Despite current vaccination protocols utilized to quell the disease, the potential for future outbreaks and the hazards of other analogous paramyxoviruses require further study of the entry mechanism. Membrane fusion to process infection is mainly mediated and coordinated by a combination of the homologous hemagglutinin-neuraminidase (HN) protein responsible for receptor binding and a fusion (F) protein undergoing irreversible conformation rearrangement coupling of the energy released with membrane coalition of the virus membrane protein (*1*).

Before participating in merging, the NDV F protein, initially synthesized as inactive form F_0, requires proteolytically cleavage to become the disulfide bonded F_1 and F_2 active complex form (*2*). F_1 has two hydrophobic regions, the N-terminal fusion peptide (FP) located at the new N-terminal after cutting, transmembrane (TM) domains, and two heptad repeat (HR) regions, HRA and HRB (Figure 1A). HRA lies at the C-terminal of FP, and HRB is adjacent to the TM domain (*3*). Atomic structures of several paramyxovirus F proteins for parainfluenza virus 5 (PIV5), respiratory syncytial virus (RSV), human metapneumovirus (hMPV), Hendra virus (HeV), and Nipah virus (NiV) in the prefusion form and hPIV3, NDV, and RSV in the post-fusion form have been determined by X-ray crystallography. While all of these protein architectures are ectodomains, the C-terminal regions are among the least well-understood (*4*).

Several studies have shown that the TM domain aids in protein folding, stability and fusion beyond merely anchoring *via* replacement with other fusion protein TM domains. Little is known about the secondary structure of the TM domain of viral fusion proteins. Researchers applied solid-state nuclear magnetic resonance to determine the backbone conformation and oligomeric structure of the TM domain of the PIV5 F protein in lipid bilayers. It was found that the secondary structure of TM domain depends on various membrane compositions (*5,6*). The TM domain can adopt a transmembrane strand-helix-strand conformation, which causes different curvatures to the two leaflets of the membrane in order to help drive the hemi-fusion to fusion pore transition. In spite of the TM domain conformation depending to a great extent on the lipid composition, the amino acid sequence of the TM domain also exhibits an intrinsic

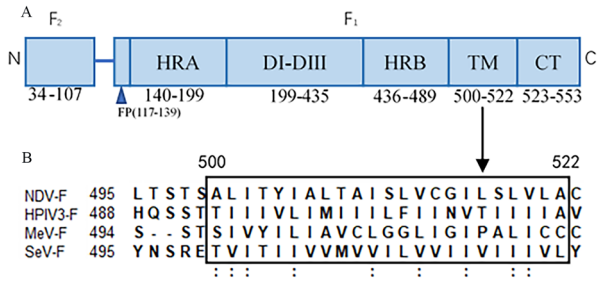

Figure 1. Schematic diagram of the locations of mutations. (A) Domain structure of the NDV F protein. Fusion peptide (FP), heptad repeat region (HR), and structural domains (DI-DIII), transmembrane region (TM), and cytoplasmic tail are shown. **(B)** Identification of the conserved amino acids in the TM domain by sequence alignment using BioEdit software. The asterisk (**) represent similar amino acids in the F protein of NDV, hPIV3, MeV and SeV.

preference for the α-helix or β-chain conformation. Importantly, β-branched residues comprise 30-75% of the TM domain sequences of 10 paramyxoviruses and the human immunodeficiency virus (HIV) (*6*). Also, the shift of β-branched residues support this notion, revealing that these residue mutations of the TM domain of the Hendra virus F seriously diminished fusion activity (*7*).

The current experiments demonstrated that the TM domain of paramyxovirus F, such as PIV5, hMPV, and HeV self-associate in a monomer-trimer equilibrium in isolation (*8,9*). It is very likely that trimeric TM-TM interactions are characteristic of F proteins throughout the paramyxovirus family. They even have similar features with other class I viral fusion proteins including the Ebola virus glycoprotein, influenza virus hemagglutinin, and severe acute respiratory syndrome coronavirus spike protein (*10*). This is helpful for the development of an antiviral target using the TM-TM interaction to destroy the fusion protein function (*11*).

Additionally, the presence or absence of certain TM motifs has been implicated in promotion of modulating protein oligomerization and function. This includes central glycine motifs (*7,12*) (*i.e.*, GXXXG, where X is any amino acid) and a leucine zipper-like (*13*) (or heptad repeat-like) arrangement of leucine/isoleucine residues. However, the PIV5 F TM L/I zipper does not significantly affect protein expression, but is critical for fusogenic activity, and only affects pre-fusion stability (*14*). These results suggest that F proteins of paramyxoviruses have inherent sequence requirements for their TM domains, rather than certain interaction motifs. Replacement of the NDV F protein TM domain with Measles virus (MeV), Sendi virus (SeV), and vesicular stomatitis virus (VSV) F proteins lead to proteins with defective fusion activities (*15*). Upon further investigation, residues L486 and I488 of PIV5 F TM domain are considered to act as a key role in fusion (*16*). Nevertheless, the key amino acids in the NDV F TM domain have not been identified. These features aroused our interest and in part motivated the present study. Therefore, we compared the TM domains among several paramyxoviruses (Figure 1B) in order to define the targets for mutagenesis.

2. Materials and Methods

2.1. Strain and plasmids

The strain was *E.coli* DH5α. Vector pBluescript SK (+) (pBSK$^+$) containing NDV-Australia-Victoria HN and F were kindly presented with Professor Iorio. The NDV F gene was cloned and inserted at *Xho* I (668), and the NDV HN gene was inserted between *Xba* I and *Sac* I.

2.2. Cell line and viruses

BHK-21 cells were maintained in Dulbecco modified Eagle medium (DMEM) (Biological Industries (BI), Beit-Haemek, Israel) supplemented with 10% (v/v) fetal bovine serum (FBS) (BI) and 1% (v/v) penicillin/streptomycin (BI). The recombinant vaccinia virus (vTF7-3), a present of Dr. Bernard Moss, provided T7 polymerase for the transient expression system of vaccinia virus-T7 RNA polymerase used to express the wild type (wt) or mutated F protein, while the wt vaccinia virus was used as the control in the content mixing assay.

2.3. Construction of F TMD mutants

The mutants for the NDV F TM domain were constructed by changing interested residues to alanine, which is the chiral amino acid with the shortest side chain and has little influence on the spatial structure of proteins according to the alignment of NDV, hPIV3, MeV, and SeV F TM domains. Using pBSK$^+$-F as a template, the mutants were obtained by Gene splicing by overlap extension PCR (SOE PCR) with the assistance of two pairs of reverse-complement primers, mutagenesis oligonucleotide primers and vector oligonucleotide primers (Table 1) (Sangon Biotech Co. Ltd., Shanghai, China) (*17*). All constructs were sequenced to verify that only the desired mutations had occurred. The recombinant plasmids were transformed into *E.coli* DH5α for amplification and extracted with the ENZA Plasmid Miniprep Kit (Omega Bio-Tek, Inc., USA) for subsequent experiments.

2.4. Transfection

BHK-21 cells were cultured in 12-well plates at a density of 4×10^5 cells per well before transfection. After 70-80% confluence, the cells were incubated with vTF7-3 (1:50) in serum-free DMEM for 1 h at 37°C in a 5% CO_2 incubator to allow for infection of vTF7-3. Subsequently, the supernatant was removed and the cells were washed with serum-free DMEM,

Table 1. Mutant primer sequences

Name	Sequence (5′-3′)
Vector-FP	GGTTATTGTCTCATGAGCGGATACA
Vector-RP	TGTATCCGCTCATGAGACAATAACC
A500T-FP	CTGACCAGCACATCTACTCTCATTACCTATATC
A500T-RP	GATATAGGTAATGAGAGTAGATGTGCTGGTCAG
L501A-FP	ACCAGCACATCTGCTGCCATTACCTATATCGCT
L501A-RP	AGCGATATAGGTAATGGCAGCAGATGTGCTGGT
I502A-FP	AGCACATCTGCTCTCGCTACCTATATCGCTTTA
I502A-RP	TAAAGCGATATAGGTAGCGAGAGCAGATGTGCT
I505A-FP	GCTCTCATTACCTATGCCGCTTTAACTGCCATA
I505A-RP	TATGGCAGTTAAAGCGGCATAGGTAATGAGAGC
I510A-FP	ATCGCTTTAACTGCCGCATCTCTTGTTTGCGGT
I510A-RP	ACCGCAAACAAGAGATGCGGCAGTTAAAGCGAT
V513A-FP	ACTGCCATATCTCTTGCTTGCGGTATACTTAGT
V513A-RP	ACTAAGTATACCGCAAGCAAGAGATATGGCAGT
I516A-FP	TCTCTTGTTTGCGGTGCACTTAGTCTGGTTCTA
I516A-RP	TAGAACCAGACTAAGTGCACCGCAAACAAGAGA
L519A-FP	GTTTGCGGTATACTTGCTCTGGTTCTAGCATGC
L519A-RP	GCATGCTAGAACCAGAGCAAGTATACCGCAAAC
V520A-FP	TGCGGTATACTTAGTGCGGTTCTAGCATGCTAC
V520A-RP	GTAGCATGCTAGAACCGCACTAAGTATACCGCA

The 9 amino acids in the TM domain were mutated to A (A500 is mutated to T) by overlapping PCR. *Xba* I digested pBSK$^+$-F was used as the template to create one PCR fragment with primers mutations-FP (forward primer) and Vector-RP (reverse primer). The same plasmid digested by *Kpn* I was used as the template to generate the other PCR fragment with primers mutations-RP and Vector-FP. Two PCR products at each mutation point with homologous ends were transformed into DH5α competent cells to obtain the desired mutants. Mutated sites are underlined in the primer sequences.

and 1 mL complete medium (DMEM with 10% FCS) was added into each well, and then transfected with 4 μL TurboFect™ Transfection Reagent (Thermo Fisher Scientific, USA) and 4 μg either wt and mutant F plasmids and/or the wt HN plasmid, the two of which were gently pre-mixed together.

2.5. Indirect immunofluorescent assay (IIFA)

After 36 h transfection, monolayers of BHK-21 cells were fixed with 4% paraformaldehyde for 15 min before washing twice with phosphate-buffered saline (PBS), followed by incubation for 4 h at 4°C with 3% PBSA (in PBS supplemented with bovine serum albumin). Then the cells were incubated with anti-NDV antiserum (ab34402, Abcam, Cambridge, UK, at a 1:1,000 dilution) recognizing the NDV F protein and an Alexa Fluor 488-conjugated goat anti-chicken IgY (H+L) (ab150169, Abcam, diluted 1:10,000) as the secondary antibody. The cells were recorded under a fluorescent microscope (Olympus, Tokyo, Japan) after the secondary antibody was washed twice with PBS.

2.6. Fluorescence-activated cell sorter (FACS) analysis

To quantify the F protein surface expression levels, transfected BHK-21 cells were transferred by PBS configured 0.02% EDTA to a centrifuge, washed twice, and blocked with PBSA for 30 min, followed by incubation with primary and secondary antibodies, the same as the IIFA. Then, the cells were immobilized with 4% paraformaldehyde and subsequently resuspended in 300 μL PBSA for analysis with the Flow Cytometer (FACSCelesta, BD, USA).

2.7. Dye transfer assay

R18, a lipolyphilic probe (Invitrogen, California, USA), which was transferred from chicken red blood cells to fuse BHK-21 cells as co-transfected with NDV HN and wt or the mutated F gene, were used to access hemi-fusion of membrane-membrane. At 22 h post-transfection, the R18-labelled RBCs were added to BHK-21 cells in 12-well plates and incubated for 0.5 h on ice. Cells were incubated 1h at 37°C after the unbound RBCs were washed by cold PBS containing 0.1 mM $CaCl_2$ and 1 mM $MgCl_2$ (PBS-CM), and then the results of the lipid mixing were photographed under a fluorescent microscope (Olympus).

2.8. Reporter gene assay

Effector cells were co-transfected with the desired F and NDV HN genes with the help of vTF7-3. Target cells infected with the WT vaccinia virus were transfected with 1 μg of plasmid pG1NT7 β-gal, which encodes β-galactosidase. After 18 h, effector cells were overlaid with target cells (which stably express the T7 polymerase) at an approximate 1:1 ratio at 37°C for 12 h in a 96-well microtiter plate. The cells were then lysed and assayed for β-galactosidase activity according to the β-galactosidase assay kit manufacturer's instructions (Beyotime Biotechnology, Shanghai, China). Values were normalized to samples containing the desired F and NDV HN, with the wild-type levels set at 100% after subtraction of the values for NDV HN alone.

2.9. Syncytium assays

BHK-21 cells seeded into 12-well plates were co-transfected with wt F or mutant F genes along with the NDV HN gene after incubation with the recombinant vaccinia virus 1h earlier at 37°C. Monolayer cells fixed with methanol and stained with Gimesa solution were examined for syncytium formation at 24 h post-transfection using an inverted microscope (Olympus).

2.10. Western Blot

At 36 h post-transfection, the lysate of cells was harvested, pelleted, and loaded in 12% polyacrylamide gels. After electrophoresis, the proteins were transferred from the gels to polyvinylidenedifluoride (PVDF) membranes, blocked with 5% nonfat milk, and incubated with primary and secondary antibody (IRDye 800CW donkey anti-chicken antibody, LI-COR,

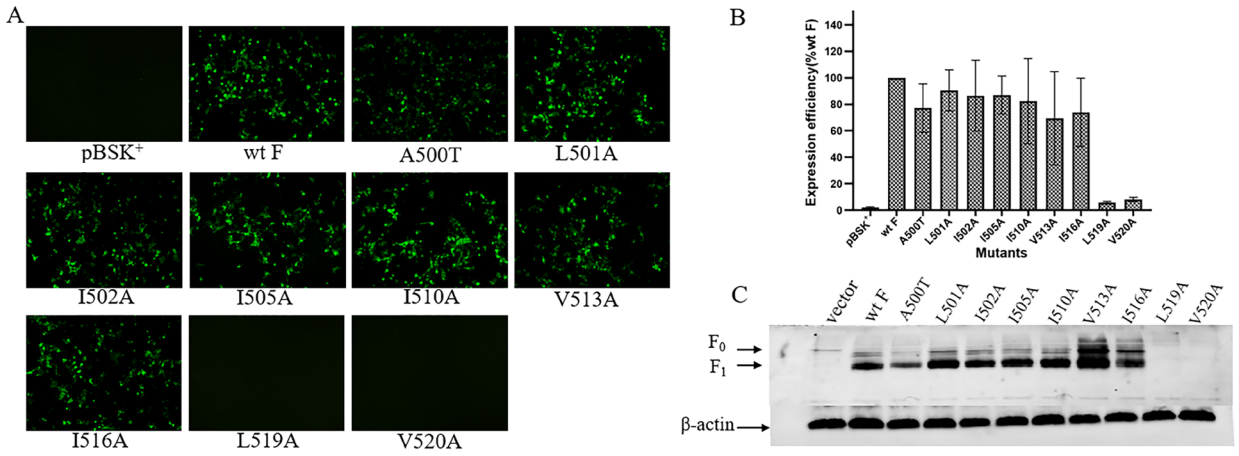

Figure 2. The results of cell surface expression and cleavage activity of wt and mutant F protein. (A) Qualitative results of cell surface expression of mutant F proteins by IIFA. Monolayers of BHK-21 cells transfected with wt or mutant F genes were incubated with anti-NDV antiserum and then with fluorescent-labeled goat anti-chicken antibody. (Magnification: 100×). **(B)** Quantitative detection results of cell surface expression efficiency of mutant F proteins by FACS analysis. Data were normalized to the value obtained with wt F. C: Expression and cleavage of NDV wt F and F mutants transfected without HN. β-actin was used as the internal reference.

Lincoln, Nebraska, USA). Protein bands were scanned and visualized with Odyssey (LI-COR).

2.11. Statistics and data analysis

All results were generated from at least three separate experiments and presented as the mean ± SD. Statistical analysis was evaluated by the Student's *t* test using SPSS 20.0 with a significance level of $p < 0.05$ (*), $p < 0.01$(**) and $p < 0.001$ (***), respectively.

3. Results

3.1. Cell surface expression of wt F and its mutants

To explore whether or not these mutated F proteins were expressed at the cell surface, indirect immunofluorescent detection and fluorescent-activated cell sorting were used to qualitatively and quantitatively analyze their protein expressions on the cell surface. As shown in Figure 2A, there were discernable fluorescent signals between most mutants and wt F, except for L519A and V520A, for which signals were barely detected. Similar to FACS analysis, most mutants expressed as much as 70-90% of wt F (Figure 2B).

3.2. Cleavage activity of NDV wt F and mutants

Only by being proteolytically cleaved can the F protein become biologically active, therefore Western Blot was applied to test cleavage activity of NDV wt F and mutants (Figure 2C). The experiment revealed that most mutants were expressed at wt levels on the surface, but mutants L519A and V520A were noncleaved and expressed less than the wt F protein as expected, in agreement with the result of IIFA and FACS. The extent of cleavage of F mirrored the surface expression levels.

3.3. Fusion activity assay for wt F and its mutants

The process of viral membrane fusion involves a series of intermediate steps such as hemifusion (local membrane approach), pore formation, and pore enlargement. In order to analyze the effect of single amino acid substitution of conserved amino acids within the TM domain of NDV F concerning their fusion activity, three types of fusion activity experiments were conducted to measure hemi-fusion, content mixing, and syncytium formation.

First, through the process of membrane fusion, merger of the contacting outer leaflet resulted in hemi-fusion *via* a stalk intermediate that occurred at an early stage. To address whether or not mutants affect the ability to mediate subsequent content mixing, a R18 dye transfer assay was used to evaluate the extent of the lipophilic probe R18 transferred from RBC membranes to transfected BHK-21 cell membranes. Figure 3A displays representative photomicrographs of the dye transfer experiment. When monolayer cells were mock transfected with F alone, most mutants behaved in a manner similar to that of wt F and HN except for L519A and V520A, but there was a slight decrease in mutants A500T, I505A, V513A, and V516A. These results substantiate the idea that the existence of these mutants does not preclude the lipid mixing stage.

Second, content mixing was measured by using a β-galactosidase reporter gene assay. When two populations of cells were mixed, one co-expressed wt or mutated F along with HN, and the other transfected with the pGINT7β-gal plasmid and the pGINT7β-gal gene was activated to synthesize galactoside, which reacted with the substrate galactopyranoside to yield a bright yellow color. The intensity of the reaction results in the shade reflects the extent of cell fusion events. As Figure 3B shows, mutant A500T, L501A, I502A, and I510A

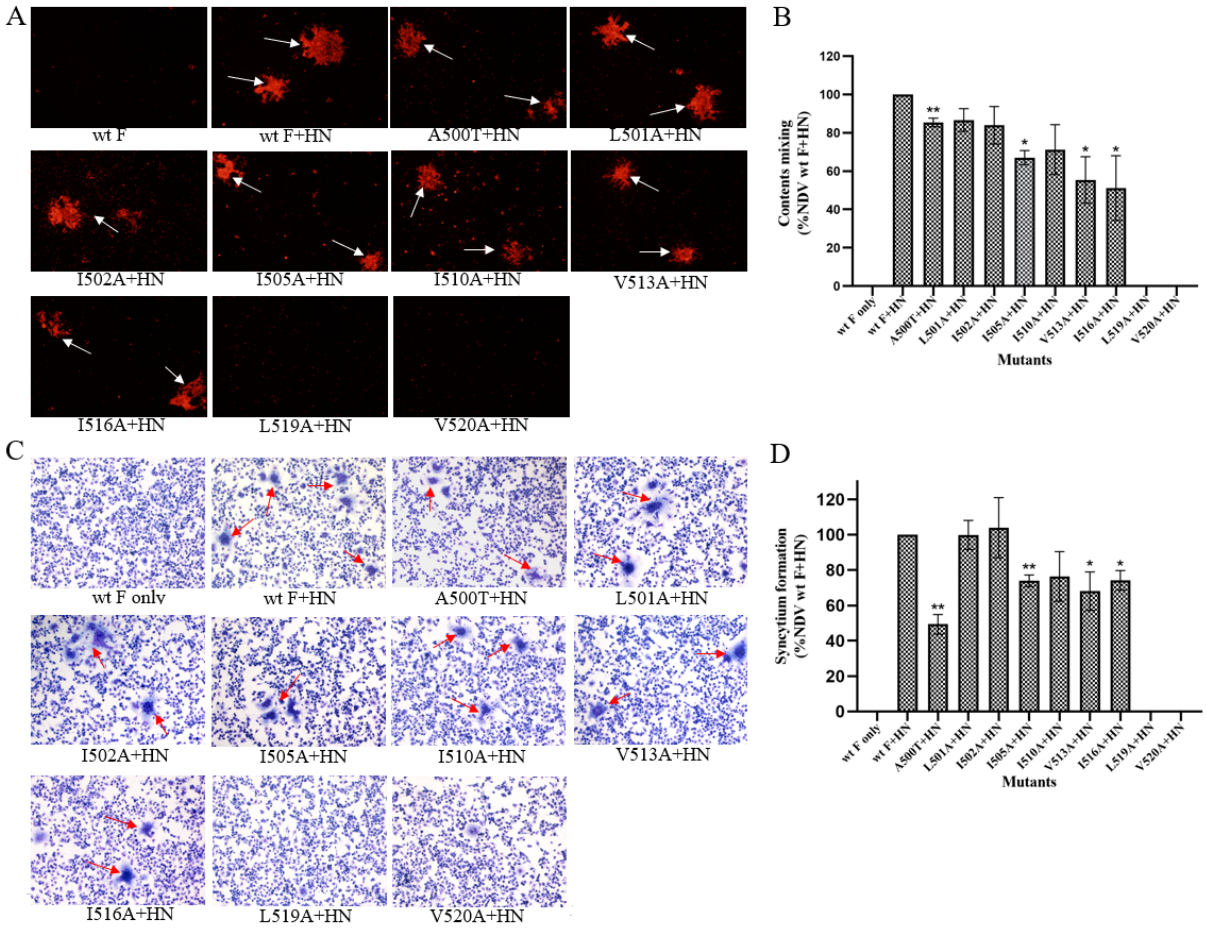

Figure 3. Fusion ability detection of F mutants. (A) Determination of lipid mixing for NDV wt and mutant F proteins (Magnification: 100×). Labeled RBCs were added to BHK-21 monolayer in order to observe the extent of lipid mixing. **(B)** Quantification of content mixing of mutants measured by the reporter gene method. The values were expressed as percentages of positive control co-transfected with wt HN and F. **(C)** The results of the syncytium formation assay of substitution mutants. The arrows point to the syncytium. (Magnification: 100×). **(D)** Quantitative results of syncytium area. Syncytia size was quantified by measuring the area covered by syncytia using Image Proplus software, referring it to the total area of the field for three random fields.

had 85.38%, 86.69%, 83.92 % and 71.24% of the levels of content mixing of the wt F protein, respectively, with L519A and V520A almost non-existent. The mutants I505A, V513A and V516A had a lower level of content mixing of 67.05%, 55.38% and 51.13% of that of wt F proteins. The preponderance of data indicated that several motifs were able to change content mixing.

Lastly, a syncytium fusion assay (Figures 3C and 3D) was used to determine whether the TM domain mutants affected the F protein function. Using cells expressing wt F only as mock, the cells that co-expressed wt or mutated F together with HN were imaged to visualize syncytia. That is, membrane fusion between neighboring cells leads to the formation of giant multinucleated cells. There was no significant difference in the number and size of syncytia formed by L501A and I502A, 100% and 104% as fusogenic as the wt F protein, respectively, and I510A was moderately fusogenic, while the mutants L519A and V520A were fusion dead. The numbers of fussed spots by the mutants A500T, I505A, V513A, and V516A in the presence of the HN protein were fewer in number than those produced by wt F and HN proteins (only 50-75% of the wt F level). These data demonstrated that individual residue replacement has various phenotypes with none to significant effects on syncytium formation.

4. Discussion

The fusion protein is generally envisioned to exist on the mature viral surface in a 'native' fusion-competent state, followed by fusion-associated conformational fold-back steps, during which the fusion subunit converts to a compact trimer-of-hairpins resembling a ball on a stick. In the prefusion structure (*18*), the spherical head consists of domains I through III (DI-DIII), HRA is located on the flanks of them, and DIII wraps HRA and FP, while the HRB domain forms a trimer coiled spiral C-terminal connected to the transmembrane domain, followed by a short cytoplasmic tail. On receiving a signal from a homotypic attachment protein, the HRB uncoils and HRA projects the FP onto the target cell membrane to closely approach and finally merging of the two membranes. This process seems to describe

only the anchoring of the transmembrane domain, but it goes far beyond that.

In the current study, we obtained nine amino acids with similar properties by aligning the TM domain sequences of the four viruses, replaced them with alanine, which was changed to the corresponding T residues at A500 of the hPIV3 F protein, in order to illustrate its effect on fusion promotion. It is clear that certain amino acids are of great importance for its structure and function. Among them, A500T, I505A, V513A, V516A, L519A, and V520A possess reduced or undetectable capacities for the mediation of membrane fusion, and the inability of two sites substitutions (519 and 520) which were fusogenically active. Alternatively, the rest of the constructs performed to an equal extent compared with wild F in fusion promotion.

The abolished capabilities to fuse cells of mutants L519A and V520A were found to be strongly associated with low expression at the cell surface, as observed in IIFA and FACS. Moreover, confirmation that mutant F proteins do not properly traffic to the cell surface came from not identifying F_0 and F_1 bands in the subsequent cleavage activity experiments. In the case of the general cycle of membrane proteins, they are initially synthesized as peptides in ribosomes, then folded and glycosylated in the endoplasmic reticulum, from where they are transported to the Golgi apparatus for cutting, and are finally secreted on the cell surface. Intracellular transport along the secretory pathway goes hand in hand with sorting of proteins and lipids (*19*). Hence, a possible role for 519 and 520 residues without expression and fusion activity is not recognized in the cellular transport and sorting machinery (*20,21*). These residues have an impact on localization of the protein in the compartment where their function is required. There are, of course, protein-specific constraints on TM domain sequences imposed by the interactions and function of a particular protein (*22*). Leucine and valine, hydrophobic residues in the TM domain proximal position of the cytoplasmic tails, may be conserved amino acids in this region. An alternative possibility is that defective conformation owing to mutation is neither properly identified by the corresponding antibody nor has fusing accessibility.

V513A and V516A showed decreased fusion activity, possibly because they affected the TM-TM effect. Among the 20 naturally occurring amino acids, proline, glycine, and alanine have a structurally unique feature that helps to explain their low or high helix propensities (*23*). The incorporation of some β-branched amino acids are deemed to facilitate textural plasticity to membrane α-helices, which may be essential to protein function for lipid disorders and subsequent steps in membrane fusion (*24,25*). Substituting alanine for them gives rise to stronger interactions favorable to stable prefusion conformation (*11*) but deleterious to the follow-up protein function due to structural rigidity (*24*). In a prevailing lipid-centric model of the fusion process, the attaching fusion peptide and transmembrane domain can concertedly act together on local membrane curvature to enhance pore opening, leading to lipid disorder, and spontaneous fusion (*26*). This has justified that fusion peptides derived from PIV5 and transmembrane domains can closely or loosely interact with homologous transmembrane domains to form thermodynamically advantageous coils in the lipid phase (*8,27*). This report is reminiscent of pivotal interaction between the FP and the TM domain of HIV gp41 (*12*). When V513 and V516 were mutated to alanine, the effect between the FP and the TM domain became weakened, resulting in the continuous expansion of fusion pores, manifested as content mixing and syncytium reduction. It is generally believed that β-strand conformation correlates with negative Gaussian curvature(NGC) (*6*), and that this curvature generation is geometrically necessary for topological changes during membrane remodeling in biological processes such as virus budding and membrane scission (*28*), while isoleucine and valine also have an inherent preference for β-strands (*29*), plus V513 and V516 are perhaps located in the core of the α-helix in the TM domain. Mutating the two together to alanine (or adding I510) may result in more failed fusion activity than a single mutation (not done in this study). In aggregate, these reasons may explain why V513A and V516A reduce fusion activity.

The construction A500T made the hypofusogenic mutant F protein, as observed in reporter gene assays (Figure 3B) and elucidated in syncytium assays (Figures 3C and 3D), where it was seen that the mutants caused 50% of wt F fusion levels. The residues that flank the hydrophobic membrane-spanning segments of membrane proteins might interact with the membrane-water interface, and strongly depend on specific properties of its amino acid side chains, including charge, hydrophobicity, polarity and potential for H-bonding (*30*). A500 could be located at the junction of the protein and the membrane. Fusion decline could be accounted for by a polarity change (from A to T), which may turn the interaction of the membrane-water interface, thus affecting its role. It was found that mutations within the membrane-proximal ectodomain region (MPER) of PIV5 (rich in serine and threonine)show both stabilizing and destabilizing activity (less fusion or increased fusion compared with wt F, respectively), suggesting that the MPER is a highly sensitive region of the protein (*31*). A500 is directly coupled to the MPER, so it might regulate fusion activity.

The fusion activity of construct I505A was decreased, as shown in previous experiment. In integral membrane proteins, tryptophan tends to locate at the membrane headgroup region, whereas isoleucine and alanine have a greater propensity to interact with the acyl chain region (*30,32,33*). I675A in MPER of HIV-1 gp41 may therefore

block the infectivity of cell-free virions by diminishing stabilizing interactions with the acyl chain region of the envelope, which predicted subtle changes in interfacial binding energy and hydrophobic moment (*34*). Likewise, the lower fusion activity of I505A is likely related to attenuated interactions with the acyl chain region, and thus adding to the mutation does not easily produce the negative curvature required for fusion.

In summary, the mutations we introduced into the TM domain of the NDV F exhibited various degrees of activity in membrane fusion, and the mutants A500T, I505A, V513A and V516A in this region altered the fusion function in BHK-21 cells. Sites L519 and V520 are crucial for F's production or architecture. This study of the F protein will provide supplementary data to further clarify the roles of this region in regulating membrane fusion activity.

Acknowledgements

We sincerely thank Dr. Bernard Moss of the National Institutes of Health for the wt and recombinant vaccinia virus vTF7-3 and Dr. Ronald M. Iorio of the University of Massachusetts Medical School for providing the recombinant plasmid vectors. Thanks to Dr. Edward C. Mignot, Shandong University, for linguistic advice.

Funding: This work was supported by grants from the National Natural Science Foundation of China (No. 81702814, No.81672011) and the Fundamental Research Funds of Shandong University (2015JC044).

Conflict of Interest: The authors have no conflicts of interest to disclose.

References

1. Harrison SC. Viral membrane fusion. Virology. 2015; 479-480:498-507.
2. Dutch RE, Hagglund RN, Nagel MA, Paterson RG, Lamb RA. Paramyxovirus fusion (F) protein: a conformational change on cleavage activation. Virology. 2001; 281:138-150.
3. Lamb RA, Parks GD. Paramyxoviridae: The viruses and their replication. In: Fields Virology (Knipe DM, Howley PM, eds.). Wolters Kluwer/Lippincott Williams & Wilkins, Philadelphia, PA, USA, 2007; pp. 1449-1496.
4. Harrison SC. Viral membrane fusion. Nat Struct Mol Biol. 2008; 15:690-698.
5. Lee M, Yao HW, Kwon B, Waring AJ, Ruchala P, Singh C, Hong M. Conformation and trimer association of the transmembrane domain of the parainfluenza virus fusion protein in lipid bilayers from solid-state NMR: Insights into the sequence determinants of trimer structure and fusion activity. J Mol Biol. 2018; 430:695-709.
6. Yao HW, Lee MW, Waring AJ, Wong GCL, Hong M. Viral fusion protein transmembrane domain adopts beta-strand structure to facilitate membrane topological changes for virus-cell fusion. Proc Natl Acad Sci U S A. 2015; 112:10926-10931.
7. Smith EC, Culler MR, Hellman LM, Fried MG, Creamer TP, Dutch RE. Beyond anchoring: the expanding role of the hendra virus fusion protein transmembrane domain in protein folding, stability, and function. J Virol. 2012; 86:3003-3013.
8. Donald JE, Zhang Y, Fiorin G, Carnevale V, Slochower DR, Gai F, Klein ML, DeGrado WF. Transmembrane orientation and possible role of the fusogenic peptide from parainfluenza virus 5 (PIV5) in promoting fusion. Proc Natl Acad Sci U S A. 2011; 108:3958-3963.
9. Smith EC, Smith SE, Carter JR, Webb SR, Gibson KM, Hellman LM, Fried MG, Dutch RE. Trimeric transmembrane domain interactions in paramyxovirus fusion proteins: roles in protein folding, stability, and function. J Biol Chem. 2013; 288:35726-35735.
10. Webb SR, Smith SE, Fried MG, Dutch RE. Transmembrane domains of highly pathogenic viral fusion proteins exhibit trimeric association *in vitro*. mSphere. 2018; 3:e00047-18.
11. Barrett CT, Webb SR, Dutch RE. A hydrophobic target: Using the paramyxovirus fusion protein transmembrane domain to modulate fusion protein stability. J Virol. 2019; 93:e00863-19.
12. Reuven EM, Dadon Y, Viard M, Manukovsky N, Blumenthal R, Shai Y. HIV-1 gp41 transmembrane domain interacts with the fusion peptide: implication in lipid mixing and inhibition of virus-cell fusion. Biochemistry. 2012; 51:2867-2878.
13. Webb S, Nagy T, Moseley H, Fried M, Dutch R. Hendra virus fusion protein transmembrane domain contributes to pre-fusion protein stability. J Biol Chem. 2017; 292:5685-5694.
14. Branttie JM, Dutch RE. Parainfluenza virus 5 fusion protein maintains pre-fusion stability but not fusogenic activity following mutation of a transmembrane leucine/isoleucine domain. J Gen Virol. 2020; 101:467-472.
15. Gravel KA, McGinnes LW, Reitter J, Morrison TG. The transmembrane domain sequence affects the structure and function of the Newcastle disease virus fusion protein. J Virol. 2011; 85:3486-3497.
16. Bissonnette MLZ, Donald JE, DeGrado WF, Jardetzky TS, Lamb RA. Functional analysis of the transmembrane domain in paramyxovirus F protein-mediated membrane fusion. J Mol Biol. 2009; 386:14-36.
17. Liu Y, Chi MM, Wen HL, Zhao L, Song YY, Liu N, Chi LL, Wang ZY. The DI-DII linker of human parainfluenza virus type 3 fusion protein is critical for the virus. Virus Genes. 2020; 56:37-48.
18. Welch BD, Liu YY, Kors CA, Leser GP, Jardetzky TS, Lamb RA. Structure of the cleavage-activated prefusion form of the parainfluenza virus 5 fusion protein. Proc Natl Acad Sci U S A. 2012; 109:16672-16677.
19. Welch LG, Munro S. A tale of short tails, through thick and thin: investigating the sorting mechanisms of Golgi enzymes. Febs Lett. 2019; 593:2452-2465.
20. Perrin J, Bary A, Vernay A, Cosson P. Role of the HIV-1 envelope transmembrane domain in intracellular sorting. Bmc Cell Biol. 2018; 19:3.
21. Singh S, Mittal A. Transmembrane domain lengths serve as signatures of organismal complexity and viral transport mechanisms. Sci Rep-Uk. 2016; 6:22352.
22. Sharpe HJ, Stevens TJ, Munro S. A comprehensive comparison of transmembrane domains reveals organelle-specific properties. Cell. 2010; 142:158-169.
23. Blaber M, Zhang XJ, Matthews BW. Structural basis

of amino-acid alpha-helix propensity. Science. 1993; 260:1637-1640.
24. Langosch D, Arkin IT. Interaction and conformational dynamics of membrane-spanning protein helices. Protein Sci. 2009; 18:1343-1358.
25. Ollesch J, Poschner BC, Nikolaus J, Hofmann MW, Herrmann A, Gerwert K, Langosch D. Secondary structure and distribution of fusogenic LV-peptides in lipid membranes. Eur Biophys J Biophy. 2008; 37:435-445.
26. Kozlov MM, McMahon HT, Chernomordik LV. Protein-driven membrane stresses in fusion and fission. Trends Biochem Sci. 2010; 35:699-706.
27. Yao HW, Lee M, Liao SY, Hong M. Solid-state nuclear magnetic resonance investigation of the structural topology and lipid interactions of a viral fusion protein chimera containing the fusion peptide and transmembrane domain. Biochemistry-Us. 2016; 55:6787-6800.
28. Schmidt NW, Lis M, Zhao K, Lai GH, Alexandrova AN, Tew GN, Wong GCL. Molecular basis for nanoscopic membrane curvature generation from quantum mechanical models and synthetic transporter sequences. J Am Chem Soc. 2012; 134:19207-19216.
29. Li SC, Deber CM. Glycine and beta-branched residues support and modulate peptide helicity in membrane environments. Febs Lett. 1992; 311:217-220.
30. Killian JA, von Heijne G. How proteins adapt to a membrane-water interface. Trends Biochem Sci. 2000; 25:429-434.
31. Zokarkar A, Lamb RA. The paramyxovirus fusion protein C-terminal region: Mutagenesis indicates an indivisible protein unit. J Virol. 2012; 86:2600-2609.
32. Senes A, Chadi DC, Law PB, Walters RFS, Nanda V, DeGrado WF. E-z, a depth-dependent potential for assessing the energies of insertion of amino acid side-chains into membranes: Derivation and applications to determining the orientation of transmembrane and interfacial helices. J Mol Biol. 2007; 366:436-448.
33. Ulmschneider MB, Sansom MSP. Amino acid distributions in integral membrane protein structures. Bba-Biomembranes. 2001; 1512:1-14.
34. Narasimhulu VGS, Bellamy-McIntyre AK, Laumaea AE, Lay CS, Harrison DN, King HAD, Drummer HE, Poumbourios P. Distinct functions for the membrane-proximal ectodomain region (MPER) of HIV-1 gp41 in cell-free and cell-cell viral transmission and cell-cell fusion. J Biol Chem. 2018; 293:6099-6120.

Received September 1, 2020; Revised December 4, 2020; Accepted January 21, 2021.

Address correspondence to:
Liyang Wang, Department of Clinical Laboratory, Qilu Hospital, Cheeloo College of Medicine, Shandong University, Ji'nan, Shandong Province, 250012, China.
E-mail: wangliyang@sdu.edu.cn

Zhiyu Wang, Department of Virology, School of Public Health, Cheeloo College of Medicine, Shandong University, Ji'nan 250012, Shandong Province, China.
E-mail: zhiyu.wang@sdu.edu.cn

Released online in J-STAGE as advance publication January 27, 2021.

Original Article

DOI: 10.5582/bst.2021.01026

A comparative study of contrast-enhanced ultrasound and contrast-enhanced CT for the detection and characterization of renal masses

Liang Fang[1,4,§], Kun Bai[2,§], Yue Chen[1,4], Jia Zhan[1,4], Yinjia Zhang[1,4], Zhiying Qiu[1,4], Lin Chen[1,4,*], Ling Wang[3,*]

[1] Department of Ultrasound, Huadong Hospital, Fudan University, Shanghai, China;
[2] Department of Ultrasound, Jiading Central Hospital, Fudan University, Shanghai, China;
[3] Department of Reproductive Immunology, Obstetrics and Gynecology Hospital, Fudan University, Shanghai, China;
[4] Shanghai Key Laboratory of Clinical Geriatric Medicine Shanghai, China.

SUMMARY This study aims to compare the value of contrast-enhanced ultrasound (CEUS) and contrast-enhanced CT (CECT) in the differential diagnosis of benign and malignant renal masses. Included in this retrospective study were 143 renal masses in 141 patients using histopathological findings as the gold standard. A comparison was made of the two modalities in image characteristics for their accuracy in the differential diagnosis of renal masses. CEUS and CECT were both used for 39 masses in 37 patients, with 31 (79.5%) being malignant and 8 (20.5%) benign. The differences between the benign and malignant groups in perfusion intensity, perfusion uniformity and entry and exit of the contrast agent were not statistically significant ($P > 0.05$). However, CEUS could better display the circular perfusion of renal cell carcinoma than CECT ($P < 0.05$). CECT alone detected 109 masses in 107 patients, with 93 (85.3%) being malignant and 16 (14.7%) benign. CEUS detected 73 masses in 71 patients, with 56 (76.7%) being malignant and 17 (23.3%) benign. No statistically significant differences were observed between CEUS and CECT in the diagnosis of renal cell carcinoma (92.8% *vs.* 90.3%), with a specificity of 52.9% *vs.* 31.2%, an accuracy of 83.5% *vs.* 81.6%, and a positive predictive value of 86.7% *vs.* 88.4% or a negative predictive value of 69.2% *vs.* 35.7% ($P > 0.05$ for all). These results suggested both CEUS and CECT are highly valuable in the differential diagnosis of renal masses, and CEUS can be used as an important supplement for CECT in diagnosis of renal cancer.

Keywords Contrast enhanced ultrasound, renal cell carcinoma, contrast enhanced CT

1. Introduction

Renal cell carcinoma (RCC), originating from epithelial cells of proximal convolutional tubules, is a common malignant tumor of the urinary system (*1*). Clinical statistics showed that about 1/3 of patients newly diagnosed with RCC had metastases and that some may have extensive metastases without any clinical symptoms. In addition, 20-40% of patients with localized RCC develop metastasis (*2*). Therefore, enhancing diagnosis and early detection rate of RCC is key to its treatment, contributing significantly to the improved survival rate of those patients.

CT, with a high definition and spatial resolution, is able to distinguish components of the lesions such as water, fat or calcification by quantifying density of the lesions and thus able to identify the nature of the lesions (*3*). However, it is often difficult to determine the nature of RCC with a plain CT scan, and contrast-enhanced CT (CECT) with iodine contrast agent can perform better for differential diagnosis. However, as CECT is timed, it is unable to obtain a continuous scan, probably resulting in missed lesion enhancement. In addition, CECT is contraindicated for patients with an allergy to iodine contrast agent, renal insufficiency, and severe hyperthyroidism. Moreover, CECT is expensive and radioactive (*4*). Therefore, it is particularly important to seek a complementary diagnostic imaging method for CECT.

At present, conventional ultrasound (US) has become one of the commonly used imaging modalities for clinical detection and diagnosis of RCC because of its intuitiveness, simplicity, non-invasiveness, accuracy and low cost. Conventional gray-scale ultrasound remains the indispensable first choice, but its sensitivity for diagnosis of RCC is reportedly low (*5*). Color Doppler

flow imaging (CDFI) can characterize blood flow of RCC, enhancing the diagnostic accuracy of RCC to some extent. However, for small RCC located in the lower pole or ventral of the kidney, CDFI has limited diagnostic value because of difficulty in detecting the signal of internal blood flow due to thin donor vessel, deep location or low blood flow velocity (*6,7*).

Contrast-enhanced ultrasound (CEUS), a technically simple imaging modality, allows real-time acquisition without the drawbacks of CECT. CEUS with microbubble contrast agents and contrast-specific US modes have been introduced to overcome the limitations of B-mode and color Doppler US. At present, CEUS has a confirmed value in detection and diagnosis of liver cancer, and its accuracy is not inferior to that of CECT (*8,9*). The diagnostic value of CEUS in RCC is, therefore, worth exploration. The objective of this study was to investigate, by comparing with pathological findings, the sensitivity and specificity of CEUS and CECT in RCC.

2. Materials and Methods

2.1. Patients

A retrospective analysis was made of the imaging data of 141 inpatients (143 masses, 2 patients with 2 masses; all masses being ipsilateral) admitted to the Department of Ultrasound from June 2015 to June 2020. CECT and CEUS were both used for 37 patients (23 male and 14 female; aged 39-81 with an average of 62.1 ± 10.2 years) and detected 39 masses with a maximum diameter of 8-100 mm and an average of 31.0 ± 19.9 mm. CECT alone examined 107 patients (71 male and 36 female; aged 28-82 with an average of 60.0 ± 11.6 years) and detected 109 masses with a maximum diameter of 7-136 mm and an average of 43.5.6 ± 27.4 mm. CEUS alone examined 71 patients (45 male and 26 female; aged 22-83 with an average of 58.2 ± 13.1 years) and detected 73 masses with a maximum diameter of 8-100 mm and an average of (31.6 ± 17.2) mm.

The study was conducted with the approval and supervision of the ethics committee of Fudan University, and the procedure followed was in accordance with the declaration of Helsinki. After informed consent was obtained, CEUS followed by CECT was performed, and all the patients were monitored for adverse events for four hours after the procedure. The clinical status, blood pressure, and heart rate were followed up.

2.2. Ultrasound examinations

Color Doppler ultrasound was performed using the Philips iU22 (Philips Ultrasound, Bothell, Washington, USA), ACUSON S2000 (Siemens Medical Solutions, Mountain View, CA, USA) and LOGIC E9 (GE Healthcare, Milwaukee, WI, USA) ultrasound systems, all being capable of real-time contrast-enhanced imaging. The 3.5 MHz transducer was used with a mechanical index (MI) of 0.06-0.09. The contrast agent used was SonoVue (Bracco SpA, Milan, Italy),which was formulated into a suspension of Sulphur hexafluoride microbubbles (8 μL/mL) by adding 5mL of physiological saline. A baseline ultrasound examination was performed to detect lesions, and the images were saved on a hard disk. For each lesion, we measured its size, position, border, shape, echogenicity, and blood flow. CEUS was performed with a bolus injection *via* cubital vein of the contrast agent at a dose of 1.5-2.0mL flushed with 5 mL saline. In this study, we defined cortical phases as 10-15 s after injection to 30-45 s, and medullary phases as approximately 30-45 s after injection until complete disappearance of microbubble echoes. In patients with multiple lesions, an additional bolus of SonoVue (1.5-2.0mL) was administered for each lesion at an interval of at least 15 min to allow for clearance of the previous contrast injection. No contrast agent was appreciable either in the renal parenchyma or masses before starting a new examination. All the CEUS examinations were digitally recorded.

2.3. CECT examinations

All examinations were performed on a dual-source, dual-energy CT scanner (Somatom Definition, Siemens Medical Solutions, Germany). Both abdominal unenhanced CT and CECT scans were performed. Parameters included a detector collimation of 64 × 0.6 mm^2, a pitch of 1.2, a gantry rotation time of 0.5 s, a tube voltage of 120 kVp, and an abdominal reference tube current of 210 mAs. Automated tube current modulation was used in all CT studies (CARE Dose 4D; Siemens Medical Solutions). All images were reconstructed from the CECT scan with a slice thickness of 0.75-mm and a reconstruction increment of 0.5-mm. The CECT scan was started by a continuous bolus injection of 80 ml iopromide (Ultravist; 300 mg I/mL, Bayer Schering Pharma, Berlin, Germany) followed by 40 mL of saline solution into an antecubital vein *via* an 18-gauge catheter at 5 mL/s. The enhanced CT scans were performed with a delay of 25-30 s for corticomedullary phase, 55-60 s for nephrographic phase, and 240 s for excretory phase.

2.4. Image analysis and data evaluation

All the conventional ultrasound images and CEUS video clips were reviewed independently offline by two experienced radiologists blinded to the final diagnosis and not involved in the scanning. They had respectively 10 and 14 years of experience in conventional liver US and more than 7 years of experience in liver CEUS interpretation. Imaging characteristics included mass position, size, echogenicity and homogeneity, presence of

a hypoechoic rim, and color flow signals on conventional and Color Doppler ultrasound imaging. The wash-in and wash-out pattern, degree of peak enhancement, homogeneity of enhancement, and peripheral rim enhancement were evaluated by CEUS imaging. The degree of enhancement was categorized as hypo-, iso-, and hyperenhancement against that in the adjacent normal renal cortex when contrast agent reached the peak in the mass. The homogeneous enhancement was defined as complete enhancement in a lesion without any defects, and heterogeneous enhancement as a lesion with unenhanced areas, regardless of various enhancement degrees. The normal renal cortex adjacent to the tumor was used as the control for comparison of enhancement. The wash-in and wash-out pattern was classified as fast, simultaneous, or slow. The peripheral rim enhancement was considered to represent the presence of a pseudocapsule, which is determined as positive with a zone of hypoechoic ring enhancement around the lesion on CEUS and negative without.

The other two experienced radiologists in CECT studies of the liver, who were blinded to the final diagnosis, recorded and analyzed changes in the dynamic enhancement images at different phases and made independent diagnoses and conclusions. The imaging parameters included mass position, size, margins, cystic components or necrosis, calcification and attenuation on unenhanced CT scan, degree of enhancement (in Hounsfield units, HU) in different phases of the CECT scan, homogeneous or heterogeneous appearance, perinephric stranding, presence or absence of a clear capsule sign, and vascular invasion.

In case of inconsistent conclusions, a mutually accepted final conclusion was made *via* consultation. Examiners engaged in CEUS and contrast enhanced magnetic resonance imaging (CEMRI) were blind to each other's diagnosis. Diagnostic criteria for RCC: CEUS was characterized by hypoenhancement, heterogeneous enhancement, fast-in or fast-out, and peripheral ring enhancement. CECT was characterized by hypoenhancement, heterogeneous enhancement, fast-in and fast-out, and peripheral ring enhancement. All images were evaluated independently by two physicians who agreed to reach a consensus in case of a disparity.

2.5. Statistical analysis

SPSS19.0 was used, continuous data were represented by frequency, and histopathological findings were used as the standards. χ^2 test was used to compare CEUS and CECT in perfusion characteristics of benign and malignant renal masses, and their sensitivity, specificity, accuracy, positive predictive value and negative predictive value in the diagnosis of RCC. The test level was 0.05, and $P < 0.05$ was considered statistically significant.

3. Results

3.1. Histopathological findings

In 141 patients, 143 renal masses were surgically treated, and histopathology was conducted. Historically, 93 (85.3%) were malignant and 16 (14.7%) benign among the 109 masses examined by CECT alone; 56 (76.7%) malignant (Figure 1) and 17 (23.3%) benign (Figure 2) among the 73 masses examined by CEUS alone; and 31 (79.5%) malignant and 8 (20.5%) benign among 39 masses in 37 patients examined by both modalities (Table 1).

3.2. Comparison between CECT and CEUS in image characteristics of benign and malignant renal masses

Among 39 masses in 37 patients examined by both CEUS and CECT (Table 2), the 31 malignant masses featured mainly fast wash-in, fast wash-out and highly heterogeneous enhancement, and the 8 benign masses featured mainly slow or equal wash-in, slow or equal wash-out and homogeneous enhancement. However, CEUS showed better peripheral rim enhancement in the malignant renal masses than CECT ($P < 0.05$).

3.3. Comparison between CECT and CEUS in the diagnosis of RCC

CECT identified 95 malignant and 14 benign masses. Of the former, 84 were accurate diagnoses and 11 misdiagnoses including 8 angiomyolipomas (AMLs), 2 complex cysts and 1 eosinoma; of the latter, 5 were accurate diagnoses and 9 misdiagnoses, including 5 clear cell carcinomas (Figure 3F-H), 2 papillary carcinomas, 1 cystic renal carcinoma and 1 renal carcinoma of another type. CEUS identified 60 malignant and 13 benign masses. Of the former, 52 were accurate diagnoses and 8 misdiagnoses including 6 AMLs, 1 complex cyst and 1 eosinoma; of the latter, 9 were accurate diagnoses and 4 misdiagnoses including 3 clear cell carcinomas (Figure 3A-E, Figure 4A-E) and 1 collecting duct carcinoma. CEUS and CECT showed no statistically significant differences in sensitivity, specificity, accuracy, positive predictive value and negative predictive value in the diagnosis of renal malignancy ($P > 0.05$) (Table 3).

4. Discussion

Most renal tumors are malignant. Of primary renal malignant tumors, RCC accounts for 85%, renal pelvis carcinoma for 7-8%, nephroblastoma for 5-6%, and sarcoma for 3%. Among them, RCC is the most fatal urogenital malignancy, accounting for 3% of all adult tumors and 90-95% of renal cancers (*10*). The three most common subtypes of RCC are clear cell carcinoma, papillary carcinoma and chromophobe cell

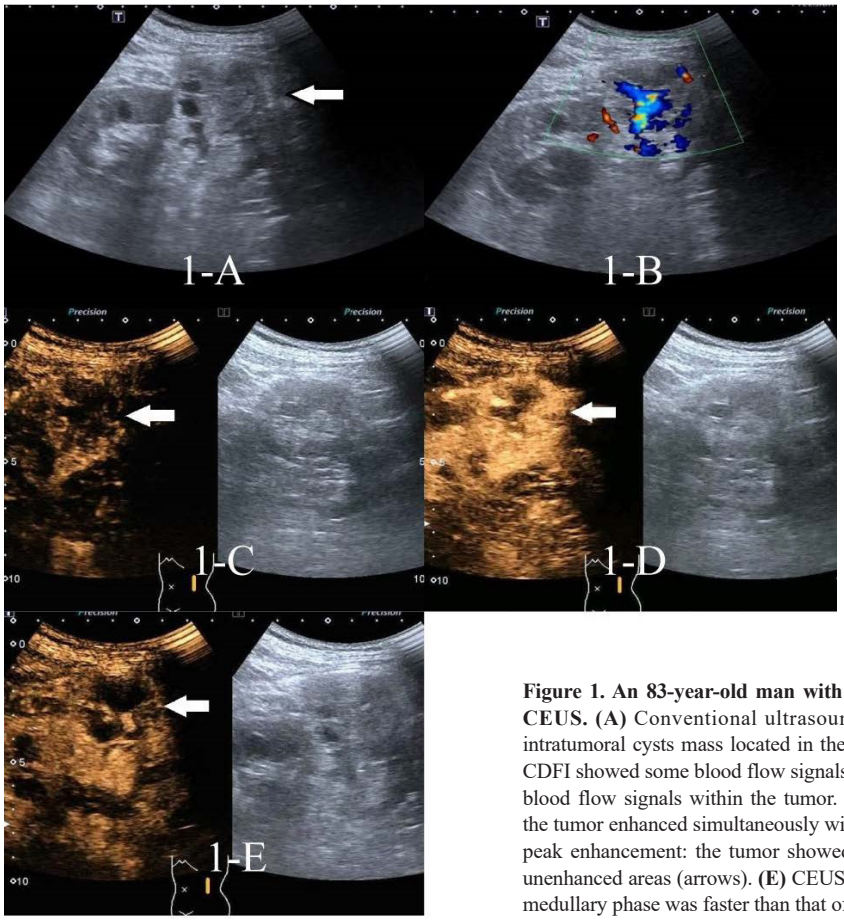

Figure 1. An 83-year-old man with a 2.6 × 1.6-cm ccRCC was diagnosed using CEUS. (A) Conventional ultrasound demonstrated a heterogeneous mass with intratumoral cysts mass located in the interpolar pole of the left kidney (arrows). **(B)** CDFI showed some blood flow signals around the tumor periphery and a few strip-like blood flow signals within the tumor. **(C)** CEUS imaging in the initial enhancement: the tumor enhanced simultaneously with the cortex (arrows). **(D)** CEUS imaging at the peak enhancement: the tumor showed heterogeneous hyperenhancement with many unenhanced areas (arrows). **(E)** CEUS imaging showed that the tumor wash-out in the medullary phase was faster than that of the renal cortex (arrows).

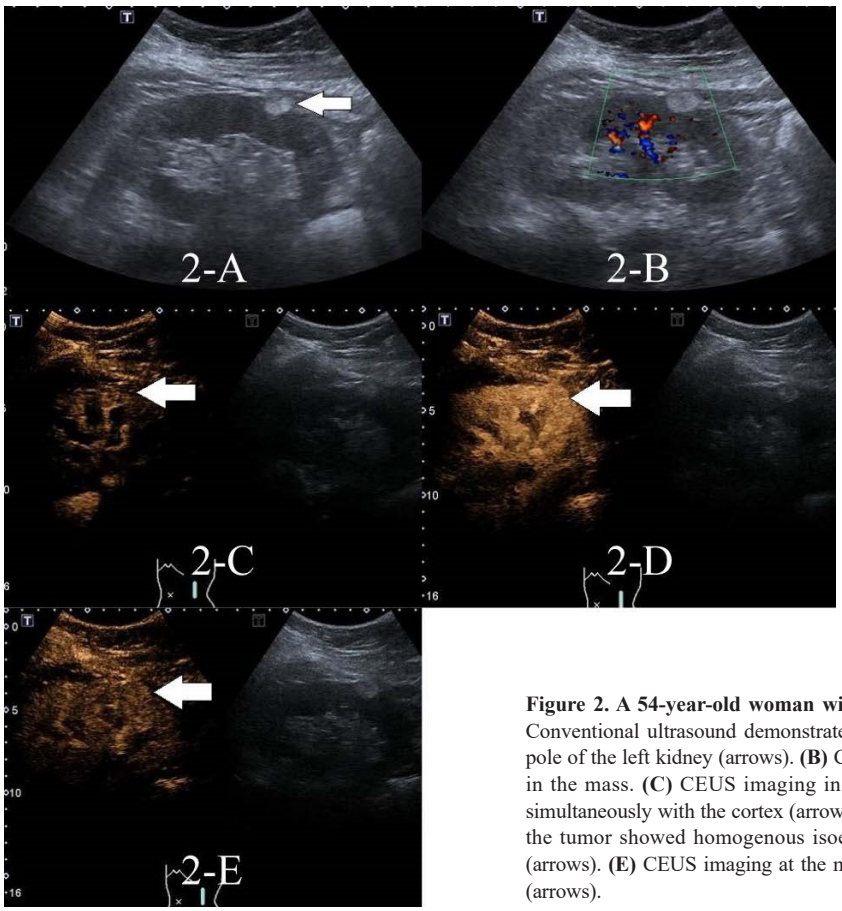

Figure 2. A 54-year-old woman with an AML was diagnosed using CEUS. (A) Conventional ultrasound demonstrated a hyperechoic mass located in the interpolar pole of the left kidney (arrows). **(B)** CDFI showed a lack of intratumoral vessel signal in the mass. **(C)** CEUS imaging in the initial enhancement: the tumor enhanced simultaneously with the cortex (arrows). **(D)** CEUS imaging at the peak enhancement: the tumor showed homogenous isoenhancement similar to the peritumoral cortex (arrows). **(E)** CEUS imaging at the medullary phase showed prolonged enhancement (arrows).

Table 1. Histopathological findings of 143 renal masses

Histopathological type		CECT	CEUS	BOTH
Malignant	ccRCC	66 (60.5)	42 (60.5)	24 (61.5)
(*n* = 31)	pRCC	7 (6.4)	5 (6.8)	3 (7.7)
	chRCC	16 (14.7)	5 (6.8)	4 (10.3)
	Collecting duct carcinoma	2 (1.8)	1 (1.4)	1 (3.6)
	Cystic RCC	1 (0.9)	1 (1.4)	0 (0)
	Other types of RCC	1 (0.9)	2 (2.7)	1 (3.6)
	ALL	93 (85.3)	56 (76.7)	31 (79.5)
Benign	AML	9 (8.3)	12 (16.4)	6 (15.4)
(*n* = 8)	Complicated cysts	6 (5.5)	4 (5.5)	1 (3.6)
	Renal oncocytoma	1 (0.6)	1 (1.4)	1 (3.6)
	ALL	16 (14.7)	17 (12.9)	8 (20.5)
	TOATL	109 (100)	73 (100)	39 (100)

AML, angiomyolipoma; ccRCC, clear cell renal cell carcinoma; pRCC, papillary renal cell carcinoma; chRCC, chromophobe renal cell carcinoma.

Table 2. Comparison between CEUS and CECT in image characteristics of benign and malignant renal masses [*N* (%)]

Histopathological results	Imaging index	Imaging features	CEUS	CECT	χ^2	*P*
Malignant	the degree of peak enhancement	hyper- enhancement	21 (67.7)	18 (58.1)	0.622	0.430
(*n* = 31)		iso-/hypo- enhancement	10 (32.3)	13 (41.9)		
	the homogeneity of enhancement	homogeneous	13 (41.9)	9 (29.0)	1.127	0.288
		inhomogeneous	18 (58.1)	22 (71.0)		
	wash-in	fast	22 (71.0)	26 (83.9)	1.476	0.224
		slow (iso-)	9 (29.0)	5 (16.1)		
	wash-out	fast	19 (61.3)	20 (64.5)	0.069	0.792
		slow (iso-)	12 (38.7)	11 (35.5)		
	Peripheral rim enhancement	Yes	12 (38.7)	5 (16.1)	3.971	0.046
		No	19 (61.3)	26 (83.9)		
Benign	degree of peak enhancement	hyper enhancement	3 (37.5)	4 (50.0)	0.254	0.614
(*n* = 8)		hypo enhancement	5 (62.5)	4 (50.0)		
	Homogeneity of enhancement	homogeneous	3 (37.5)	4 (50.0)	0.254	0.614
	wsh-in	inhomogeneous	5 (62.5)	4 (50.0)		
		fast	1 (87.5)	0 (100.0)	1.067	0.302
		slow (iso-)	7 (12.5)	8 (0)		
	wash-out	fast	1 (12.5)	2 (25.0)	0.410	0.522
		slow (iso-)	7 (87.5)	6 (75.0)		
	Peripheral rim enhancement	Yes	1 (12.5)	0 (25.0)	1.067	0.302
		No	7 (87.5)	8 (100)		

carcinoma, accounting for 70-80%, 10-15% and 5% respectively (*11*). In recent years, the rising incidence of renal malignancies has made early diagnosis and treatment increasingly important. CEUS and CECT are the main modalities for the diagnosis of renal tumors at present. CECT scanning is often used clinically to detect renal lesions, providing important evidence for the qualitative diagnosis of renal tumors. The development degree of space-occupying lesions can be inferred based on enhancement in the lesions, the presence of tumor thrombi in the renal vein and infiltration around the lesions (*12*). CEUS compensates for the low accuracy of traditional gray-scale ultrasound and color Doppler ultrasound through contrast imaging and can clearly reflect hemodynamic changes in the lesions, which is of great help to determine benign and malignant tumors (*13*). In this study, RCC was the main malignancy diagnosed by CECT and CEUS (89/93 or 95.7% *vs.* 52/56 or 92.9%), followed by papillary carcinoma, chromophobe cell carcinoma, collecting duct carcinoma, and cystic renal carcinoma. The proportions were much higher than those in SUN D' possibly because fewer cases were included in our present study. AML is the most common benign tumor of the kidney, containing different proportions of thick-walled blood vessels, smooth muscle and adipose tissue (*14*). In our study, AML was the dominant benign tumor (9/16 or 56.3% *vs.* 12/17 or 70.6%), while complex cysts and eosinophils were fewer.

At present, CEUS has been used for the differential diagnosis of benign and malignant renal lesions, and it is generally believed that CEUS is helpful in the

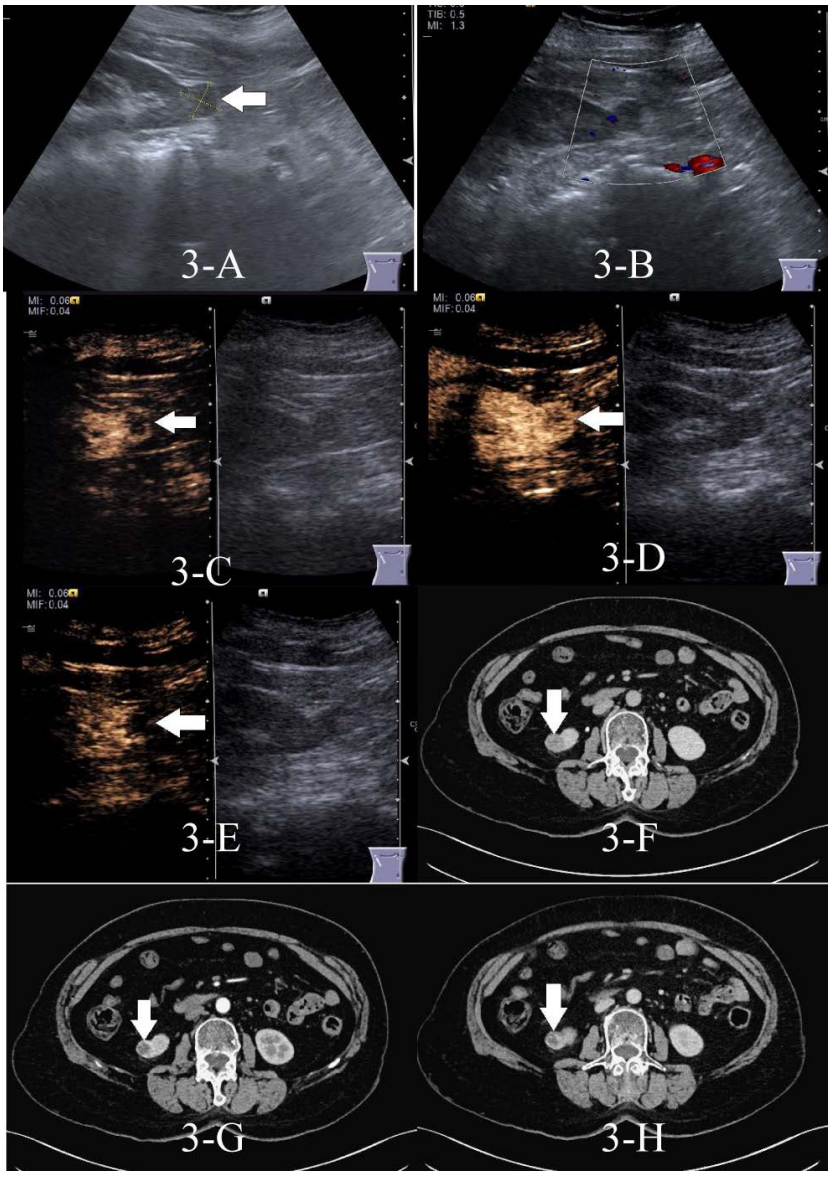

Figure 3. A 75-year-old woman with a 2.2 × 1.9-cm oncocytoma but was misdiagnosed using CEUS and CECT as RCC. (A) Conventional ultrasound demonstrated a mildly hyperechoic mass located in the lower pole of the right kidney (arrows). (B) CDFI showed a few periphery tumoral vessel signals in the mass (arrows). (C) CEUS imaging in the initial enhancement: the tumor enhanced simultaneously with the cortex (arrows). (D) CEUS imaging at the peak enhancement: the tumor showed heterogeneous hyperenhancement (arrows). (E) CEUS imaging at the medullary phase: the central region of tumor showed faster wash-out than the renal cortex (arrows). (F) Unenhanced CT demonstrated a heterogeneous mass (big arrow). (G) Corticomedullary phase: the edge of the lesion was obviously enhanced (big arrow). (H) Nephrographic phase: the tumor showed faster wash out than the renal cortex (big arrow).

diagnosis and differentiation of RCC. In this current study, among 39 masses in 37 patients detected by CEUS and CECT, the 31 malignant masses mainly featured fast wash-in, fast wash-out and heterogeneous enhancement, and the 8 benign masses mainly featured slow or equal wash-in, slow wash-out and homogeneity enhancement. Benign and malignant renal tumors have characteristic manifestations on CEUS, which was consistent with the studies by Bertolotto *et al.*, Kahna *et al.*, and Kazmierski *et al.* (*15-17*). However, some researchers believed that RCCs did not have a typical CEUS pattern and overlapped to some extent with the appearance of other renal masses (*18-21*). Haendl *et al.* (*19*) used SonoVue, a microbubble contrast agent, in 30 patients with solid renal tumors before surgery. They claimed that RCCs showed chaotic vascularization on CEUS without a typical vascularization pattern. However, only 25 RCCs, 2 uROTHelial carcinomas and 3 eosinomas were included in their study, and the results might not be universal. Quaia *et al.* (*20*) performed Levovist-enhanced pulse-inverted harmonic imaging on 26 patients with renal masses, and they reported that CEUS was still limited in differentiating between solid and cystic renal masses. Therefore, further study of a larger sample size and the inclusion of other types of renal lesions are necessary to validate the results of this series.

Heterogeneous perfusion was associated with the presence of hemorrhage, necrosis, and cystic changes in the mass (*22*). In this study, inhomogeneous perfusion in the benign and malignant renal masses was not statistically significant. The reason lies in the rapid growth of malignant tumors and their increasing demand for nutrients. When the needs cannot be met, changes such as necrosis and cystic degeneration will occur inside the tumor (*21,23,24*). Internal echoes in most AMLs were uniform, but some AMLs, especially those larger than 4cm, may also have spontaneous hemorrhage, and CEUS presents inhomogeneous perfusion (*25*).

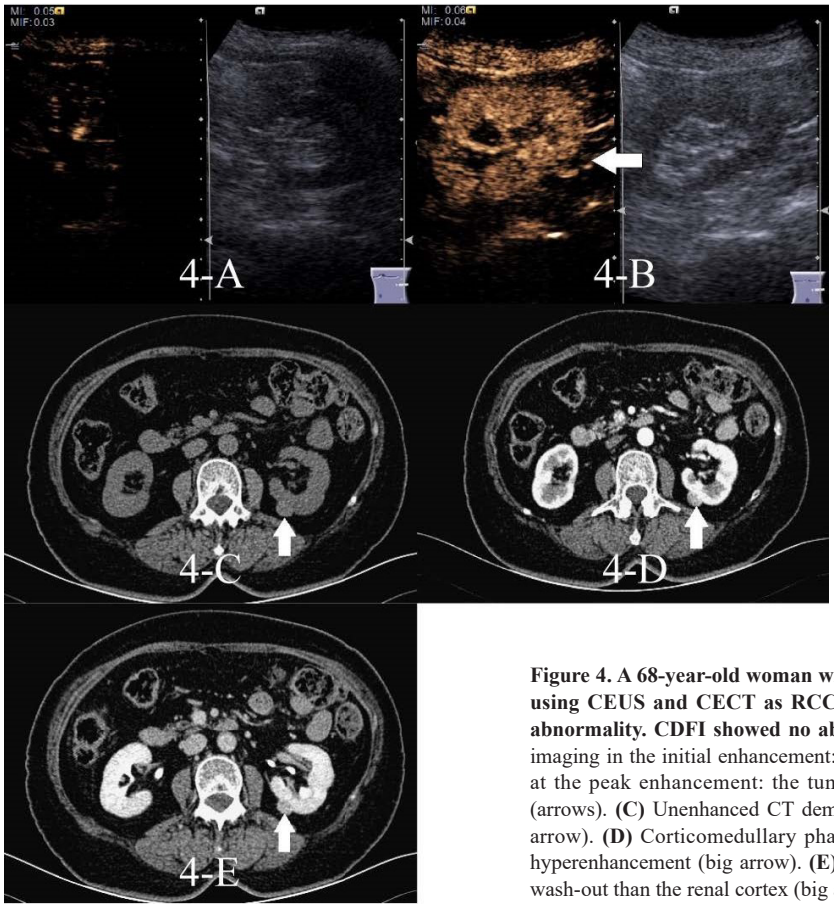

Figure 4. A 68-year-old woman with a 1.7 × 1.3-cm AML but was misdiagnosed using CEUS and CECT as RCC. Conventional ultrasound demonstrated no abnormality. CDFI showed no abnormal vessel signals in the mass. (A) CEUS imaging in the initial enhancement: the cortex enhanced in 19s. **(B)** CEUS imaging at the peak enhancement: the tumor showed heterogeneous hyperenhancement (arrows). **(C)** Unenhanced CT demonstrated a homogenous low density mass (big arrow). **(D)** Corticomedullary phase: the mass showed obviously heterogeneous hyperenhancement (big arrow). **(E)** Nephrographic phase: the tumor showed faster wash-out than the renal cortex (big arrow).

Table 3. Comparison of the accuracy between CEUS and CECT in the diagnosis of RCC

Methods	Sensitivity	specificity	accuracy	PPV	NPV
CECT	84/93(90.3%)	5/16(31.2%)	89/109(81.6%)	84/95(88.4%)	5/14(35.7%)
CEUS	52/56(92.8%)	9/17(52.9%)	61/73(83.5%)	52/60(86.7%)	9/13(69.2%)
χ^2	0.282	1.588	0.110	0.105	3.033
P	0.595	0.208	0.740	0.746	0.128

Peripheral rim enhancement, referring to the annular enhanced area around the tumor, is pathologically based on the high degree of malignancy and rapid growth of RCC masses, which compresses the adjacent normal renal tissue and leads to ischemia, necrosis and fibrosis, and the formation of a false envelope (*26,27*). Circumferential perfusion can better indicate renal malignancy. It may also be a standard for kidney preservation surgery (*28*). In our study, CEUS could display annular perfusion better than CECT ($P < 0.05$). Tamai *et al.* (*29*) used a high-MI CEUS technique and Levovist (SHU 508A; Schering AG, Berlin, Germany) and found tumor blood flow in all 29 patients with renal lesions, while contrast CT failed to show it in 5 patients, and among clear cell carcinomas, hypervascularity on CEUS was observed in 17 of 18 patients. Consistent with our study, CEUS was believed to be able to detect blood flow with contrast microbubbles, the true blood pool agent and could show more characteristic features of RCCs than CECT.

In this study, pathological findings were used as the gold standard to determine the sensitivity (92.8% *vs.* 90.3%), specificity (52.9% *vs.* 31.2%), accuracy (83.5% *vs.* 81.6%), positive predictive value (86.7% *vs.* 88.4%), and negative predictive value (69.2% *vs.* 35.7%) of CEUS and CECT in the diagnosis of RCC, with no statistical difference between the five groups. Therefore, CEUS is expected to be an independent imaging modality for the diagnosis of RCC. However, when RCC is associated with hemorrhage, liquefaction and necrosis, it loses its typical characteristics and, on CEUS, often shows atypical enhancement patterns.

In this study, most RCCs showed fast wash-in and fast wash-out and hyperenhancement, and almost all of the cases were diagnosed as clear cell carcinoma with a high diagnostic accuracy. The misdiagnoses were basically those with hypoenhancement, that is, those with fewer blood vessels. In the CEUS group, 6

AMLs were misdiagnosed as RCCs, and 3 RCCs as AML. In the CECT group, 8 AMLs were misdiagnosed as RCC, and 4 RCCs as AML. It is worth noting that AMLs were misdiagnosed as RCC when both CEUS and CECT were used. It is of great significance to distinguish AMLs from RCCs. AMLs, composed of malformed blood vessels, spindle smooth muscle and fat cells, can be simply divided into "typical AMLs" and "atypical AMLs" (*30*). As most AMLs, referred to as "typical AML," contain a large amount of adipose tissue, they can be detected by CT or MRI (*31*). However, studies have also shown that about 5% of AMLs are fat-free and are often misdiagnosed as RCC (*32*). In this study, 2 AMLs with fast wash-in, fast wash-out and hyperenhancement on CEUS and CECT were misdiagnosed as RCC, and it was speculated that the AMLs were rich in blood vessels. Lee-Felker SA *et al.* suggested that accurate measurements of CT values on plain and enhanced scans of the cortex-medulla, parenchyma, and excretory phases may help to distinguish clear cell renal cell carcinoma (ccRCC), papillary renal cell carcinoma (pRCC), chromophobe renal cell carcinoma (chRCC), renal oncocytoma, and minimal fat AMLs (*33*). However, due to the small sample size of their study and the fact that the speed of renal contrast media wash-in and wash-out of the kidneys may be influenced by the patient's own factors, more research is needed to determine whether quantitative analysis CT can be used to differentiate AML from RCC. Xu ZF *et al.* believed that AMLs have no false envelop in pathology, and the false envelop can be used to accurately identify RCC and AML (*21*), but some RCCs have no false envelop, which makes it difficult to accurately identify RCC and AML on CEUS and CECT.

Totally 3 complicated cysts were misdiagnosed as RCC, 1 being in the CEUS group and 2 in the CECT group. Complicated cysts, according to their progression possibility, fall into levelI, II, III, and IV, with a progression probability of 0%, 15%, 50% and 95%, respectively. RCC is the most common sequel of progression, this could be the reason that complicated cysts and RCCs are difficult to distinguish on both CEUS and CECT, especially with high-level (IIIand above) complicated cysts. Multilocular cystic renal cell carcinoma (MCRCC), a special type of RCCs, is almost entirely cystic with varying lumen sizes and fluid filling. Nodules of soft tissues can be seen in the cyst wall and uneven thickening of the septum. A few cystic walls or septal calcifications are seen. The boundary is generally clear, being separated with fibrous capsule from surrounding normal renal tissues, and irregular enhancement of cyst wall and septum can be observed. Complicated cysts, especially those of level IIIand above, have similar presentations to multilocular RCC and are difficult to distinguish on CEUS and CECT. This may account for the misdiagnoses in this study.

Three limitations are mentionable. First, only the masses histopathologically confirmed after surgical resection were enrolled in this study, which might have resulted in selection bias. Many benign lesions at follow-up without histopathologic diagnosis were excluded; thus, the sample of AMLs was relatively smaller than that of RCCs. Second, this study included few cases examined by both CEUS and CECT, and a larger sample size is needed for further investigation. Finally, our study was retrospective in nature.

In conclusion, CEUS and CECT play an equally important role in the diagnosis of RCCs. CEUS may serve as a substitute for CECT when the latter is impossible in iodipin-allergic patients or in patients with renal inadequacy. A small number of atypical RCCs require employment of the two imaging modalities as justified by the patient's medical history, clinical manifestations and findings in laboratory tests. Such comprehensive judgment by the radiologist, sonographer, and clinician improves the diagnosis of RCC.

Funding: This work was supported by the 2016 program of the Shanghai Municipal Health and Family Planning Commission (grant no.201640285 to Lin Chen).

Conflict of Interest: The authors have no conflicts of interest to disclose.

References

1. Motzer RJ, Jonasch E, Agarwal N, *et al.* Kidney cancer, version 3.2015. J Natl Compr Canc Netw. 2015; 13:151-159.
2. Wasserman M, Sobel D, Pareek G. Choice of Surgical Options in Kidney Cancer and Surgical Complications. Semin Nephrol. 2020; 40:42-48.
3. Leveridge MJ, Bostrom PJ, Koulouris G, Finelli A, Lawrentschuk N. Imaging renal cell carcinoma with ultrasonography, CT and MRI. Nat Rev Urol. 2010; 7:311-325.
4. Marschner CA, Ruebenthaler J, Schwarze V, Negrão de Figueiredo G, Zhang L, Clevert DA. Comparison of computed tomography (CT), magnetic resonance imaging (MRI) and contrast-enhanced ultrasound (CEUS) in the evaluation of unclear renal lesions. Rofo. 2020; 192:1053-1059.
5. Chen L, Wang L, Diao X, Qian W, Fang L, Pang Y, Zhan J, Chen Y. The diagnostic value of contrast-enhanced ultrasound in differentiating small renal carcinoma and angiomyolipoma. Biosci Trends. 2015 9:252-258.
6. Sparchez Z, Radu P, Sparchez M, Crisan N, Kacso G, Petrut B. Contrast enhanced ultrasound of renal masses. A reappraisal of EFSUMB recommendations and possible emerging applications. Med Ultrason. 2015; 17:219-226.
7. Lu Q, Wang WP, Huang BJ, Li CL, Li C. Minimal fat renal angiomyolipoma: the initial study with contrast-enhanced ultrasonography. Ultrasound Med Biol. 2012; 38:1896-1901.
8. Wilson SR, Burns PN, Kono Y. Contrast-Enhanced Ultrasound of Focal Liver Masses: A Success Story. Ultrasound Med Biol. 2020; 46:1059-1070.

9. Yang DP, Zhuang BW, Wang W, Xie XY, Xie XH. Differential diagnosis of liver metastases of gastrointestinal stromal tumors from colorectal cancer based on combined tumor biomarker with features of conventional ultrasound and contrast-enhanced ultrasound. Abdom Radiol (NY). 2020; 45:2717-2725.
10. Vázquez Estévez S, Anido U, Lázaro M, Fernández O, Fernández Núñez N, de Dios Álvarez N, Varela V, Campos Balea B, Agraso S, Areses MC, Iglesias L, Blanco M, Maciá S, Anton Aparicio LM. A new scenario in metastatic renal cell carcinoma: a SOG-GU consensus. Clin Transl Oncol. 2020; 22:1565-1579.
11. Sun D, Wei C, Li Y, Lu QJ, Zhang W, Hu B. Contrast-enhanced Ultrasonography with Quantitative Analysis allowing Differentiation of Renal Tumor Tumor types. Sci Rep. 2016; 6:35081.
12. Jin L, Xie F. Untargeted Contrast-Enhanced Ultrasound Versus Contrast-Enhanced Computed Tomography: A Differential Diagnostic Performance (DDP) Study for Kidney Lesions. Clinics (Sao Paulo). 2020; 75:e1489.
13. Wei SP, Xu CL, Zhang Q, Zhang QR, Zhao YE, Huang PF, Xie YD, Zhou CS, Tian FL, Yang B. Contrast-enhanced ultrasound for differentiating benign from malignant solid small renal masses: comparison with contrast-enhanced CT. Abdom Radiol (NY). 2017; 42:2135-2145.
14. Boudaouara O, Kallel R, Dhieb D, Smaoui W, Ayed HB, Keskes L, Sellami Boudawara T. Renal angiomyolipoma: Clinico-pathologic study of 17 cases with emphasis on the epithelioid histology and p53 gene abnormalities. Ann Diagn Pathol. 2020; 47:151538.
15. Bertolotto M, Bucci S, Valentino M, Currò F, Sachs C, Cova MA. Contrast-enhanced Ultrasound for characterizing renal masses. Eur J Radiol. 2018; 105:41-48.
16. Kahna AE, Ostrowski, AK, Caserta MP, Galler, IJ, Thiel, DD. Contrast enhanced ultrasound characterization of surgically resected renal masses in patients on dialysis. Scand J Urol. 2019; 53:344-349.
17. Kazmierski B, Deurdlian C, Tchelepi H, Grant EG. Applications of contrast-enhanced ultrasound in the kidney. Abdom Radiol (NY). 2018; 43:880-898.
18. Cokkinos DD, Antypa EG, Skilakaki M, Kriketou D, Tavernaraki E, Piperopoulos PN. Contrast Enhanced Ultrasound of the Kidneys: What is it capable of? Biomed Res Int. 2013; 2013:595873.
19. Haendl T, Strobel D, Legal W, Frieser M, Hahn EG, Bernatik T. Renal cell cancer does not show a typical perfusion pattern in contrast-enhanced ultrasound. Ultraschall Med. 2009; 30:58-63.
20. Quaia E, Siracusano S, Bertolotto M, Monduzzi M, Mucelli PR. Characterization of renal tumours with pulse inversion harmonic imaging by intermittent high mechanical index technique: initial results. Eur Radiol. 2003; 13:1402-1412.
21. Xu ZF, Xu HX, Xie XY, Liu GJ, Zheng YL, Liang JY, Lu MD. Renal cell carcinoma: real-time contrast-enhanced ultrasound findings. Abdom Imaging. 2010c; 35:750-756.
22. Li CX, Lu Q, Huang BJ, Xue LY, Yan LX, Zheng FY, Wen JX, Wang WP. Quantitative evaluation of contrast-enhanced ultrasound for differentiation of renal cell carcinoma subtypes and angiomyolipoma. Eur J Radiol. 2016; 85:795-802.
23. Jiang J, Chen YQ, Zhou YC, Zhang HZ. Clear cell renal cell carcinoma: contrast-enhanced ultrasound features relation to tumor size. Eur J Radiol. 2010; 73:162-167.
24. Xue LY, Lu Q, Huang BJ, Li CX, Yan LX, Wang WP. Differentiation of subtypes of renal cell carcinoma with contrast-enhanced ultrasonography. Clin Hemorheol Microcirc. 2016; 63:361-371.
25. King KG, Gulati M, Malhi H, Hwang D, Gill IS, Cheng PM, Grant EG, Duddalwar VA. Quantitative assessment of solid renal masses by contrast-enhanced ultrasound with time-intensity curves: how we do it. Abdom Imaging. 2015; 40:2461-2471.
26. Yamashita Y, Honda S, Nishiharu T, Urata J, Takahashi M. Detection of pseudocapsule of renal cell carcinoma with MR imaging and CT. AJR Am J Roentgenol. 1996; 166:1151-1155.
27. Dai WB, Yu B, Diao XH, Cao H, Chen L, Chen Y, Zhan J. Renal Masses: Evaluation with Contrast-Enhanced Ultrasound, with a Special Focus on the Pseudocapsule Sign. Ultrasound Med Biol. 2019; 45:1924-1932.
28. Pretorius ES, Siegelman ES, Ramchandani P, Cangiano T, Banner MP. Renal neoplasms amenable to partial nephrectomy: MR imaging. Radiology.1999; 212:28-34.
29. Tamai H, Takiguchi Y, Oka M, *et al.* Contrast-enhanced ultrasonography in the diagnosis of solid renal tumors. J Ultrasound Med. 2005; 24:1635-1640.
30. Srigley JR, Delahunt B, Eble JN, Egevad L, Epstein JI, Grignon D, Hes O, Moch H, Montironi R, Tickoo SK, Zhou M, Argani P; ISUP Renal Tumor Panel. The International Society of Urological Pathology (ISUP) Vancouver Classification of Renal Neoplasia. Am J Surg Pathol. 2013; 37:1469-1489.
31. Lane BR, Aydin H, Danforth TL, Zhou M, Remer EM, Novick AC, Campbell SC. Clinical correlates of renal angiomyolipoma subtypes in 209 patients: classic, fat poor, tuberous sclerosis associated and epithelioid. J Urol. 2008; 180:836-843
32. Nicolau C, Pano B, Sebastia C. Managing focal incidental renal lesions. Radiologia. 2016; 58:81-87
33. Lee-Felker SA, Felker ER, Tan N, Margolis DJ, Young JR, Sayre J, Raman SS. Qualitative and quantitative MDCT features for differentiating clear cell renal cell carcinoma from other solid renal cortical masse. AJR Am J Roentgenol. 2014; 203:W516-24.

Received January 15, 2021; Revised February 18, 2021; Accepted February 24, 2021.

[§]These authors contributed equally to this work.
**Address correspondence to:*
Lin Chen, Department of Ultrasound, Huadong Hospital, Fudan University, 211 West Yan'an Rd, Shanghai 200040, China.
E-mail: cl_point@126.com

Ling Wang, Laboratory for Reproductive Immunology, Hospital & Institute of Obstetrics and Gynecology, Fudan University, 419 Fangxie Road, Shanghai 200011, China.
E-mail: Dr.wangling@fudan.edu.cn

Released online in J-STAGE as advance publication February 26, 2021.

Original Article

DOI: 10.5582/bst.2020.03437

Impact of patient age on outcome after resection for hepatocellular carcinoma

Masaharu Harada, Osamu Aramaki*, Yutaka Midorikawa, Tokio Higaki, Hisashi Nakayama, Masamichi Moriguchi, Tadatoshi Takayama

Department of Digestive Surgery, Nihon University School of Medicine, Tokyo, Japan.

SUMMARY There is little information on the impact of aging on liver resection of hepatocellular carcinoma (HCC). The aim of study was to evaluate the prognostic impact of the patient's age on the long-term survival after resection of HCC. The postoperative outcomes of the 291 elderly (≥ 70 years) and 340 younger (< 70 years) patients underwent curative liver resection for HCC were analyzed using multivariate and propensity-score matching. Risk score were calculated from the results of Cox regression analysis. The overall survival rate was significantly lower in the elderly group than that in the younger group (p = 0.01). Factors related to overall survival were vascular invasion (absent vs. present, HR 2.25; 95% CI 1.52-3.33, p = 0.0001), albumin level (< 3.0 *vs*. ≥ 3.0 g/dl, HR 2.23; 95% CI 1.31-3.79, p = 0.003), and number of tumors (solitary *vs*. multiple, HR 1.68; 95% CI 1.24-2.27, p = 0.001). The results of risk-score analysis with a Cox proportional-hazards model indicated that the proportion of poor-risk patients was significantly higher in the elderly than in the younger group. Propensity-score matching analysis yielded 234 pairs of patients. There were no significant differences in baseline profiles or risk scores between the two groups (p = 0.43). There were also no significant differences in the overall survival between the two groups (p = 0.23). Advanced age does not have a significant impact on the outcomes of patients after resection of HCC.

Keywords elderly, hepatocellular carcinoma, liver resection, propensity score matching analysis, risk scores

1. Introduction

The average age of patients with hepatocellular carcinoma (HCC) is advancing, and the mean ages at diagnosis of HCC are estimated to be 65-69 years in Japan and 63-65 years in Europe and North America (*1-3*). Age at diagnosis of HCC depends primarily on etiological factors, *i.e*., hepatitis B (HBV) and C (HCV) virus infections and alcohol abuse, which have different peak ages of exposure (*4,5*). Although there have been many reports of liver resection in elderly patients with HCC, there have been few large studies of long-term outcomes in such cases (*6-15*). Moreover, previous studies indicated a wide range of long-term outcomes among elderly patients with HCC following liver resection, and it was suggested that the discrepancy in survival may be attributable to differences in patient backgrounds, including etiologic factors, between groups (*6,10,14*). However, nearly all previous studies compared patients solely on the basis of whether they were elderly or not, and only a few studies have attempted to adjust for bias associated with other demographic and clinical characteristics (*5,7,8*). One of these studies had a small sample size of less than 50 elderly patients after liver resection, and so the statistical power was low (*5*). One of the remaining two studies defined elderly as age more than 75 years and had a sample size of less than 150 elderly patients after liver resection (*7*). The other of these studies defined elderly as age more than 55 years, which was the median age of patients in their cohort; however, this cutoff value is too young (*8*). These two studies investigated patients undergoing liver resection for HCC mainly caused by HBV (*7,8*).

It has been difficult to identify the specific role of advanced age in the outcome of patients with HCC undergoing liver resection. Even sophisticated multivariate analyses were probably inadequate to clarify whether advanced age itself is a risk factor. Instead of performing a randomized controlled trial, a one-to-one match created by propensity score analysis has been used to overcome bias between two groups (*16,17*).

The aim of this study was to investigate the impact of advanced age (≥ 70 years) on long-term survival in patients undergoing liver resection for HCC caused

mainly by HCV. Propensity score matching was performed to compare groups of patients who had similar preoperative and operative profiles.

2. Patients and Methods

2.1. Patients

The study population consisted of 631 consecutive patients who had undergone initial curative liver resection for HCC between 2001 and 2012. Clinicopathological data and outcomes after liver resection were prospectively followed up and compared. The patients were divided into two groups according to age at initial diagnosis: 340 patients were < 70 years old (younger group) and 291 patients were ≥ 70 years old (elderly group). We defined elderly as ≥ 70 years for the following reasons: the majority of previous studies have defined elderly as 70 years or older (*5-14*), age ≥ 70 years is related to systemic complications after liver resection (*11*), and 70 years old is the lower limit of senescence associated with age-related changes occurring after this age (*18*).

The study design conformed to the ethical guidelines of the Declaration of Helsinki. This retrospective study was approved by the institutional review board of the Nihon University School of Medicine (approval number: RK-200908-7).

2.2. Liver resection

The indications for liver resection and the surgical procedures were determined according to a decision tree based on the indocyanine green retention rate at 15 minutes (ICG-R_{15}), the presence or absence of uncontrolled ascites, and the presence or absence of jaundice (*19*). Other types of organ failure, including ischemic heart disease, were examined, and the decision to operate or not was made after consultation with the attending physician and an anesthesiologist. Age was not an exclusion criterion for liver resection. Performance status was used as a criterion for patient selection. In principle, patients with a performance status of 0-2 were considered candidates for surgery (*20*).

Anatomical resection of a subsegment, Couinaud's segment, sector, or hemiliver was the preferred surgical procedure (*21*). All liver resections were performed using the clamp crushing method (*22*). The total inflow occlusion technique (Pringle's maneuver) was applied in an intermittent manner, with 15 minutes of occlusion alternating with 5 minutes of reperfusion. Postoperative complications were defined and classified according to the modified Clavien-Dindo classification (*23*).

2.3. Postoperative management

After discharge, all patients were examined for recurrence by dynamic computed tomography every 3 to 4 months. Recurrence was defined as the appearance of a new lesion with radiological features typical of HCC (*21*). The disease-free survival period was defined as the interval between surgery for HCC and the date of diagnosis of the first recurrence or the last follow-up visit. When recurrence was diagnosed, the candidates for treatments were selected according to the same criteria used to select primary treatment (*21*).

2.4. Statistical Analysis

The statistical significance of differences between the two groups was assessed using the Mann-Whitney *U* test and the chi-square test for continuous and categorical data, respectively. Standardized differences were also estimated for all variables considered (*24*). The survival curves of the two groups were compared by the log-rank test. Factors that were significantly related to overall survival on univariate analysis were included in multivariate analysis, performed using a Cox proportional-hazards model. The assumption of proportional hazards was checked by examination of plots of log cumulative hazard for parallelism, and in no case was this assumption materially violated.

To overcome bias due to the different distributions of covariates between the two groups, we performed propensity analysis using logistic regression to create propensity scores for younger and older patients (*16,17*). To identify the propensity of being elderly, multiple logistic regression analysis was performed using forward stepwise variable selection. The model was then used to provide a one-to-one match between two groups using the nearest-neighbor matching method. Model calibration was assessed using the Hosmer-Lemeshow statistic. We used the standardized difference to measure covariate balance, whereby an absolute standardized difference above 10% on a covariate indicates a meaningful imbalance (*24*). After matching, the statistical significance of differences between the two groups was assessed using the Wilcoxon signed-rank test and McNemar's test to analyze continuous and categorical data, respectively.

To develop the risk score for poor prognosis and to determine the cutoff value of the risk score, we used the following equation with β regression coefficients that were estimated with the Cox proportional-hazards model: risk score = $X1\beta1 + X2\beta2 + \ldots + Xk\beta k$ (*25*). Next, to determine the cutoff value for poor prognosis, the risk score was distributed according to whether the patient died within 1, 3, or 5 years after the operation (*26*). The most suitable cutoff value was derived from the area under the receiver operating characteristic (ROC) curve (AUC) of the score, based on the highest Youden index, to achieve the highest sensitivity and specificity (*27*).

All analyses were performed using IBM SPSS Statistics 19 software (IBM SPSS, Tokyo, Japan). In

all analyses, $p < 0.05$ was taken to indicate statistical significance.

3. Results

3.1. Preoperative Characteristics

The elderly group had a lower rate of seropositivity for HBs antigen (4.1%) and of habitual alcohol consumption (24.4%) and a higher rate of seropositivity for HCV antibody (65.9%) than did the younger group (22.6%, 33.8%, and 52.1%; $p = 0.01$, 0.01, and 0.01, respectively). The elderly group had a lower hemoglobin concentration [median, 12.8; range (8.1-16.6) g/dL], a lower serum albumin level [3.8; range (2.3-4.9) g/dL], and a higher ICG-R_{15} [13.2; range (3.0-48.5)%] than did the younger group [13.5; range (8.3-17.3) g/dL, 3.9; range (2.4-5.3) g/dL, and 11.4; range (1.3-82.3)%; $p = 0.0001$, 0.001, and 0.001, respectively]. The elderly group had worse renal function as estimated by creatinine clearance (CCr) [79.9; range (29.7-180.1) %] than did the younger group [96.5; range (5.9-281.5) %, $p = 0.0001$]. Although the elderly group had lower blood loss [270; range (5-2725) mL] than did the younger group [322; range (5-3777) mL, $p = 0.03$], there were no significant differences in other perioperative variables between the two groups (Table 1A). Regarding the site of recurrence and cause

Table 1A. Clinical and operative variables

Items	All patients, *n* = 631	younger, *n* = 340	elderly, *n* = 291	*p*-value
Clinical variable				
Age	69 (36-85)	63 (36-69)	74 (70-85)	0.00001
Gender	Male	276 (81.2%)	206 (70.8%)	0.01
Hepatitis type				
HBV, positive	Present	77 (22.6%)	12 (4.1%)	0.01
HCV, positive	Present	177 (52.1%)	191 (65.9%)	0.01
Alcohol	Present	115 (33.8%)	71 (24.4%)	0.01
Child-Pugh classification	A	327 (96.2%)	282 (96.9%)	0.62
	B+C	13 (3.8%)	9 (3.1%)	
Hemoglobin (g/dL)[d]	13.1 (8.1-17.3)	13.5 (8.3-17.3)	12.8 (8.1-16.6)	0.00001
Platelets ($10^4/\mu L$)[d]	14.2 (2.6-68.6)	14.3 (2.6-68.6)	14.0 (3.2-44.3)	1.00
Total protein (g/dL)[d]	7.1 (5.0-8.9)	7.2 (5.6-8.9)	7.0 (5.0-8.8)	0.04
Albumin (g/dL)[d]	3.8 (2.3-5.3)	3.9 (2.4-5.3)	3.8 (2.3-4.9)	0.0001
Total bilirubin (mg/dL)[d]	0.6 (0.2-3.4)	0.6 (0.2-2.0)	0.6 (0.3-3.4)	0.78
AST (IU/L)[d]	41 (12-295)	41 (12-295)	41 (13-265)	0.81
ALT (IU/L)[d]	37 (5-296)	40 (5-253)	35 (7-296)	0.07
Prothrombin time (%)[d]	98 (53-100)	97 (62-100)	99 (53-100)	0.36
ICG-R_{15}[a,d]	12.3 (1.3-82.3)	11.4 (1.3-82.3)	13.2 (3.0-48.5)	0.001
α-fetoprotein (ng/mL)[d]	12.3 (0.6-91725)	19.1 (0.8-91725)	14.1 (0.6-24275)	0.16
Ccr[b,d]	88.9 (5.9-281.5)	96.5 (5.9-281.5)	79.9 (29.7-180.1)	0.00001
Operative variable				
Tumor size	32 (7-205)	31 (7-205)	32 (9-180)	0.38
Number of tumors	Solitary	281 (82.6%)	231 (79.4%)	0.30
Vascular invasion	Present	36 (10.6%)	43 (14.8%)	0.11
Anatomical resection	Present	125 (36.8%)	100 (34.4%)	0.53
Major hepatic resection	Present	19 (5.6%)	17 (5.8%)	0.89
UICC stage[c]	1, 2	306 (90.0%)	267 (91.8%)	0.45
	3	34 (10.0%)	24 (8.2%)	
Blood loss[d]	301 (5-3777)	322 (5-3777)	270 (5-2725)	0.03
Clamp time[d]	75 (0-860)	76 (11-860)	72 (0-222)	0.07
Operative time[d]	330 (120-1590)	339 (130-1590)	318 (120-803)	0.06
Differentiation	Mod, well	305 (89.7%)	258 (88.7%)	0.03
	Poor	35 (10.3%)	33 (11.3%)	
Complications	0-II	260 (76.5%)	226 (77.7%)	0.72
	III-V	80 (23.5%)	65 (22.3%)	

[a]ICG15: indocyanine green retention rate at 15 minutes; bCCr: Creatinine clearance; [c]International Union Against Cancer (UICC) TNM staging classification; [d]Median (range)

Table 1B. Site of recurrence and cause of death

Variable	All patients	younger	elderly	*p*-value
Site of recurrence	*n* = 370	*n* = 199	*n* = 171	0.67
Intrahepatic	331 (89.5%)	180 (90.50%)	151 (88.3%)	
Extrahepatic	27 (7.3%)	14 (7.0%)	13 (7.6%)	
Intra- and Extrahepatic	12 (3.2%)	5 (2.50%)	7 (4.1%)	
Cause of death	*n* = 223	*n* = 113	*n* = 110	0.83
Hepatocellular carcinoma	183 (82.1%)	91 (80.50%)	92 (83.6%)	
Liver failure	10 (4.5%)	6 (5.30%)	4 (3.6%)	
Other carcinoma	8 (3.6%)	5 (4.40%)	3 (2.7%)	
Other	22 (9.9%)	11 (9.70%)	11 (10.0%)	

Table 2. Univariate analysis of clinical variables

Variables	No.	Overall survival rate (%) 1 yr	3 yr	5 yr	*p*-value
Age					0.01
< 70	340	92.8	76.0	61.8	
≥ 70	291	89.1	72.9	52.9	
Platelet count (104/μL)					0.03
< 15	353	91.4	74.7	54.6	
≥ 15	278	90.8	74.4	62.2	
Albumin (g/dL)					0.004
< 3.0	30	72.7	53.4	40.7	
≥ 3.0	601	92.1	75.6	58.7	
Total bilirubin (g/dL)					0.31
< 1.0	549	91.5	74.7	59.2	
≥ 1.0	82	88.8	74.2	48.9	
AST (IU/L)					0.0001
< 35	250	94.3	82.0	67.0	
≥ 35	381	89.0	69.8	52.0	
α-fetoprotein (ng/mL)					0.001
< 20	336	95.7	79.6	63.9	
≥ 20	295	85.9	68.9	51.1	
ICG-R_{15}[a]					0.04
< 15	391	92.7	76.1	61.0	
≥ 15	240	88.5	72.1	51.8	
CCr[b] (%)					0.04
< 70	144	88.0	68.1	49.6	
≥ 70	487	92.0	76.4	60.2	
Tumor size					0.01
< 5cm	490	93.3	77.5	60.4	
≥ 5cm	141	83.5	64.2	49.3	
Number of tumors					0.001
Solitary	512	92.4	77.1	62.2	
Multiple	119	85.6	64.4	41.3	
Vascular invasion					0.001
Absent	552	93.0	76.4	59.6	
Present	79	78.2	61.2	43.4	

[a]ICG15: indocyanine green retention rate at 15 minutes; [b]CCr; Creatinine clearance.

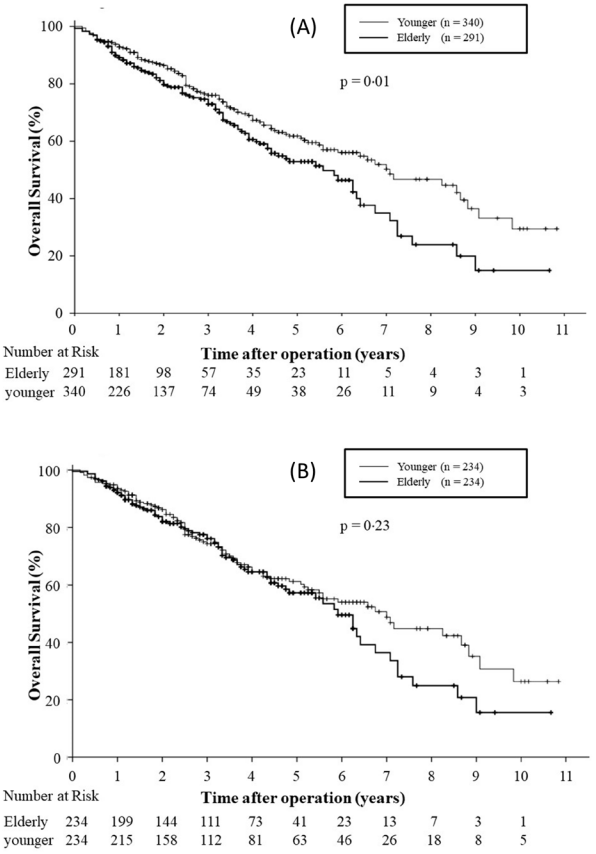

Figure 1. (A) Cumulative overall survival in patients with hepatocellular carcinoma stratified by age. The younger group had a higher overall survival rate than the elderly group ($p = 0.01$). (B) Cumulative overall survival in patients with hepatocellular carcinoma by propensity score matching analysis. There were no significant differences between the two groups ($p = 0.23$).

of death after liver resection, there were no significant differences between the two groups ($p = 0.67$ and 0.83, respectively; Table 1B).

3.2. Survival Outcomes

There was no significant difference in recurrence-free survival between the two groups ($p = 0.24$; supplementary Figure S1A). Overall survival rates in the elderly group at 1, 3, and 5 years were 89.1% [95% confidence interval (CI), 84.9 to 92.2], 72.9% [95% CI, 66.8 to 78.3], and 52.9% [95% CI, 45.1 to 60.5], respectively, whereas those in the younger group were 92.8% [95% CI, 89.5 to 95.2], 76.0% [95% CI, 70.6 to 80.7], and 61.8% [95% CI, 55.1 to 68.0], respectively (Table 2). The overall survival was significantly shorter in the elderly group than in the younger group ($p = 0.01$; Figure 1A).

3.3. Multivariate Analysis

Multivariate analysis with a Cox proportional-hazards model showed that macroscopic vascular invasion (present *vs*. absent, hazard ratio (HR) 2.25; 95% CI 1.52-3.33, $p = 0.0001$), albumin level (< 3.0 *vs*. ≥ 3.0 g/dL, HR 2.23; 95% CI 1.31-3.79, $p = 0.003$), number of tumors (multiple *vs*. solitary, HR 1.68; 95% CI 1.24-2.27, $p = 0.001$), and platelet count (< 15 *vs*. ≥ 15 × 10^4/μL, HR 1.46; 95% CI 1.11-1.93, $p = 0.01$) were independent risk factors for overall survival (Table 3).

3.4. Preoperative Characteristics of the Matched Series

Propensity score matching analysis yielded 234 pairs of patients. There were no significant differences in baseline profiles (Table 4).

3.5. Survival Outcomes of the Matched Series

There were no significant differences in recurrence-free survival between the two groups ($p = 0.42$; supplementary Figure S1B). Overall survival rates in the elderly group at 1, 3, and 5 years were 92.1% [95% CI, 87.8 to 95.0], 76.1% [95% CI, 69.4 to 81.8], and 57.3% [95% CI, 48.7 to 65.4], respectively, whereas those in the younger group were 93.5% [95% CI, 89.6

Table 3. Multivariate logistic-regression analysis

Variable		Hazard ratio	95% confidence interval	*p*-value	Regression coefficients
Vascular invasion:	Present *vs*. Absent	2.25	1.52 - 3.33	0.0001	0.81
Albumin (g/dL):	< 3.0 *vs*. ≥ 3.0	2.23	1.31 - 3.79	0.003	0.80
Number of tumors:	Multiple *vs*. Solitary	1.68	1.24 - 2.27	0.001	0.52
Platelet count (g/dL):	< 15 *vs*. ≥ 15	1.46	1.11 - 1.93	0.01	0.38

Table 4. Clinical and operative variables after propensity match

Items	All patients, *n* = 468	younger, *n* = 234	elderly, *n* = 234	*p*-value
Clinical variable				
Age	69 (36-85)	64 (36-69)	73 (70-85)	0.00001
Gender	Male	177 (75.6%)	166 (70.9%)	0.25
Hepatitis type				
HBV, positive	Present	11 (4.7%)	11 (4.7%)	1.0
HCV, positive	Present	155 (66.2%)	159 (67.9%)	0.69
Alcohol	Present	60 (25.6%)	58 (24.8%)	0.83
Child-Pugh classification	A	223 (95.3%)	228 (97.4%)	0.22
	B+C	11 (4.7%)	6 (2.6%)	
Hemoglobin (g/dL)[d]	13.0 (8.1-17.3)	13.0 (8.3-17.3)	12.9 (8.1-16.6)	0.03
Platelets (10^4/μL)[d]	14.0 (2.6-68.6)	14.0 (2.6-68.6)	13.8 (3.2-38.7)	0.85
Total protein (g/dL)[d]	7.1 (5.0-8.9)	7.2 (5.6-8.9)	7.1 (5.0-8.8)	0.06
Albumin (g/dL)[d]	3.8 (2.4-5.3)	3.9 (2.4-5.3)	3.8 (2.6-4.9)	0.06
Total bilirubin (mg/dL)[d]	0.6 (0.2-3.4)	0.6 (0.2-2.0)	0.6 (0.3-3.4)	0.73
AST (IU/L)[d]	40 (12-295)	41 (12-295)	40 (13-265)	0.3
ALT (IU/L)[d]	37 (5-296)	40 (5-253)	35 (10-296)	0.06
Prothrombin time (%)[d]	97 (53-100)	96 (62-100)	99 (53-100)	0.21
ICG-R_{15}[a,d]	12.8 (1.3-82.3)	12.0 (1.3-82.3)	13.2 (3.0-48.5)	0.05
α-fetoprotein (ng/mL)[d]	15.2 (0.6-60340)	20.7 (0.8-60340)	12.9 (0.6-24275)	0.03
Ccr[b,d]	87.9 (5.9-281.5)	92.0 (5.9-281.5)	82.1 (29.7-180.1)	0.06
Operative variable				
Tumor size	31 (7-205)	31 (7-205)	30 (9-180)	0.69
Number of tumors	Solitary	178 (76.1%)	173 (73.9%)	0.59
Vascular invasion	Present	28 (12.0%)	26 (11.1%)	0.77
Anatomical resection	Present	84 (35.9%)	83 (35.5%)	0.92
Major hepatic resection	Present	10 (4.3%)	15 (6.4%)	0.3
UICC stage[c]	1, 2	217 (92.7%)	217 (92.7%)	1.0
	3	17 (7.3%)	17 (7.3%)	1.0
Blood loss[d]	285 (5-3378)	320 (10-3378)	252 (5-2725)	0.02
Clamp time[d]	73 (0-860)	76 (13-860)	71 (0-221)	0.2
Operative time[d]	326 (130-1590)	338 (130-1590)	314 (139-803)	0.1
Differentiation	Mod, well	214 (91.5%)	206 (88.0%)	0.22
	Poor	20 (8.5%)	28 (12.0%)	
Complications	0-II	174 (74.4%)	183 (78.2%)	0.33
	III-V	60 (25.6%)	51 (21.8%)	

[a]ICG15: indocyanine green retention rate at 15 minutes; bCCr: Creatinine clearance; [c]International Union Against Cancer (UICC) TNM staging classification; [d]Median (range)

Table 5. Rate of high-risk patients before and after propensity matched analysis

Whole study	All patients, *n* = 631	Younger, *n* = 340	Elderly, *n* = 291	*p*-value
Risk score < 0.45	418 (66.2%)	241 (70.9%)	177 (60.8%)	
Risk score ≥ 0.45	213 (33.8%)	99 (29.1%)	114 (39.2%)	0.01
After propensity matching analysis	All patients, *n* = 468	Younger, *n* = 234	Elderly, *n* = 234	0.43
Risk score < 0.45	316 (67.5%)	162 (69.2%)	154 (65.8%)	
Risk score ≥ 0.45	152 (32.5%)	72(30.8%)	80 (34.2%)	

Risk score = 0.81 X (with vascular invasion) + 0.80 X (albumin level less than 3.0 g/dL) + 0.52 X (multiple nodules) + 0.38 X (platelet count less than 15×10^4/μL).

to 96.1], 74.3% [95% CI, 67.5 to 80.1], and 61.2% [95% CI, 53.3 to 68.6], respectively. There was no significant difference in overall survival between the two groups ($p = 0.23$) (Figure 1B).

3.6. Calculation and Determination of Cutoff Value of Risk Score

Risk scores for individual patients were calculated by combining their four prognostic values with the regression coefficients from the results of analysis with the Cox proportional-hazards model (Table 3), *i.e*., risk score = 0.81 X (with vascular invasion) + 0.80 X (albumin level < 3.0 g/dL) + 0.52 X (multiple nodules) + 0.38 X (platelet count < 15×10^4/μL). The ROC curve

indicated that the optimal cutoff value of risk score was 0.45, and the AUC was 0.74 (95% CI: 0.67-0.81, p = 0.000001). Although the elderly group had a higher proportion of high-risk patients (39.2%) than the younger group (29.1%; p = 0.01), after propensity analysis, the proportion of high-risk patients in the elderly group (34.2%) was comparable to that in the younger group (30.8%; p = 0.43) (Table 4).

3.7. Survival Outcomes of patients with high and low risk score.

The overall survival and recurrence-free survival were significantly shorter in the patients with high-risk than in the low-risk score (p = 0.000000004 and 0.000001, respectively: supplementary Figure S2A and B).

4. Discussion

We showed that elderly patients with HCC who underwent liver resection had a lower overall survival rate than younger patients; however, after matching, the overall survival rates were similar in both groups. Thus, our results showed no impact of advanced age on the outcome of patients after resection of HCC. Furthermore, we examined why elderly patients with HCC who underwent liver resection had a lower overall survival rate than younger patients, and poor outcomes in the elderly group were probably attributable to the higher proportion of "high-risk patients" who had either vascular invasion, lower albumin level, or multiple nodules in the elderly group.

To our knowledge, even after propensity matching and reduction of the number of patients, our study group of 234 elderly patients after liver resection represents one of the largest contemporary series of elderly patients undergoing liver resection for HCC reported to date. Therefore, our results represent useful information for the management of HCC in this subgroup of patients.

We performed propensity analysis to adjust for age-related differences in the background characteristics of the younger and elderly groups, and the overall survival rates were comparable in the two groups. This finding suggests that differences in background characteristics between the groups led to the observed difference in survival. Only three previous studies used propensity score matching analysis to investigate the relation between the age and outcomes of patients with HCC after liver resection (*5,7,8*). One of these studies performed in Italy showed the overall survival rate as one of several treatment results, and therefore the relation between the age and outcomes of HCC patients after liver resection was not discussed sufficiently in this paper. Although this study defined elderly as 70 years or older as in our study, the cohort consisted of less than 50 patients. The study showed that overall survival rates were similar in elderly and younger patients after propensity matching, consistent with our results regarding long-term survival (*5*). In the other two studies performed in Taiwan, HBV was the main cause of HCC (61.0% and 63.4%) (*7,8*). In one of the two studies, the overall survival rate was also shown as one of several treatment results, and therefore the relation between age and outcomes of HCC patients after liver resection was not discussed sufficiently in this paper. Although this study defined elderly as 75 years or older, the cohort consisted of only 118 patients (*7*). The remaining study defined elderly as 55 years or older, based on the median age of patients in their cohort (*8*). The results showed that the younger group had better liver functional reserve but more aggressive tumor factors than the elderly group. In our study, we defined elderly as 70 years or older, and liver functional reserve and tumor factors were comparable in the two groups in contrast to the study from Taiwan. The differences between this study and our study may be ascribed to the differences in patients according to whether HCC is associated with underlying HBV or HCV. These two studies performed in Taiwan showed that the elderly group had a lower overall survival rate than the younger group before matching; consistent with our results, however, the overall survival rates were similar in the two groups after matching (*7,8*). HCV is currently the main cause of HCC in Japan and Southern Europe, accounting for 70% of cases (*3,4*). In the present study, HCV was the main cause of HCC in the younger group (52.1%) as well as in the elderly group (65.9%). Therefore, our results may be most applicable to countries in which a high proportion of HCC is caused by HCV infection.

Although there were no significant differences between the two groups in assumed prognostic factors, such as tumor size, vascular invasion, and the number of tumors, the overall survival rate was significantly lower in the elderly group than the younger group. Furthermore, the site of recurrence, the cause of death, and the recurrence-free survival were also similar in the two groups. Therefore, we could not determine why the elderly patients had poorer outcomes. To investigate what background characteristics negatively affected outcomes in the elderly group, we defined and calculated risk scores from the results of Cox regression analysis, and the optimal cutoff value of the risk score, calculated by ROC analysis, was 0.45. As the β regression coefficient of the platelet count was 0.38 and lower than the optimal cutoff value, the platelet count could be excluded from the risk score, and all three other variables had β regression coefficients of 0.45 or higher. According to the equation used to calculate our risk score, patients who had either vascular invasion, lower albumin level, or multiple nodules were defined as "high-risk patients". Among these variables, vascular invasion and multiple nodules are common prognostic factors for poor survival in patients with HCC after liver resection (*18,28,29*). Hypoalbuminemia is common in the elderly (*12,18*), and previous studies indicated that the incidences of vascular

invasion and hypoalbuminemia were significantly higher in elderly than younger patients with HCC (*12,13*). In our study, although the albumin level was lower in the elderly group (median, 3.8 g/dL; range, 2.3-4.9 g/dL) than in the younger group (3.9 g/dL; 2.4-5.3 g/dL; $p = 0.0001$), there were no significant differences between the two groups in vascular invasion or the number of tumors ($p = 0.11$ and $p = 0.30$, respectively); therefore, these three variables seem to be unrelated to aging. However, the proportions of high-risk patients were significantly higher in the elderly group than in the younger group. After propensity matching, the effects of the high-risk factors were apparently cancelled by other factors, and overall survival was comparable in both groups. Taken together, these findings indicated that the poor outcomes in the elderly group were not due to advanced age itself, but were probably attributable to the higher proportion of high-risk patients who had either vascular invasion, lower albumin level, or multiple nodules in the elderly group.

Although we used a cutoff age of 70 years or older to define elderly patients, there was no apparent impact of patient age on long-term outcome after liver resection for HCC mainly caused by HCV. Our results suggest that surgeons should not hesitate to perform liver resection because of advanced age in patients with HCC.

Funding: This work was mainly supported by Japan Agency for Medical Research and Development (AMED), Grant/Award Number: JP20hk0102049.

Conflict of Interest: The authors have no conflicts of interest to disclose.

References

1. El-Serag HB. Hepatocellular carcinoma: recent trends in the United States. Gastroenterology 2004; 127:S27–S34.
2. El-Serag HB. Epidemiology of viral hepatitis and hepatocellular carcinoma. Gastroenterology. 2012; 142:1264-1273.
3. Ikai I, Arii S, Okazaki M, Okita K, Omata M, Kojiro M, Takayasu K, Nakanuma Y, Makuuchi M, Matsuyama Y, Monden M, Kudo M. Report of the 17th Nationwide Follow-up Survey of Primary Liver Cancer in Japan. Hepatol Res. 2007; 37:676-691.
4. Michielsen PP, Francque SM, van Dongen JL. Viral hepatitis and hepatocellular carcinoma. World J Surg Oncol. 2005; 3:27.
5. Mirici-Cappa F, Gramenzi A, Santi V, *et al*. Treatments for hepatocellular carcinoma in elderly patients are as effective as in younger patients: a 20-year multicentre experience. Gut. 2010; 59:387-396.
6. Huang J, Li BK, Chen GH, Li JQ, Zhang YQ, Li GH, Yuan YF. Long-term outcomes and prognostic factors of elderly patients with hepatocellular carcinoma undergoing hepatectomy. J Gastrointest Surg. 2009; 13:1627-1635.
7. Liu PH, Hsu CY, Lee YH, Hsia CY, Huang YH, Su CW, Chiou YY, Lin HC, Huo TI. Uncompromised treatment efficacy in elderly patients with hepatocellular carcinoma: a propensity score analysis. Medicine (Baltimore). 2014; 93:e264
8. Su CW, Lei HJ, Chau GY, Hung HH, Wu JC, Hsia CY, Lui WY, Su YH, Wu CW, Lee SD. The effect of age on the long-term prognosis of patients with hepatocellular carcinoma after resection surgery: a propensity score matching analysis. Arch Surg. 2012; 147:137-144.
9. Oishi K, Itamoto T, Kobayashi T, Oshita A, Amano H, Ohdan H, Tashiro H, Asahara T. Hepatectomy for hepatocellular carcinoma in elderly patients aged 75 years or more. J Gastrointest Surg. 2009; 13:695-701.
10. Lee CR, Lim JH, Kim SH, Ahn SH, Park YN, Choi GH, Choi JS, Kim KS. A comparative analysis of hepatocellular carcinoma after hepatic resection in young versus elderly patients. J Gastrointest Surg. 2012; 16:1736-1743.
11. Nanashima A, Abo T, Nonaka T, Fukuoka H, Hidaka S, Takeshita H, Ichikawa T, Sawai T, Yasutake T, Nakao K, Nagayasu T. Prognosis of patients with hepatocellular carcinoma after hepatic resection: are elderly patients suitable for surgery? J Surg Oncol. 2011; 104:284-291.
12. Kaibori M, Matsui K, Ishizaki M, Saito T, Kitade H, Matsui Y, Kwon AH. Hepatic resection for hepatocellular carcinoma in the elderly. J Surg Oncol. 2009; 99:154-160.
13. Hanazaki K, Kajikawa S, Shimozawa N, Shimada K, Hiraguri M, Koide N, Adachi W, Amano J. Hepatic resection for hepatocellular carcinoma in the elderly. J Am Coll Surg. 2001; 192:38-46.
14. Namieno T, Kawata A, Sato N, Kondo Y, Uchino J. Age-related, different clinicopathologic features of hepatocellular carcinoma patients. Ann Surg. 1995; 221:308-314.
15. Kaibori M, Yoshii K, Yokota I, Hasegawa K, Nagashima F, Kubo S, Kon M, Izumi N, Kadoya M, Kudo M, Kumada T, Sakamoto M, Nakashima O, Matsuyama Y, Takayama T, Kokudo N; Liver Cancer Study Group of Japan. Impact of Advanced Age on Survival in Patients Undergoing Resection of Hepatocellular Carcinoma: Report of a Japanese Nationwide Survey. Ann Surg. 2019; 269 :692-699.
16. Layer P, Zinsmeister AR, DiMagno EP. Effects of decreasing intraluminal amylase activity on starch digestion and postprandial gastrointestinal function in humans. Gastroenterology. 1986; 91:41-48.
17. Zinsmeister AR, Connor JT. Ten common statistical errors and how to avoid them. Am J Gastroenterol. 2008; 103:262-266.
18. Balducci L. Geriatric oncology: challenges for the new century. Eur J Cancer. 2000; 36:1741-1754.
19. Makuuchi M, Kosuge T, Takayama T, Yamazaki S, Kakazu T, Miyagawa S, Kawasaki S. Surgery for small liver cancers. Semin Surg Oncol. 1993; 9:298-304.
20. DRIPPS RD, LAMONT A, ECKENHOFF JE. The role of anesthesia in surgical mortality. JAMA. 1961; 178:261-266.
21. Takayama T, Makuuchi M, Hirohashi S, Sakamoto M, Yamamoto J, Shimada K, Kosuge T, Okada S, Takayasu K, Yamasaki S. Early hepatocellular carcinoma as an entity with a high rate of surgical cure. Hepatology. 1998; 28:1241-1746.
22. Takayama T, Makuuchi M, Kubota K, Harihara Y, Hui AM, Sano K, Ijichi M, Hasegawa K. Randomized comparison of ultrasonic vs clamp transection of the liver. Arch Surg. 2001; 136:922-928.
23. Dindo D, Demartines N, Clavien PA. Classification of

surgical complications: a new proposal with evaluation in a cohort of 6336 patients and results of a survey. Ann Surg. 2004; 240:205-213.
24. Smetana GW, Lawrence VA, Cornell JE; American College of Physicians. Preoperative pulmonary risk stratification for noncardiothoracic surgery: systematic review for the American College of Physicians. Ann Intern Med. 2006; 144:581-595.
25. Dickson ER, Grambsch PM, Fleming TR, Fisher LD, Langworthy A. Prognosis in primary biliary cirrhosis: model for decision making. Hepatology. 1989; 10:1-7.
26. Chevret S, Trinchet JC, Mathieu D, Rached AA, Beaugrand M, Chastang C. A new prognostic classification for predicting survival in patients with hepatocellular carcinoma. J Hepatol. 1999; 31:133-141.
27. Perkins NJ, Schisterman EF. The inconsistency of "optimal" cutpoints obtained using two criteria based on the receiver operating characteristic curve. Am J Epidemiol. 2006; 163:670-675.
28. Poon RT, Ng IO, Fan ST, Lai EC, Lo CM, Liu CL, Wong J. Clinicopathologic features of long-term survivors and disease-free survivors after resection of hepatocellular carcinoma: a study of a prospective cohort. J Clin Oncol. 2001; 19:3037-3044.
29. Arii S, Tanaka J, Yamazoe Y, Minematsu S, Morino T, Fujita K, Maetani S, Tobe T. Predictive factors for intrahepatic recurrence of hepatocellular carcinoma after partial hepatectomy. Cancer. 1992; 69:913-919.

Received December 14, 2020; Revised January 23, 2021; Accepted February 3, 2021.

*Address correspondence to:
Osamu Aramaki, Department of Digestive Surgery, Nihon University School of Medicine, 30-1 Oyaguchikami-machi, Itabashi-ku, Tokyo173-8610, Japan.
E-mail: aramaki.osamu@nihon-u.ac.jp

Released online in J-STAGE as advance publication February 7, 2021.

Supplementary Figures

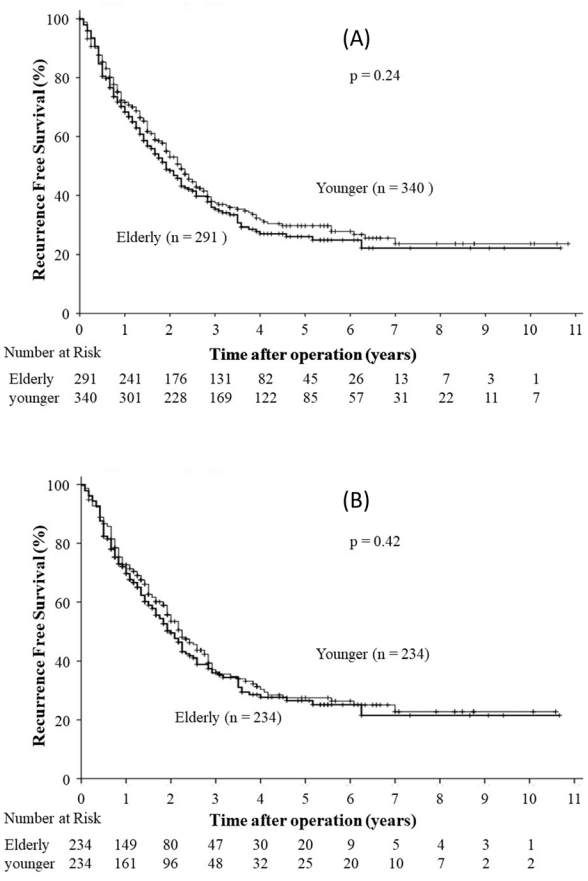

Figure S1. (A) Cumulative recurrence-free survival in patients with hepatocellular carcinoma stratified by age. There were no significant differences between the two groups (p = 0.24). (B) Cumulative recurrence-free survival in patients with hepatocellular carcinoma by propensity score matching analysis. There were no significant differences between the two groups (p = 0.42).

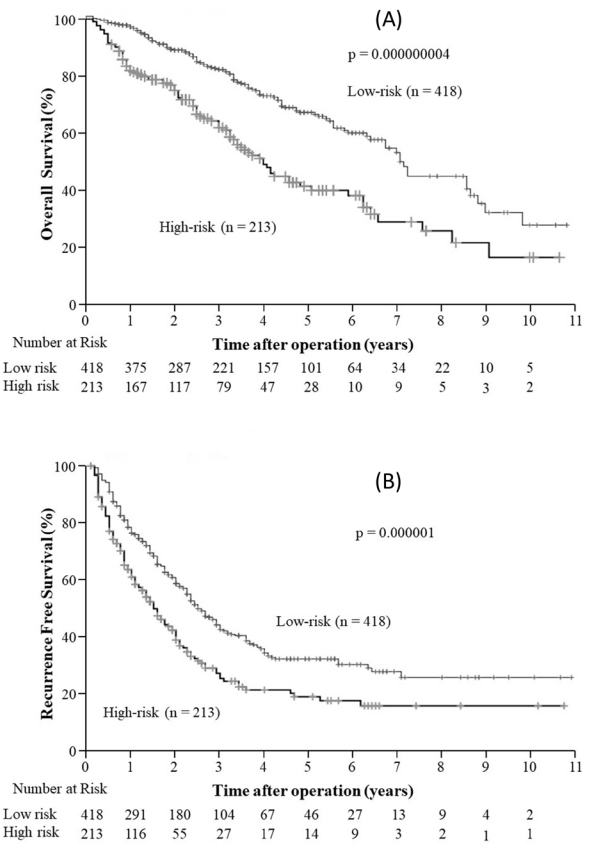

Figure S2. (A) Cumulative overall survival in patients with hepatocellular carcinoma stratified by risk score. The patients with low-risk had a higher overall survival rate than the low-risk score (p = 0.000000004). (B) Cumulative recurrence-free in patients with hepatocellular carcinoma stratified by risk score. The patients with low-risk had a higher recurrence-free rate than the low-risk score (p = 0.000001).

Original Article

DOI: 10.5582/bst.2021.01064

Combination of albumin-bilirubin grade and clinically significant portal hypertension predicts the prognosis of patients with hepatocellular carcinoma after liver resection

Li Qin[1,2], Chuan Li[1,*], Fei Xie[3], Zhenxia Wang[4], Tianfu Wen[1]

[1] Department of Liver Surgery, West China Hospital of Sichuan University, Chengdu, Sichuan, China;
[2] West China School of Nursing, Sichuan University, Chengdu, Sichuan, China;
[3] Department of Hepato-pancreato-biliary Surgery, First People's Hospital of Neijiang, Neijiang, Sichuan, China;
[4] Department of Hepato-pancreato-biliary Surgery, Chengdu Second People's Hospital, Chengdu, Sichuan, China.

SUMMARY There is little information concerning whether incorporating clinically significant portal hypertension (CSPH) into albumin-bilirubin (ALBI) grading could improve its predictive capacity. In this study, we investigated the predictive ability of ALBI grade plus CSPH (ALBI-P score) for patients with hepatocellular carcinoma (HCC) after liver resection. Data from 1,679 patients were retrospectively reviewed. The ALBI-P score was calculated from the ALBI grade and a point for CSPH (0 for absence of CSPH and 1 for presence of CSPH). Independent risk factors for recurrence-free survival (RFS) and overall survival (OS) were analyzed. Multivariate analysis suggested that the ALBI-P score was an independent risk factor for both postoperative recurrence (HR = 1.441, 95% CI = 1.328-1.563, $P < 0.001$) and mortality (HR = 1.332, 95% CI = 1.156-1.535, $P < 0.001$). Both the RFS and OS of patients with an ALBI-P score of 1 were significantly better than those of patients with ALBI-P scores of 2 and 3 (5-year RFS of 38.9%, 26.1%, and 14.7%, respectively, $P < 0.001$; 5-year OS of 52.7%, 42.6%, and 29.3%, $P < 0.001$). When the ALBI-P score and BCLC stage were combined, the ALBI-P-BCLC score showed the highest area under the receiver operating characteristic curve to predict both postoperative recurrence and mortality compared with BCLC stage alone, BCLC stage combined with ALBI grade, or platelet-albumin-bilirubin grade. These results suggested incorporating CSPH into the ALBI grade could strengthen its prognostic power. The ALBI-P score may serve as a surrogate marker to predict HCC patient outcomes after liver resection.

Keywords hepatocellular carcinoma, albumin-bilirubin grade, clinically significant portal hypertension

1. Introduction

Hepatocellular carcinoma (HCC) is a heavy public health burden and is a leading cause of cancer-related mortality in many parts of the world, ranking as the fifth most common malignancy and third most frequent cause of cancer-related death worldwide (*1*). Chronic hepatitis virus infections, including chronic hepatitis B virus (HBV) and hepatitis C virus (HCV) infections, are the most important causes of HCC. Every year, approximately 1-8% of patients with cirrhosis from chronic HBV and HCV infections will develop HCC (*2*). Previous investigations revealed that chronic hepatitis infections may contribute to approximately 80% of HCC cases globally (*1*). Since many patients with HCC suffer from chronic hepatitis virus infections, many HCC patients also have cirrhosis and even portal hypertension.

In contrast to other kinds of cancers, liver function greatly impacts the prognosis of HCC following many treatments, such as liver resection, radiofrequency ablation, and transarterial chemoembolization (*2,3*). Currently, the Child-Pugh score is the most commonly used tool to assess liver function. However, the accuracy of the Child-Pugh score varies due to subjective variables, including hepatic encephalopathy and ascites. In 2015, Johnson *et al.* (*4*) developed the albumin-bilirubin (ALBI) grade, which only includes total bilirubin and albumin as two objective parameters, to evaluate a patient's liver function. Subsequently, a number of studies confirmed that ALBI was better than the Child-Pugh score in predicting the prognosis of patients with HCC after many management strategies. For example, Na *et al.* (*5*) suggested that ALBI provided better prognostic performance in survival analysis and a more accurate distribution of grades than the Child-Pugh score for HCC patients. Moreover, portal hypertension

is also often detected in cirrhosis and could adversely influence the outcomes of patients with HCC after liver resection. The Barcelona Clinic Liver Cancer (BCLC) system does not recommend liver resection for HCC patients with portal hypertension (2). In our clinical practice, portal hypertension occurs not only in patients with poor liver function but also in those with compensated liver function. However, neither the Child-Pugh score nor the ALBI grade involved variables that could assess portal hypertension. Accordingly, we suspected that the combination of liver function assessed by ALBI grade and clinical portal hypertension could more exactly predict the prognosis of patients with HCC following liver resection.

2. Patients and Methods

The records of patients with HCC who had undergone liver resection between 2012 and 2020 at West China Hospital of Sichuan University were retrospectively analyzed. Patients who underwent re-resection, had ruptured HCC, received preoperative antitumor treatment, had a positive surgical margin, or had other types of tumors were excluded. All HCC cases were confirmed by postoperative pathology. This study was approved by the ethics committee of West China Hospital. In our center, Clinically significant portal hypertension (CSPH) is not a contraindication of liver resection for patients with HCC. Liver function of patients who underwent liver resection should be in Child-Pugh A grade. For patients with cirrhosis, if the indocyanine green retention rate at 15 minutes < 10%, the future liver remnant should be at least 40%. If the indocyanine green retention rate at 15 minutes is between 10% and 20%, the future liver remnant should be at least 50%. Additionally, for patients with liver fibrosis, the future liver remnant volume should be greater than 30%, and for patients without an underlying liver disease, the future liver remnant volume should be greater than 20% (*6*). Simultaneous splenectomy will be performed on patients with a preoperative platelet count of less than 50 $\times 10^9$/L.

2.1. Follow-up

All preoperative blood tests were performed 1 week before the operation. After liver resection, the patients were regularly followed up every 3 months. Before and after the operation, antiviral drugs (entecavir, lamivudine or tenofovir) were conventionally administered to patients with a positive HBV-DNA load. The routine follow-up included blood cell tests, liver function tests, serum alpha-fetoprotein (AFP) measurement, HBV-DNA tests, visceral ultrasonography, computed tomography or magnetic resonance imaging and chest radiography. Bone scintigraphy was performed whenever HCC recurrence was suspected. Postoperative recurrence was defined as positive imaging findings compared with the preoperative examination values or as confirmed by biopsy or resection (*7*).

2.2. Definitions

High alpha-fetoprotein (AFP) was defined as > 400 ng/mL (*7*). The neutrophil-to-lymphocyte ratio (NLR) was defined as the absolute neutrophil count divided by the lymphocyte count (*8*). An NLR greater than 3 was defined as being high (*8*). The prognostic nutrition index (PNI) was the sum of serum albumin (g/L) and 5× lymphocyte count (10^9/L) (*9*). The cut-off value of PNI was 45, as reported in the literature (*9*). ALBI grade was calculated according to the following formula: ALBI = ($\log_{10}$ bilirubin (μmol/L) × 0.66) + (albumin (g/L) × -0.085) (*4*). ALBI values were divided into 3 grades as follows: grade 1 (less than -2.60), grade 2 (between -2.60 and -1.39) and grade 3 (above -1.39) (*4*). Platelet-albumin-bilirubin (PALBI) was calculated based on the following equation: $2.02 \times \log_{10}$ bilirubin (μmol/L) - $0.37 \times (\log_{10}$ bilirubin (μmol/L))^2 - $0.04 \times$ albumin (g/L) - $348 \times \log_{10}$ platelets (1,000/μL) + $1.01 \times (\log_{10}$ platelets (1,000/μL))^2 (*10*). PALBI was divided into 3 grades as follows: grade 1 (≤ -2.53), grade 2 (> -2.53 and ≤-2.09), and grade 3 (>-2.09) (*10*). Clinically significant portal hypertension (CSPH) was defined by the presence of esophagogastric varices and/or a platelet count < 100 × 10^9/L in association with splenomegaly (*11*). The ALBI-portal hypertension (ALBI-P) score was defined as the summary of the ALBI grade and status of CSPH: (1 for the presence of CSPH and 0 for the absence of CSPH). For example, if a patient with ALBI grade 1 (score of 1) and CSPH (score of 1), the ALBI-P score of this patient is 2. If a patient with ALBI grade 2 (score 2), but without CSPH (score 0), the ALBI-P score of this patient is also 2. We also analyzed the predictive ability of the combination of BCLC stage and ALBI grade, PALBI grade, or ALBI-P score, where we allocated 0 to BCLC stage 0, 1 to BCLC stage A, 2 to BCLC stage B and 3 to BCLC stage C. The ALBI-BCLC score was defined as the summary of the ALBI grade and BCLC score. The PALBI-BCLC score was defined as the summary of the PALBI grade and BCLC score. The ALBI-P-BCLC score was defined as the summary of the ALBI-P score and BCLC score.

2.3. Statistical analysis

All statistical analyses were performed by SPSS 26.0 (SPSS Company, Chicago, IL) for Windows. All continuous variables were analyzed using one-way analysis of variance. The χ^2 test or Fisher's exact test was used to compare the categorical variables. The Kaplan-Meier method was applied to determine recurrence-free survival (RFS) and overall survival, and the log-rank test was performed to test the survival differences.

Multivariable analysis was carried out using Cox regression analysis to identify independent risk factors for OS and RFS. All variables with a *P* value < 0.1 in the univariate analysis were included in the multivariate analysis. The area under the receiver operating characteristic (ROC) curve (AUC) was used to estimate the predictive accuracy. MedCalc software version 11.2 was used to compare the ROC curves. A *P*-value of < 0.05 was considered statistically significant.

3. Results

3.1. Patient characteristics

A total of 1,679 patients were enrolled in this study. The mean age of the patients was 51.3 ± 12.1 years. According to the ALBI grade, 1,156 patients were ALBI grade 1, and 523 patients were ALBI grade 2. There were no patients with ALBI grade 3. According to the PALBI grade, 1,173 patients were PALBI grade 1, 445 patients were PALBI grade 2, and 61 patients were PALBI grade 3. CSPH was detected in 597 patients. According to the definition of the ALBI-P score, 791 patients were classified as ALBI-P score 1, 655 as ALBI-P score 2, and 233 as ALBI-P score 3. The mean tumor size was 6.7 ± 3.6 cm in this study. Multiple tumors were found in 362 patients. High preoperative AFP levels were observed in 690 patients. A total of 757 patients had positive preoperative HBV DNA. Microvascular invasion (MVI) was detected in 871 patients. Satellite lesions were found in 249 patients. Thirty-six patients were in BCLC stage 0, 849 patients were in BCLC stage A, 167 patients were in BCLC stage B, and 627 patients were in BCLC stage C.

During a median 39.8 months of follow-up, 1,128 patients experienced recurrence, and 825 patients died. The 1-, 3-, and 5-year RFS rates of the whole cohort were 72.8%, 41.2% and 30.2%, respectively (Figure 1A), whereas the 1-, 3-, and 5-year OS rates were 91.5%, 62.1%, and 45.1% (Figure 1B).

3.2. Prognostic factors for RFS

The prognostic factors for RFS according to the univariate and multivariate analyses are listed in Table 1. The potential risk factors for RFS detected by univariate analysis were tumor size > 5 cm, multiple tumors, tumor differentiation, AFP > 400 ng/mL, presence of microvascular invasion (MVI), satellite lesions, cirrhosis, Milan criteria, platelet count < 100 (10^9/L), NLR > 3, PNI < 45, ALBI grade, PALBI grade, ALBI-P score and BCLC stage. In the multivariate analysis, the independent risk factors for RFS were only tumor size > 5 cm (HR = 1.737, 95% CI = 1.459-2.068, *P* < 0.001), MVI (HR = 1.574, 95% CI = 1.321-1.877, *P* < 0.001), satellite lesions (HR = 1.435, 95% CI = 1.229-1.676, *P* < 0.001), ALBI-P score (HR = 1.441, 95% CI = 1.328-

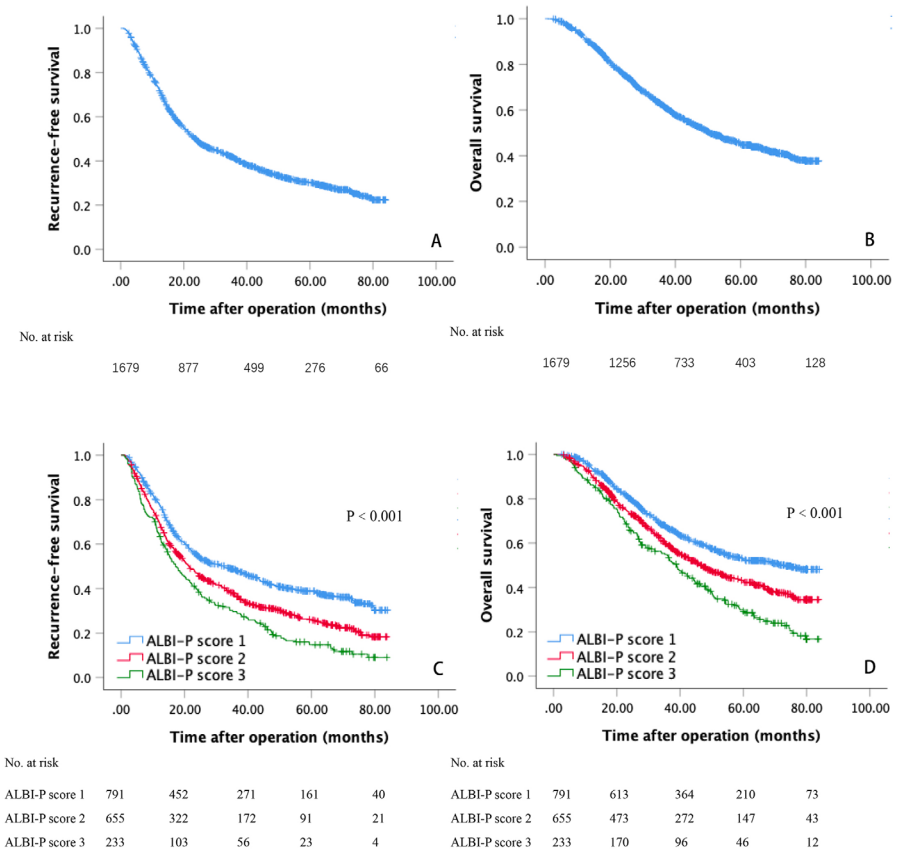

Figure 1. Recurrence-free (A) and overall (B) survival in all patients. Recurrence-free (C) and overall (D) survival comparison of patients with different ALBI-P scores. Patients with a high ALBI-P score had a high risk of postoperative recurrence and death.

1.563, $P < 0.001$), and BCLC stage (HR = 1.125, 95% CI = 1.018-1.242, $P = 0.020$).

3.3. Prognostic factors for OS

As shown in Table 2, tumor size > 5 cm, multiple tumors, tumor differentiation, AFP > 400 ng/mL, presence of microvascular invasion (MVI), satellite lesions, cirrhosis, Milan criteria, platelet count < 100 (10^9/L), NLR >3, PNI <45, ALBI grade, PALBI grade, ALBI-P score and BCLC stage were associated with poor OS in the univariate analysis. In multivariate analysis, only tumor size > 5 cm (HR = 1.647, 95% CI = 1.317-2.059, $P < 0.001$), platelet count < 100 (10^9/L) (HR = 1.282, 95% CI = 1.037-1.585, $P = 0.022$), MVI (HR = 1.549, 95% CI = 1.238-1.937, $P < 0.001$), satellite lesions (HR = 1.295, 95% CI = 1.080-1.552, $P = 0.005$), ALBI-P score (HR = 1.332, 95% CI = 1.156-1.535, $P < 0.001$), and BCLC stage (HR = 1.589, 95% CI = 1.404-1.799, $P < 0.001$) were independent prognostic factors of poor OS.

3.4. Comparison of the clinicopathological data of patients according to different ALBI-P scores

As presented in Table 3, a higher proportion of patients with older age, multiple tumors, poor tumor

Table 1. Variables associated with recurrence-free survival according to the Cox proportional hazards model

Variables	Univariate analysis			Multivariate analysis		
	HR	95% CI	*P*	HR	95% CI	*P*
Age > 60 years	0.981	0.856-1.123	0.776			
Male	1.023	0.870-1.203	0.781			
Tumor size > 5 cm	2.542	2.224-2.907	< 0.001	1.737	1.459-2.068	< 0.001
Multiple tumors	1.528	1.330-1.756	< 0.001			
Differentiation	1.183	1.075-1.302	0.001			
AFP > 400 ng/mL	1.269	1.128-1.427	< 0.001			
High positive HBV DNA	1.034	0.920-1.163	0.575			
MVI	2.424	2.145-2.740	< 0.001	1.574	1.321-1.877	< 0.001
Satellite lesion	1.580	1.353-1.846	< 0.001	1.435	1.229-1.676	< 0.001
Fulfill Milan criteria	0.407	0.357-0.465	< 0.001			
Cirrhosis	1.220	1.027-1.449	0.023			
Platelet < 100 (10^9/L)	1.357	1.205-1.528	< 0.001			
NLR > 3	1.347	1.182-1.536	< 0.001			
PNI < 45	1.337	1.167-1.532	< 0.001			
ALBI grade	1.463	1.295-1.653	< 0.001			
ALBI-P score	1.353	1.249-1.466	< 0.001	1.441	1.328-1.563	< 0.001
PALBI grade	1.216	1.094-1.352	< 0.001			
BCLC stage	1.366	1.309-1.426	< 0.001	1.125	1.018-1.242	0.020

Table 2. Variables associated with overall survival according to the Cox proportional hazards model

Variables	Univariate analysis			Multivariate analysis		
	HR	95% CI	*P*	HR	95% CI	*P*
Age > 60 years	1.114	0.917-1.353	0.276			
Male	0.944	0.805-1.107	0.479			
Tumor size > 5 cm	3.499	2.961-4.134	< 0.001	1.647	1.317-2.059	< 0.001
Multiple tumors	1.646	1.403-1.931	< 0.001			
Differentiation	1.338	1.194-1.500	< 0.001			
AFP >400 ng/mL	1.377	1.201-1.579	< 0.001			
High positive HBV DNA	0.919	0.801-1.055	0.231			
MVI	3.561	3.065-4.137	< 0.001	1.549	1.238-1.937	< 0.001
Satellite lesion	1.448	1.209-1.733	< 0.001	1.295	1.080-1.552	0.005
Fulfill Milan criteria	0.304	0.258-0.358	< 0.001			
Cirrhosis	1.344	1.090-1.657	0.006			
Platelet < 100 (10^9/L)	1.371	1.195-1.573	< 0.001	1.282	1.037-1.585	0.022
NLR > 3	1.419	1.220-1.650	< 0.001			
PNI < 45	1.391	1.190-1.625	< 0.001			
ALBI grade	1.549	1.346-1.782	< 0.001			
ALBI-P score	1.391	1.269-1.525	< 0.001	1.332	1.156-1.535	< 0.001
PALBI grade	1.309	1.161-1.476	< 0.001			
BCLC stage	1.668	1.584-1.757	< 0.001	1.589	1.404-1.799	< 0.001

Table 3. Comparison of the clinicopathological characteristics of patients with different ALBI-P scores

Characteristics	ALBI-P score 1	ALBI-P score 2	ALBI-P score 3	*P* values
Age > 60 years (yes/no)	172/619	152/503	76/157	0.003
Sex (female/male)	129/662	104/551	28/205	0.270
Multiple tumors (yes/no)	156/635	140/515	66/167	0.019
Tumor size > 5 cm	520/271	421/234	137/96	0.151
Cirrhosis	625/166	583/72	220/13	< 0.001
Satellite lesion	128/662	91/564	30/203	0.331
MVI	402/389	361/294	108/125	0.051
Differentiation	130/483/178	130/377/148	26/138/69	0.012
AFP > 400 ng/mL	327/464	274/381	89/144	0.614
Positive HBV DNA	423/476	319/336	114/119	0.006
NLR > 3	172/619	170/485	68/165	0.034
PNI < 45	39/752	191/464	134/99	< 0.001
BCLC stage (0/A *vs.* B/C)	427/364	331/423	127/106	0.357

differentiation, positive HBV DNA, cirrhosis, high NLR, and low PNI were observed in patients with a high ALBI-P score. The 1-, 3-, and 5-year RFS rates were 78.0%, 48.7%, and 38.9% for patients with an ALBI-P score of 1; 69.7%, 36.6% and 26.1% for patients with an ALBI-P score of 2; and 63.9%, 29.7% and 14.7% for patients with an ALBI-P score of 3 respectively. Statistically significant differences were observed ($P < 0.001$, Figure 1C). The 1-, 3-, and 5-year OS rates were 93.8%, 66.6%, and 52.7% for patients with an ALBI-P score of 1; 90.6%, 59.5% and 42.6% for patients with an ALBI-P score of 2; and 86.2%, 54.4% and 29.3% for patients with an ALBI-P score of 3 respectively ($P < 0.001$, Figure 1D).

3.5. Comparison of the RFS and OS of HCC patients with different ALBI-P scores when stratified by BCLC stage

We performed a subgroup analysis stratified by BCLC stage. Because there were few patients in BCLC stage 0, we combined BCLC stage 0 and BCLC stage A for analysis. As shown in Figure 2, significant differences were observed among patients with different ALBI-P scores, regardless of whether they were BCLC stage 0/A, B or C, for both RFS and OS. In each BCLC stage, patients with a high ALBI-P score had a high incidence of postoperative recurrence and mortality.

3.6. Comparison of predictive capacity when integrating ALBI-P score and BCLC stage

We also compared the prognostic ability of the combination of the ALBI-P score and BCLC stage. As shown in Figure 3A, for predicting postoperative recurrence, the ALBI-P-BCLC score showed the highest AUC (0.681), with a sensitivity of 60.1% and a specificity of 69.7%, followed by the ALBI-BCLC score (0.653, $P_{\text{ALBI-P-BCLC } vs. \text{ ALBI-BCLC}} = 0.002$), PALBI-BCLC score (0.633, $P_{\text{ALBI-P-BCLC } vs. \text{ PALBI-BCLC}} < 0.001$), and BCLC stage (0.632, $P_{\text{ALBI-P-BCLC } vs. \text{ BCLC}} < 0.001$). For predicting postoperative mortality (Figure 3B), the ALBI-P-BCLC score also had the highest AUC (0.723), with a sensitivity of 69.5% and a specificity of 68.2%, followed by the ALBI-BCLC score (0.705, $P_{\text{ALBI-P-BCLC } vs. \text{ ALBI-BCLC}} = 0.003$), BCLC stage (0.683, $P_{\text{ALBI-P-BCLC } vs. \text{ BCLC}} < 0.001$), and PALBI-BCLC score (0.680, $P_{\text{ALBI-P-BCLC } vs. \text{ PALBI-BCLC}} < 0.001$).

4. Discussion

Cirrhosis is often observed in patients with HCC and could also cause poor liver function and CSPH. In the past, investigations have suggested that both liver function and CSPH could adversely influence both short-term and long-term outcomes of patients with HCC following liver resection (*12,13*). Although some studies suggested liver transplantation provided better prognosis than liver resection for HCC patients with CSPH (*14,15*). However, due to the scarcity of liver grafts, many HCC patients with CSPH received liver resection in many centers (*11,15*). In our clinical practice, some HCC patients had poor liver function only or CSPH only. However, some HCC patients may suffer from both poor liver function and CSPH. Unfortunately, there is little information regarding whether incorporating CSPH into ALBI could strengthen its predictive ability. In the current study, we clarified this issue. Patients with both poor liver function and CSPH had a poorer prognosis than those with only one or none of the above-mentioned risk factors.

Johnson and his colleagues introduced the ALBI grade to assess liver function (*4*). Many studies have confirmed that the ALBI grade is better than the Child-Pugh score to assess patients' liver function (*16,17*). The ALBI grade is calculated with total bilirubin and serum albumin, two objective variables that could be easily obtained from laboratory tests. In contrast, the Child-Pugh score uses ascites and hepatic encephalopathy, two subjective parameters that could negatively affect its accuracy. Many studies have also suggested that ALBI grade could predict the outcomes of patients with

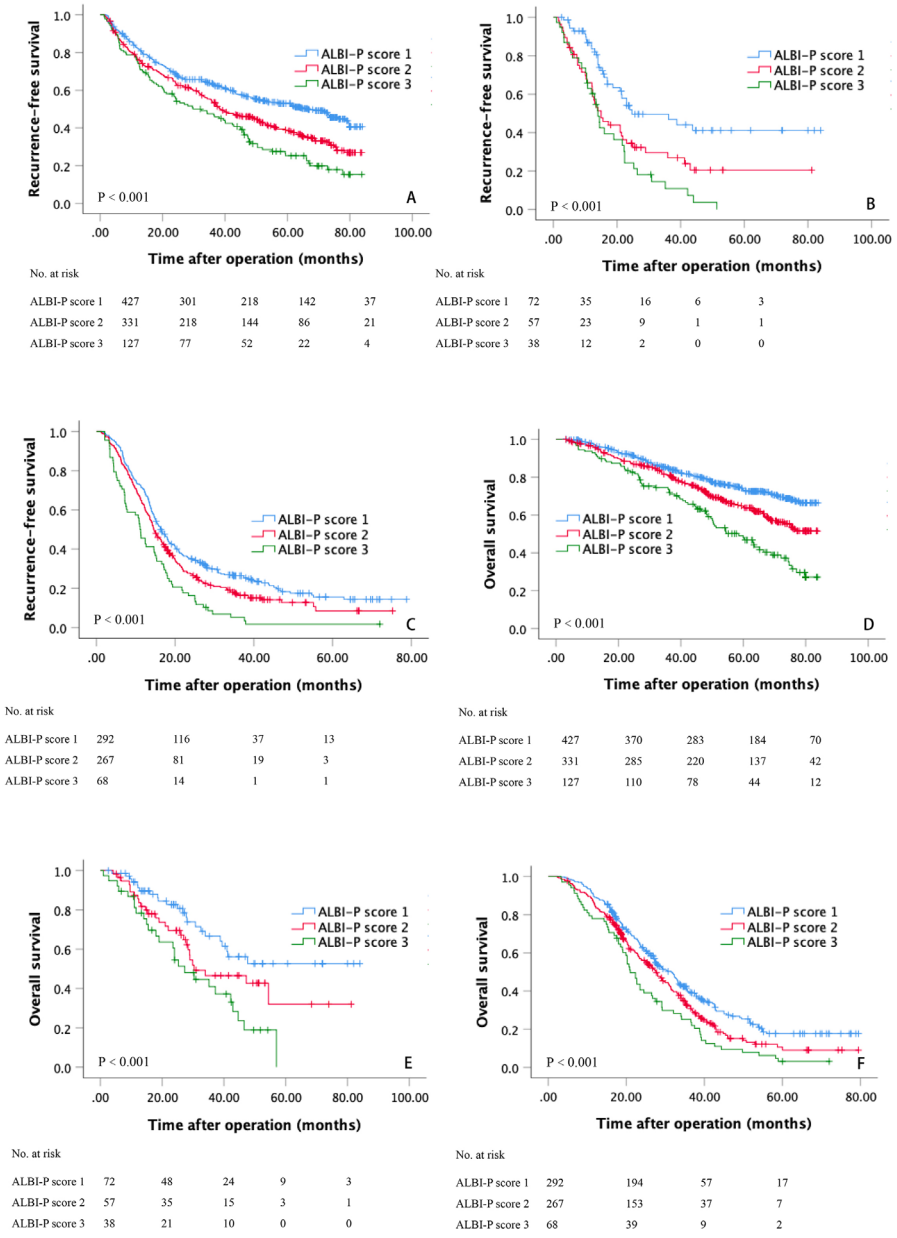

Figure 2. Kaplan-Meier survival plots comparing recurrence-free survival (RFS) and overall survival (OS) in Barcelona Clinic Liver Cancer (BCLC) stage 0/A (A for RFS and D for OS), BCLC stage B (B for RFS and E for OS) and BCLC stage C (C for RFS and F for OS) patients. Patients with high ALBI-P scores showed both poor RFS and OS regardless of BCLC stage.

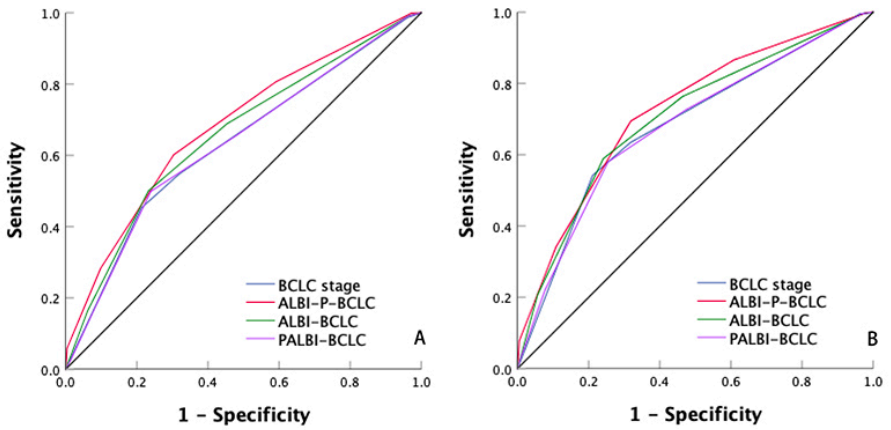

Figure 3. Comparison of the area under the receiver operating characteristic curves of the ALBI-P-BCLC score, ALBI-BCLC score, PALBI-BCLC score and BCLC stage in predicting postoperative recurrence (A) and survival (B).

HCC after liver resection (*12,18,19*). Toyoda *et al.* (*20*) suggested that for post liver resection HCC patients, the overall survival (OS) of those with ALBI grade 1 was approximately two times longer than that of patients with ALBI grade 2, although all patients were in Child-Pugh grade A. Ho *et al.* (*21*) also suggested that ALBI is a surrogate marker for predicting the postoperative recurrence of HCC patients who underwent liver resection. However, CSPH may also be observed in patients with very good liver function. Some authors suggested that failure to incorporate portal hypertension may be a potential weakness of the ALBI grade (*10,22*). Some investigations suggested that PALBI, which integrates platelets, albumin, and bilirubin, could also assess patient liver function and predict the outcomes of HCC patients (*10*). However, in our study, PALBI was not an independent risk factor for RFS or OS, although it showed significance in the univariate analysis. This result suggested that perhaps using scores including CSPH may be better than using a model incorporating platelets to predict HCC patient outcomes.

According to the treatment guidelines for HCC proposed by both the European Association for the Study of the Liver and the American Association for the Study of Liver Diseases, liver resection is not recommended for HCC patients with CSPH, even though the liver function of these patients may be Child-Pugh class A (*2,23*). Previous studies have confirmed that low preoperative platelet counts contribute to a high incidence of postoperative complications and poor long-term survival (*24,25*). Some investigators argued that liver resection may be safely performed in selected HCC patients with portal hypertension (*11,26-28*). However, several meta-analyses confirmed that CSPH could negatively impact the prognosis of HCC patients following liver resection (*29-32*). For instance, Liu *et al.* suggested that compared to those without CSPH, patients with CSPH had a higher incidence of morbidity and 5-year mortality (*30*). A meta-analysis performed by Berzigotti *et al.* (*29*) confirmed that CSPH could increase 3-year and 5-year mortality and clinical decompensation after surgery regardless of the evaluation methods for CSPH. In fact, CSPH can also occur in patients with relatively healthy liver function, such as those in Child-Pugh class A. ALBI can subdivide Child-Pugh grade A liver function. However, previous investigations did not consider the impact of relatively poor liver function on the outcomes of patients with CSPH although they were in Child-Pugh grade A. In this study, our results suggested that the combination of CSPH and high ALBI grade could further adversely affect HCC patient prognosis after liver resection.

Our study also revealed that many unfavorable clinicopathological variables were observed in patients with high ALBI-P scores, such as high NLR and low PNI. Portal hypertension could cause splenomegaly and even hypersplenism, which could result in not only low platelet counts but also low lymphocyte counts. This may be why more patients with high NLR and low PNI were observed in those with high ALBI-P scores. The patient's anticancer response mainly depends on lymphocytes. Accordingly, the anticancer response was impaired in patients with low lymphocyte counts. Moreover, the NLR and PNI were also considered two markers that mirror a patient's systemic inflammatory response (*8*). Many studies have indicated that high NLR and low PNI are associated with a poor systemic inflammatory response and poor prognosis after liver resection (*9,33-35*).

Interestingly, the ALBI-P-BCLC score showed better prognostic ability than the ALBI-BCLC score and BCLC stage. The BCLC staging system is recommended by many associations for staging HCC, including the European Association for the Study of the Liver and the American Association for the Study of Liver Diseases (*2,23*). The BCLC staging system considers liver function to influence the choice of treatments and uses the Child-Pugh score to evaluate liver function. Pinato *et al.* (*18*) confirmed that the ALBI grade offered exact hepatic reserve evaluation across each BCLC stage of HCC. Chan *et al.* (*19*) even suggested that integrating ALBI into the BCLC system could achieve a similar prognostic performance to that of the Child-Pugh score-based BCLC system. However, neither the ALBI-based BCLC nor the Child-Pugh score-based BCLC consider the influence of portal hypertension. For example, if an HCC patient had multiple extrahepatic metastases, Child-Pugh class A liver function and a healthy physical status, he or she would be classified as BCLC stage C. According to the BCLC staging system, oral targeted drugs may be the first choice for this patient. However, if the platelet count of this patient was very low, *e.g.*, 20×10^9/L, it would not be suitable to administer oral targeted drugs to him or her. Accordingly, portal hypertension could also influence the management and prognosis of HCC patients. This may be one potential explanation why integrating the ALBI-P score into the BCLC stage achieved better predictive capacity.

There are also some limitations in this study. This is a single center retrospective study. Therefore, the prognostic performance of the ALBI-P score lacks external validation. Moreover, the ALBI-P score's suitability to predict the prognosis of HCC patients who receive other treatments needs further study. Additionally, in the current study, CSPH as defined used only clinical parameters, rather than using duplexsonography or measurement of hepatic venous pressure gradient. We acknowledge that the current standard for assessing the severity of portal hypertension is the measurement of hepatic venous pressure gradient. However, this is an invasive procedure which is not conventionally used in our clinical practice.

In conclusion, our study suggested that incorporating CSPH into ALBI strengthened its prognostic ability.

The ALBI-P score may serve as a surrogate marker for predicting HCC patient prognosis after liver resection in different BCLC stages. A high ALBI-P score was associated with a high incidence of postoperative recurrence and poor long-term survival.

Funding: This study was supported by grants from the State Key Scientific and Technological Research Programs (2017ZX10203207-003-0020), the National Natural Science Foundation of China (81900576), and the Science and Technological Supports Project of Sichuan Province (2019YJ0149).

Conflict of Interest: The authors have no conflicts of interest to disclose.

References

1. Yang JD, Hainaut P, Gores GJ, Amadou A, Plymoth A, Roberts LR. A global view of hepatocellular carcinoma: trends, risk, prevention and management. Nat Rev Gastroenterol Hepatol. 2019; 16:589-604.
2. European Association for the Study of the Liver. Electronic address eee, European Association for the Study of the L. EASL Clinical Practice Guidelines: Management of hepatocellular carcinoma. J Hepatol. 2018; 69:182-236.
3. Sayiner M, Golabi P, Younossi ZM. Disease Burden of Hepatocellular Carcinoma: A Global Perspective. Dig Dis Sci. 2019; 64:910-917.
4. Johnson PJ, Berhane S, Kagebayashi C, *et al.* Assessment of liver function in patients with hepatocellular carcinoma: a new evidence-based approach-the ALBI grade. J Clin Oncol 2015; 33:550-558.
5. Na SK, Yim SY, Suh SJ, Jung YK, Kim JH, Seo YS, Yim HJ, Yeon JE, Byun KS, Um SH. ALBI versus Child-Pugh grading systems for liver function in patients with hepatocellular carcinoma. J Surg Oncol. 2018; 117:912-921.
6. Wen T, Jin C, Facciorusso A, *et al.* Multidisciplinary management of recurrent and metastatic hepatocellular carcinoma after resection: an international expert consensus. Hepatobiliary Surg Nutr. 2018; 7:353-371.
7. Li C, Shen JY, Zhang XY, Peng W, Wen TF, Yang JY, Yan LN. Predictors of Futile Liver Resection for Patients with Barcelona Clinic Liver Cancer Stage B/C Hepatocellular Carcinoma. J Gastrointest Surg. 2018; 22:496-502.
8. Yamamura K, Sugimoto H, Kanda M, Yamada S, Nomoto S, Nakayama G, Fujii T, Koike M, Fujiwara M, Kodera Y. Comparison of inflammation-based prognostic scores as predictors of tumor recurrence in patients with hepatocellular carcinoma after curative resection. J Hepatobiliary Pancreat Sci. 2014; 21:682-688.
9. Chan AW, Chan SL, Wong GL, Wong VW, Chong CC, Lai PB, Chan HL, To KF. Prognostic Nutritional Index (PNI) Predicts Tumor Recurrence of Very Early/Early Stage Hepatocellular Carcinoma After Surgical Resection. Ann Surg Oncol. 2015; 22:4138-4148.
10. Liu PH, Hsu CY, Hsia CY, Lee YH, Chiou YY, Huang YH, Lee FY, Lin HC, Hou MC, Huo TI. ALBI and PALBI grade predict survival for HCC across treatment modalities and BCLC stages in the MELD Era. Journal of gastroenterology and hepatology. 2017; 32:879-886.
11. Takemura N, Aoki T, Hasegawa K, Kaneko J, Arita J, Akamatsu N, Makuuchi M, Kokudo N. Hepatectomy for hepatocellular carcinoma after perioperative management of portal hypertension. Br J Surg. 2019; 106:1066-1074.
12. Ho SY, Hsu CY, Liu PH, Hsia CY, Lei HJ, Huang YH, Ko CC, Su CW, Lee RC, Hou MC, Huo TI. Albumin-bilirubin grade-based nomogram of the BCLC system for personalized prognostic prediction in hepatocellular carcinoma. Liver Int. 2020; 40:205-214.
13. Choi GH, Park JY, Hwang HK, Kim DH, Kang CM, Choi JS, Park YN, Kim DY, Ahn SH, Han KH, Chon CY, Lee WJ. Predictive factors for long-term survival in patients with clinically significant portal hypertension following resection of hepatocellular carcinoma. Liver Int. 2011; 31:485-493.
14. Li Y, Ruan DY, Jia CC, Zhao H, Wang GY, Yang Y, Jiang N. Surgical resection versus liver transplantation for hepatocellular carcinoma within the Hangzhou criteria: a preoperative nomogram-guided treatment strategy. Hepatobiliary Pancreat Dis Int. 2017; 16:480-486.
15. Lee WC, Lee CF, Cheng CH, Wu TJ, Chou HS, Wu TH, Soong RS, Chan KM, Yu MC, Chen MF. Outcomes of liver resection for hepatocellular carcinoma in liver transplantation era. Eur J Surg Oncol. 2015; 41:1144-1152.
16. Zou H, Yang X, Li QL, Zhou QX, Xiong L, Wen Y. A Comparative Study of Albumin-Bilirubin Score with Child-Pugh Score, Model for End-Stage Liver Disease Score and Indocyanine Green R15 in Predicting Posthepatectomy Liver Failure for Hepatocellular Carcinoma Patients. Dig Dis. 2018; 36:236-243.
17. Wang YY, Zhong JH, Su ZY, Huang JF, Lu SD, Xiang BD, Ma L, Qi LN, Ou BN, Li LQ. Albumin-bilirubin versus Child-Pugh score as a predictor of outcome after liver resection for hepatocellular carcinoma. Br J Surg. 2016; 103:725-734.
18. Pinato DJ, Sharma R, Allara E, *et al.* The ALBI grade provides objective hepatic reserve estimation across each BCLC stage of hepatocellular carcinoma. J Hepatol. 2017; 66:338-346.
19. Chan AW, Kumada T, Toyoda H, Tada T, Chong CC, Mo FK, Yeo W, Johnson PJ, Lai PB, Chan AT, To KF, Chan SL. Integration of albumin-bilirubin (ALBI) score into Barcelona Clinic Liver Cancer (BCLC) system for hepatocellular carcinoma. J Gastroenterol Hepatol. 2016; 31:1300-1306.
20. Toyoda H, Lai PB, O'Beirne J, *et al.* Long-term impact of liver function on curative therapy for hepatocellular carcinoma: application of the ALBI grade. Br J Cancer. 2016; 114:744-750.
21. Ho SY, Hsu CY, Liu PH, Hsia CY, Su CW, Huang YH, Hou MC, Huo TI. Albumin-bilirubin (ALBI) grade-based nomogram to predict tumor recurrence in patients with hepatocellular carcinoma. Eur J Surg Oncol. 2019; 45:776-781.
22. Huo TI. ALBI grade as a new player in hepatocellular carcinoma. J Chin Med Assoc. 2019; 82:1.
23. Heimbach JK, Kulik LM, Finn RS, Sirlin CB, Abecassis MM, Roberts LR, Zhu AX, Murad MH, Marrero JA. AASLD guidelines for the treatment of hepatocellular carcinoma. Hepatology. 2018; 67:358-380.
24. Tomimaru Y, Eguchi H, Gotoh K, Kawamoto K, Wada H, Asaoka T, Noda T, Yamada D, Ogawa H, Umeshita K,

Nagano H, Doki Y, Mori M. Platelet count is more useful for predicting posthepatectomy liver failure at surgery for hepatocellular carcinoma than indocyanine green clearance test. J Surg Oncol. 2016; 113:565-569.
25. Maithel SK, Kneuertz PJ, Kooby DA, Scoggins CR, Weber SM, Martin RC, 2nd, McMasters KM, Cho CS, Winslow ER, Wood WC, Staley CA, 3rd. Importance of low preoperative platelet count in selecting patients for resection of hepatocellular carcinoma: a multi-institutional analysis. J Am Coll Surg. 2011; 212:638-648; discussion 648-650.
26. Jang CW, Kwon HJ, Kong H, Ha H, Han YS, Chun JM, Kim SG, Hwang YJ. Impact of clinically significant portal hypertension on surgical outcomes for hepatocellular carcinoma in patients with compensated liver cirrhosis: a propensity score matching analysis. Ann Hepatobiliary Pancreat Surg. 2016; 20:159-166.
27. Ohkubo T, Midorikawa Y, Nakayama H, Moriguchi M, Aramaki O, Yamazaki S, Higaki T, Takayama T. Liver resection of hepatocellular carcinoma in patients with portal hypertension and multiple tumors. Hepatol Res. 2018; 48:433-441.
28. Lim C, Osseis M, Lahat E, Doussot A, Sotirov D, Hemery F, Lanteri-Minet M, Feray C, Salloum C, Azoulay D. Safety of laparoscopic hepatectomy in patients with hepatocellular carcinoma and portal hypertension: interim analysis of an open prospective study. Surg Endosc. 2019; 33:811-820.
29. Berzigotti A, Reig M, Abraldes JG, Bosch J, Bruix J. Portal hypertension and the outcome of surgery for hepatocellular carcinoma in compensated cirrhosis: a systematic review and meta-analysis. Hepatology. 2015; 61:526-536.
30. Liu J, Zhang H, Xia Y, Yang T, Gao Y, Li J, Wu Y, Shen F. Impact of clinically significant portal hypertension on outcomes after partial hepatectomy for hepatocellular carcinoma: a systematic review and meta-analysis. HPB (Oxford). 2019; 21:1-13.
31. Choi SB, Kim HJ, Song TJ, Ahn HS, Choi SY. Influence of clinically significant portal hypertension on surgical outcomes and survival following hepatectomy for hepatocellular carcinoma: a systematic review and meta-analysis. J Hepatobiliary Pancreat Sci. 2014; 21:639-647.
32. Tang YH, Zhu WJ, Wen TF. Influence of clinically significant portal hypertension on hepatectomy for hepatocellular carcinoma: a meta-analysis. Asian Pac J Cancer Prev. 2014; 15:1649-1654.
33. Pinato DJ, North BV, Sharma R. A novel, externally validated inflammation-based prognostic algorithm in hepatocellular carcinoma: the prognostic nutritional index (PNI). Br J Cancer. 2012; 106:1439-1445.
34. Shiraki T, Ishizuka M, Kubota K, Kato M, Matsumoto T, Mori S, Shimizu T, Aoki T. An elevated neutrophil-to-lymphocyte ratio predicts a poor postoperative survival in primary hepatocellular carcinoma patients with a normal preoperative serum level of alpha-fetoprotein. Surg Today. 2019; 49:661-669.
35. Li C, Wen TF, Yan LN, Li B, Wang WT, Yang JY, Xu MQ. Postoperative neutrophil-to-lymphocyte ratio plus platelet-to-lymphocyte ratio predicts the outcomes of hepatocellular carcinoma. J Surg Res. 2015; 198:73-79.

Received February 8, 2021; Revised February 20, 2021; Accepted February 22, 2021.

*Address correspondence to:
Chuan Li, Department of Liver Surgery, West China Hospital of Sichuan University, Chengdu 610041, Sichuan, China.
E-mail: lichuan@scu.edu.cn

Released online in J-STAGE as advance publication February 24, 2021.

Brief Report

DOI: 10.5582/bst.2020.03399

Cisatracurium attenuates LPS-induced modulation of MMP3 and junctional protein expression in human microvascular endothelial cells

Rana W. Kadry, Mir S. Adil, Andrea Sikora Newsome*, Payaningal R. Somanath*

Clinical and Experimental Therapeutics, University of Georgia, and Charlie Norwood VA Medical Center, Augusta, GA, USA.

SUMMARY Acute respiratory distress syndrome (ARDS) is a life-threatening form of acute lung injury (ALI) associated with hypoxemic lung damage and inflammation. Matrix metalloproteinase protein-3 (MMP3 or Stromelysin-1) is known to promote vascular injury in ALI/ARDS. Cisatracurium, a nicotinic neuromuscular blocker, is used in ARDS patients to decrease mechanical ventilator dyssynchrony, increase oxygenation, and improve mortality. However, the magnitude and the underlying mechanisms of these potential benefits of cisatracurium remains unclear. We investigated the effect of cisatracurium on lipopolysaccharide-induced MMP3 expression in human microvascular endothelial cells. In our results, cisatracurium treatment significantly decreased LPS-induced MMP3 expression and increased expression of cell junction proteins such as vascular endothelial cadherin (VE-cadherin) and claudin-5.

Keywords Cisatracurium, MMP3, stromelysin-1, lipopolysaccharide, cell junction

1. Introduction

Acute respiratory distress syndrome (ARDS) results in life-threatening hypoxemia secondary to lung injury from diffuse alveolar damage and subsequent edema (*1*). A myriad of clinical trials have been conducted to develop strategies to manage ARDS patients with minimal success (*2*), and the 2018 guidelines for ARDS management recommend only supportive care treatments (*e.g.*, mechanical ventilation) (*3*). Neuromuscular blocking agents (NMBAs) are used in supportive care to decrease patient-ventilator dyssynchrony (and the associated lung damage) in mechanically ventilated ARDS patients (*4*). The most common NMBA used in ARDS is cisatracurium as it has been evaluated in two large-scale clinical trials (ACURASYS and ROSE) (*5-7*).

At the cellular level, the exudative stage of ARDS results from the extensive damage to the alveolar-capillary unit (*8*), which in turn, results in neutrophil infiltration and edema (*9*). Hence, preventing injury to the alveolar-capillary unit may be a potential strategy to halt ARDS disease progression. We have demonstrated the integral role of the Akt pathway in endothelial-barrier protection (*10,11*), which acts by removing the transcriptional suppression by FoxO and β-catenin necessary for barrier function (*11-13*). Inhibition of the Akt pathway resulted in the reduced expression of tight-junction (TJ) proteins, mainly claudin-5 (*14*) in the endothelial cells and the lung blood vessels, leading to lung injury and edema (*15*) and ultimately endothelial-to-mesenchymal transition and lung scarring (*16*). Apart from the transcriptional suppression of TJ proteins, activated FoxO was also observed to increase the expression of matrix metalloproteinases-3 (MMP-3/stromelysin-1) (*15*) a protease previously known to break up the junctional protein complexes (*17*). The potential therapeutic role of MMP3 was further confirmed with increased expression and activity of MMP3 in the LPS-injured lungs and bronchoalveolar lavage fluid (BALF) in mice (*15*) and ARDS patient plasma samples (*18*). In the current study, we investigated the direct effect of cisatracurium to suppress LPS-induced MMP3 expression in human microvascular endothelial cells.

2. Materials and Methods

2.1. Cell culture

Human dermal (Telomerase-immortalized) microvascular ECs (HMECs) (CRL-4025; ATCC, Manassas, VA, USA) were maintained in EC Basal Medium-2 with a Growth Medium-2 Bullet Kit (Lonza; Walkersville, MD, USA). Cells were maintained in a humidified 5% CO_2 incubator at 37°C and routinely passaged when 80-90% confluent. Cisatracurium (cat. No S2113, Selleckchem) was reconstituted according to the manufacturer's protocol.

Cells were treated with 100 ng/mL LPS and different doses of cisatracurium 0.32, 0.64, and 1.28 μM and PBS (vehicle), respectively, in a 5% serum-containing medium for 24 hours. The optimal doses of cisatracurium were determined based on a similar study performed previously (*19*).

2.2. Western blot analysis

Western analysis was performed as described previously (*20*). Cell lysates were prepared using complete lysis buffer (EMD Millipore, San Diego, CA) with protease and phosphatase inhibitor cocktails (Roche Diagnostics, Indianapolis, IN). Protein quantification was performed using DC protein assay from Bio-Rad (Hercules, and CA). Western blot analysis was performed as described previously (*21,22*). Antibodies used include stromelysin1 (cat. No. 14351-S) dilution 1:1,000 in milk, vascular endothelial cadherin (VE-cadherins; cat No. 2158) dilution 1:1,000 in BSA, P-P38 MAPK (cat No. 9112-S) dilution 1:1,000 in BSA, T-P38MAPK (cat No. 9212-S) dilution 1:1,000 in BSA, P-SRC Tyr-416 (cat No. 6943-S) dilution 1:1,000 in BSA and T-SRC (cat No. 2109-S) dilution 1:1,000 in BSA all from Cell Signaling Technology (Danvers, MA). β-actin (dilution in milk, primary antibodies 1:10,000 and secondary antibodies 1:20,000) from Sigma (St. Louis, MO) and Claudin-5 antibodies (cat No. ab15106) 1:1,000 and secondary antibodies 1:5,000 dilution in milk from Abcam (Cambridge, MA). Band densitometry was done using NIH Image J software.

2.3. Immunofluorescence staining

Immunofluorescent staining of HMEC monolayers was performed using the 8-well chamber slides as described previously (*23*). Cells were then washed twice with PBS, fixed using 2% paraformaldehyde for 30 min, permeabilized with 0.1% Triton X-100 for 15 min, and blocked with 4% BSA in sterile PBS. Cell monolayers were then incubated with antibody against VE-cadherin (1:100, Catalog# 2158S, Rabbit antibody, Cell Signaling Technology, Danvers, MA) at 4°C overnight. Immunofluorescence was revealed using Alexa Fluor 488 secondary antibody (1:1,000, Goat anti-Rabbit, Life Technologies, Grand Island, NY). Cells were mounted onto a glass slide using DAPI containing mounting medium (Vector Laboratories). Samples were observed under KEYENCE Fluorescence Microscope BZ-X800 (Itasca, IL). Controls were performed by omitting primary antibodies and all controls gave negative results with no detectable non-specific labeling.

2.4. Statistical analysis

All the data are presented as mean ± SD and were calculated from multiple independent experiments performed in triplicates. The 'n' value for each figure implies the multiple independent experiments performed. All the data were analyzed by parametric testing using the Student's unpaired *t*-test or one-way ANOVA, followed by the posthoc test using the GraphPad Prism 6.01 software. Data with $p < 0.05$ were considered significant.

3. Results and Discussion

3.1. Treatment with cisatracurium reduced LPS-induced MMP3 expression in HMECs

Our results indicated a significantly higher MMP3 expression in HMECs with LPS treatment for 24 hours, which was blunted by co-treatment with cisatracurium (Figures 1A and 1B) indicating that cisatracurium reduces LPS-induced MMP3 expression in HMECs.

3.2. Cisatracurium inhibits LPS-induced Src and P38MAPK phosphorylation in HMECs

Since Src has been demonstrated to break up adherens junction (AJ) cell interactions through the cadherins (*24*), we determined how LPS and cisatracurium treatment affect Src activating phosphorylation at Tyrosine-416 residue. In HMECs, treatment with LPS for 24 hours resulted in increased pY416Src, which was significantly inhibited by co-treatment with cisatracurium (Figures 1A and 1C), thus indicating that cisatracurium protects the cell-barriers by inhibiting Src activity.

Since P38MAPK is a stress and inflammation associated kinase, we next determined if cisatracurium protects the endothelial cells from cell stress associated with pro-inflammatory stimuli such as the bacterial LPS. Our results indicated that although LPS stimulation of HMECs modestly increased phosphorylated P38MAPK, the effect was not reversed upon co-treatment with cisatracurium, except at a lower dose (Figures 1A and 1D). Overall, our data suggested that cisatracurium does not affect P38 MAPK activity in endothelial cells.

3.3. Cisatracurium rescued LPS-induced loss of claudin-5 and VE-cadherin

To determine if cisatracurium could preserve AJ and TJ complexes in HMECs, we treated them with LPS alone or in combination with cisatracurium for 24 hours and subjected them to the Western analysis of VE-cadherin and claudin-5. Our analysis indicated that 24 hours of treatment with LPS significantly reduced VE-cadherin expression in HMECs, which was reversed upon co-treatment with cisatracurium (Figures 2A and 2B). Akin to VE-cadherin, treatment with LPS significantly reduced claudin-5 expression in HMECs, which was reversed upon co-treatment with cisatracurium (Figures 2A and 2C). Together, these results indicated that cisatracurium

modulates AJ and TJ protein expression in endothelial cells.

3.4. Cisatracurium preserves HMEC monolayer integrity upon LPS insult

Immunofluorescence staining on HMEC monolayer in LPS alone or combination with cisatracurium for 24 hours was performed to determine the sub-cellular compartment involved in the VE-cadherin alterations witnessed at the protein level (Figure 2A and 2B). The drug was used at a dose of 0.64 μM since it resulted in a significant increase in protein expression on Western blot analysis (Figure 3). As anticipated, we observed disruption of VE-cadherin distribution in HMEC monolayers by LPS insult thereby disturbing the continuity of the AJ bands in the cell junctions. Treatment with cisatracurium, however, prevented the LPS-induced disruption of VE-cadherin cell-cell contacts to preserve cell cohesion thus maintaining integrity. These findings confirm the beneficial effects of cisatracurium in HMECs during LPS-induced injury.

NMBA, particularly cisatracurium, is recommended by the guidelines for severe ARDS and is thought to improve mortality by optimizing pulmonary airflow mechanics and oxygenation (*3,5*). Cisatracurium has also been shown to exert anti-inflammatory effects and may play a role in mitigating the deleterious effects of inflammation in the early stages of ARDS, with support largely based

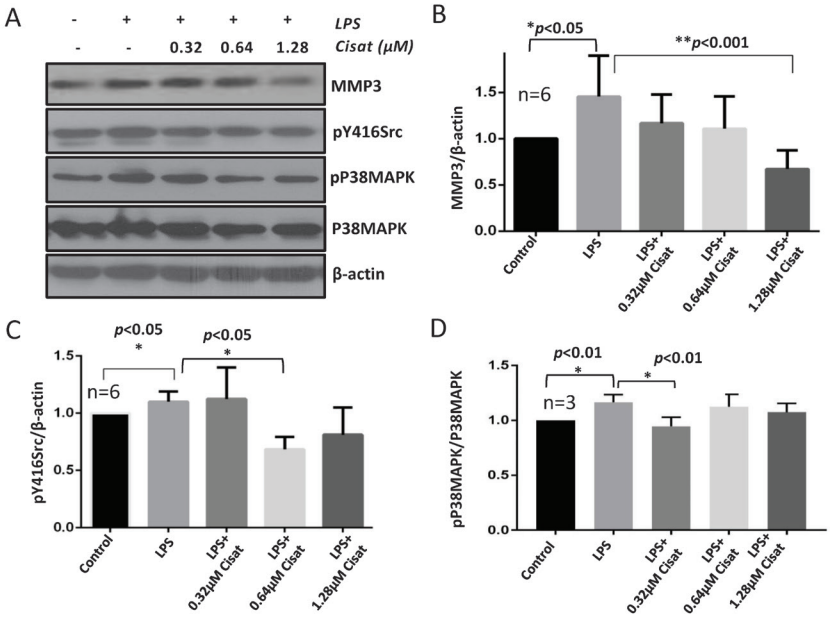

Figure 1. Cisatracurium inhibited LPS-induced increase in MMP3 expression and Src phosphorylation. (A-B) Representative Western blot images and a bar graph with band densitometry analysis indicating increased MMP3 expression in HMECs with LPS treatment and its reversal by co-treatment with cisatracurium after 24 hours of incubation. **(C)** Bar graph with band densitometry analysis indicating increased pY416Src expression in HMECs with LPS treatment and its reversal by co-treatment with cisatracurium after 24 hours of incubation. **(D)** Bar graph with band densitometry analysis indicating a modest increase in pP38MAPK expression in HMECs with LPS treatment and its partial inhibition by co-treatment with a very low dose of cisatracurium after 24 hours of incubation. Data are shown as Mean + SD.

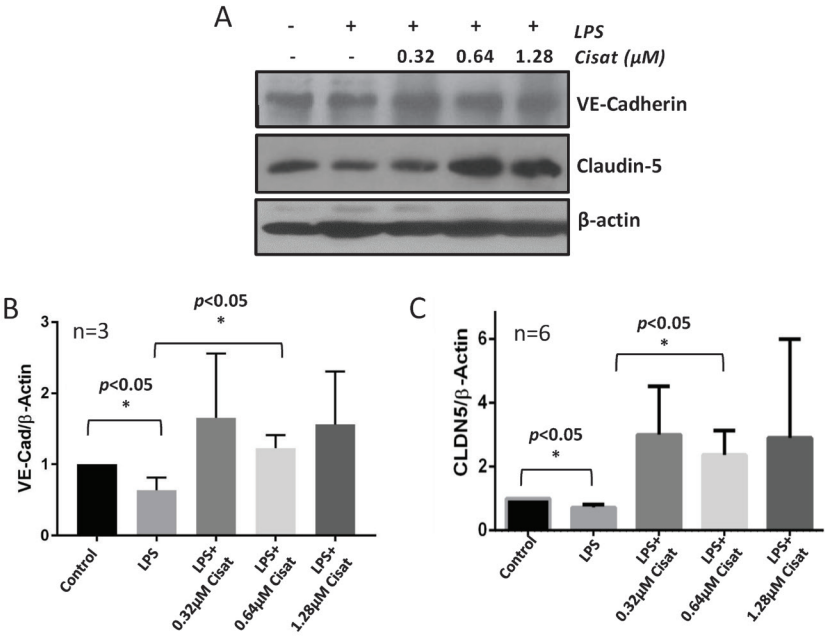

Figure 2. Cisatracurium prevented LPS-induced loss of VE-cadherin and claudin-5 in HMECs. (A) Representative Western blot images showing reduced VE-cadherin and claudin-5 expressions in HMECs with LPS treatment and its reversal by co-treatment with cisatracurium after 24 hours of incubation. **(B)** Bar graph with band densitometry analysis indicating reduced VE-cadherin expression in HMECs with LPS treatment and its reversal by co-treatment with cisatracurium after 24 hours of incubation. **(C)** Bar graph with band densitometry analysis indicating reduced claudin-5 expression in HMECs with LPS treatment and reversal by co-treatment with cisatracurium after 24 hours of incubation. Data are shown as Mean + SD.

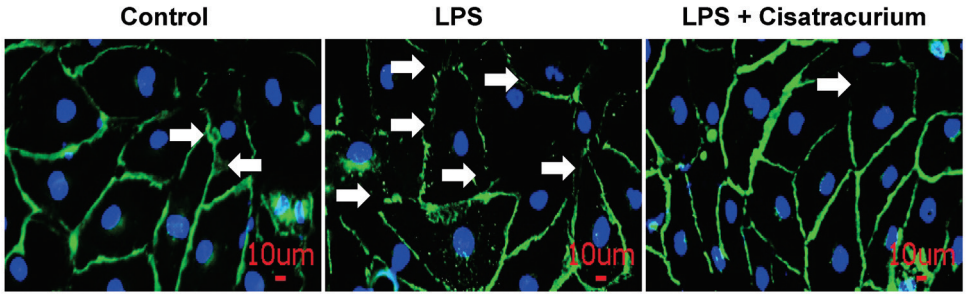

Figure 3. Representative images of VE-cadherin staining in human microvascular endothelial cells post LPS treatment alone, or in combination with cisatracurium at 24 hours.

on the results of the ACURASYS study, which showed reduced 90-day mortality (*6,7,25-27*). In 2019, the efficacy of NMBA in ARDS was called into question by the Reevaluation of Systemic Early Neuromuscular Blockade (ROSE) trial, which evaluated cisatracurium versus no cisatracurium in moderate-to-severe ARDS and observed no difference in 90-day mortality (*6*). These conflicting results have prompted the scientific community to evaluate the potential confounders in these studies and further investigate the molecular mechanisms of cisatracurium-induced effects. Our study demonstrated the ability of cisatracurium to reduce the expression of LPS-induced MMP3 by the endothelial cells. Although the direct effects of cisatracurium on the endothelial barrier protein expression were modest, these were significant.

Preclinical studies in our laboratory demonstrated that ARDS/ALI was associated with elevated expression and activity of MMP3 (*15*), a matricellular protease that is known to breakdown the endothelial barrier junctions and promote vascular permeability (*28*). MMP3 is also known to have an essential role in the innate immunity and inflammatory response, and cause degradation for the extracellular matrix (ECM) (*17*). Several inflammatory lung diseases such as ARDS, asthma, and pulmonary fibrosis are characterized by an increase in the expression of one or more of the MMPs (*29,30*). Recent studies from our laboratory have identified that pharmacological inhibition of MMP3 or its upstream regulator, FoxO transcription factors, has been demonstrated to reverse LPS-induced lung injury and edema (*15*). The studies also demonstrated elevated MMP3 expression and activity in LPS-administered mouse BALF. Another study demonstrated increased MMP3 expression/activity in the plasma samples collected from human ARDS patients compared to healthy subjects (*18*). Increased MMP3 expression was correlated with reduced expression of claudin-5 in endothelial cells and mouse lung lysates, and increased neutrophil activity in the lungs (*15*) indicating the importance of MMP3 in the promotion of lung inflammation and ARDS disease progression. The disruption of the ECM by MMPs intra- and intercellularly in the ALI experimental model has also reported disruption of the TJ and AJ complexes that preserve the lung vascular integrity (*31*). Studies conducted on cisatracurium in different disease models have shown its effects on decreasing inflammation and cell migration involving various pathways (*19,32*).

In the current study, we investigated the effect of cisatracurium to modulate the pro-inflammatory and cell-barrier modulating pathways in HMECs and determined its efficacy to inhibit the injury-response elicited by bacterial LPS treatment. The ability of cisatracurium to reverse the LPS-induced increase in MMP3 expression and Src phosphorylation and preventing the loss of AJ protein VE-cadherin and TJ protein claudin-5 in HMECs are indications of its potential benefits in preventing pathological vascular permeability and inflammation. However, the fact that cisatracurium had no direct effect on the activity of pro-inflammatory P38MAPK suggests that cisatracurium has no direct effect on the HMECs in reducing the inflammatory response. However, the study has limitations as it has been conducted in individual cell lines *in vitro* that a clear understanding of the collective effect and molecular mechanisms of cisatracurium in a disease model is lacking. Further studies will be required to fully understand the benefits and mechanisms of cisatracurium in the treatment of ARDS patients.

Funding: Funds were provided by the NHLBI (R01HL103952), NCATS (UL1TR002378), Georgia-CTSA (KL2TR002381), and Wilson Pharmacy Foundation (intramural). This work has been accomplished using the resources and facilities at the VA Medical Center in Augusta, GA.

Conflict of Interest: Authors declare that there are no financial or other conflicts of interest exist.

References

1. Matthay MA, Zemans RL, Zimmerman GA, Arabi YM, Beitler JR, Mercat A, Herridge M, Randolph AG, Calfee CS. Acute respiratory distress syndrome. Nat Rev Dis Primers. 2019; 5:18.
2. Cepkova M, Matthay MA. Pharmacotherapy of acute lung injury and the acute respiratory distress syndrome. J Intensive Care Med. 2006; 21:119-143.

3. Papazian L, Aubron C, Brochard L, *et al*. Formal guidelines: management of acute respiratory distress syndrome. Ann Intensive Care. 2019; 9:69.
4. Hall JB. Point: Should paralytic agents be routinely used in severe ARDS? Yes. Chest. 2013; 144:1440-1442.
5. Murray MJ, DeBlock H, Erstad B, *et al*. Clinical practice guidelines for sustained neuromuscular blockade in the adult critically ill patient. Crit Care Med. 2016; 44:2079-2103.
6. National Heart L, Blood Institute PCTN, Moss M, *et al*. Early neuromuscular blockade in the acute respiratory distress syndrome. N Engl J Med. 2019; 380:1997-2008.
7. Papazian L, Forel JM, Gacouin A, *et al*. Neuromuscular blockers in early acute respiratory distress syndrome. N Engl J Med. 2010; 363:1107-1116.
8. Herrero R, Sanchez G, Lorente JA. New insights into the mechanisms of pulmonary edema in acute lung injury. Ann Transl Med. 2018; 6:32.
9. Han S, Mallampalli RK. The acute respiratory distress syndrome: from mechanism to translation. J Immunol. 2015; 194:855-860.
10. Chen J, Somanath PR, Razorenova O, Chen WS, Hay N, Bornstein P, Byzova TV. Akt1 regulates pathological angiogenesis, vascular maturation and permeability *in vivo*. Nat Med. 2005; 11:1188-1196.
11. Gao F, Sabbineni H, Artham S, Somanath PR. Modulation of long-term endothelial-barrier integrity is conditional to the cross-talk between Akt and Src signaling. J Cell Physiol. 2017; 232:2599-2609.
12. Alwhaibi A, Verma A, Adil MS, Somanath PR. The unconventional role of Akt1 in the advanced cancers and in diabetes-promoted carcinogenesis. Pharmacol Res. 2019; 145:104270.
13. Adil MS, Narayanan SP, Somanath PR. Cell-cell junctions: structure and regulation in physiology and pathology. Tissue Barriers. 2020;1848212.
14. Gao F, Artham S, Sabbineni H, Al-Azayzih A, Peng XD, Hay N, Adams RH, Byzova TV, Somanath PR. Akt1 promotes stimuli-induced endothelial-barrier protection through FoxO-mediated tight-junction protein turnover. Cell Mol Life Sci. 2016; 73:3917-3933.
15. Artham S, Gao F, Verma A, Alwhaibi A, Sabbineni H, Hafez S, Ergul A, Somanath PR. Endothelial stromelysin1 regulation by the forkhead box-O transcription factors is crucial in the exudative phase of acute lung injury. Pharmacol Res. 2019; 141:249-263.
16. Sabbineni H, Verma A, Artham S, Anderson D, Amaka O, Liu F, Narayanan SP, Somanath PR. Pharmacological inhibition of beta-catenin prevents EndMT *in vitro* and vascular remodeling *in vivo* resulting from endothelial Akt1 suppression. Biochem Pharmacol. 2019; 164:205-215.
17. Nagase H, Visse R, Murphy G. Structure and function of matrix metalloproteinases and TIMPs. Cardiovasc Res. 2006; 69:562-573.
18. Artham S, Verma A, Newsome AS, Somanath PR. Patients with acute respiratory distress syndrome exhibit increased stromelysin1 activity in the blood samples. Cytokine. 2020; 131:155086.
19. Fanelli V, Morita Y, Cappello P, Ghazarian M, Sugumar B, Delsedime L, Batt J, Ranieri VM, Zhang H, Slutsky AS. Neuromuscular blocking agent cisatracurium attenuates lung injury by inhibition of nicotinic acetylcholine receptor-alpha1. Anesthesiology. 2016; 124:132-140.
20. Abdalla M, Sabbineni H, Prakash R, Ergul A, Fagan SC, Somanath PR. The Akt inhibitor, triciribine, ameliorates chronic hypoxia-induced vascular pruning and TGFbeta-induced pulmonary fibrosis. Br J Pharmacol. 2015; 172:4173-4188.
21. Sabbineni H, Verma A, Somanath PR. Isoform-specific effects of transforming growth factor beta on endothelial-to-mesenchymal transition. J Cell Physiol. 2018; 233:8418-8428.
22. Goc A, Al-Azayzih A, Abdalla M, Al-Husein B, Kavuri S, Lee J, Moses K, Somanath PR. P21 activated kinase-1 (Pak1) promotes prostate tumor growth and microinvasion *via* inhibition of transforming growth factor beta expression and enhanced matrix metalloproteinase 9 secretion. J Biol Chem. 2013; 288:3025-3035.
23. Gao F, Al-Azayzih A, Somanath PR. Discrete functions of GSK3alpha and GSK3beta isoforms in prostate tumor growth and micrometastasis. Oncotarget. 2015; 6:5947-5962.
24. Dejana E, Orsenigo F, Lampugnani MG. The role of adherens junctions and VE-cadherin in the control of vascular permeability. J Cell Sci. 2008; 121:2115-2122.
25. Forel JM, Roch A, Marin V, Michelet P, Demory D, Blache JL, Perrin G, Gainnier M, Bongrand P, Papazian L. Neuromuscular blocking agents decrease inflammatory response in patients presenting with acute respiratory distress syndrome. Crit Care Med. 2006; 34:2749-2757.
26. Gainnier M, Roch A, Forel JM, Thirion X, Arnal JM, Donati S, Papazian L. Effect of neuromuscular blocking agents on gas exchange in patients presenting with acute respiratory distress syndrome. Crit Care Med. 2004; 32:113-119.
27. Paton WD. Mode of action of neuromuscular blocking agents. Br J Anaesth. 1956; 28:470-480.
28. McKeown S, Richter AG, O'Kane C, McAuley DF, Thickett DR. MMP expression and abnormal lung permeability are important determinants of outcome in IPF. Eur Respir J. 2009; 33:77-84.
29. Ito JT, Lourenco JD, Righetti RF, Tiberio I, Prado CM, Lopes F. Extracellular matrix component remodeling in respiratory diseases: What has been found in clinical and experimental studies? Cells. 2019; 8:342.
30. Vandenbroucke RE, Dejonckheere E, Libert C. A therapeutic role for matrix metalloproteinase inhibitors in lung diseases? Eur Respir J. 2011; 38:1200-1214.
31. Schlingmann B, Molina SA, Koval M. Claudins: Gatekeepers of lung epithelial function. Semin Cell Dev Biol. 2015; 42:47-57.
32. Yabasin IB, Sanches JGP, Ibrahim MM, Huidan J, Williams W, Lu ZL, Wen Q. Cisatracurium retards cell migration and invasion upon upregulation of p53 and inhibits the aggressiveness of colorectal cancer. Front Physiol. 2018; 9:941.

Received November 2, 2020; Revised January 30, 2021; Accepted February 9, 2021.

**Address correspondence to:*
Payaningal R. Somanath and Andrea Sikora Newsome, College of Pharmacy, University of Georgia, Augusta, GA 30912, USA.
E-mail: sshenoy@augusta.edu (Somanath PR); sikora@uga.edu (Newsome AS)

Released online in J-STAGE as advance publication February 23, 2021.

Communication

DOI: 10.5582/bst.2021.01056

Transitional care during COVID-19 pandemic in Japan: Calls for new strategies to integrate traditional approaches with information and communication technologies

Yuka Sumikawa*, Noriko Yamamoto-Mitani

Department of Community Health Nursing, Division of Health Sciences and Nursing, Graduate School of Medicine, The University of Tokyo, Bunkyo-ku, Tokyo, Japan.

SUMMARY Transitional care is indispensable in successfully transitioning patients from hospital to home and preventing adverse events during this process. There were restricted services in several hospitals for minimizing the spread of COVID-19. Therefore, hospitals could not provide adequate transitional care that possibly resulted in poor post-discharge outcomes in patients. Some hospitals have now combined infection prevention with face-to-face opportunities, *i.e*., requiring reservations for transitional care consultation and restricting pre-discharge conferences. Several hospitals started providing pre-discharge conferences using apps, where patients/family caregivers and care teams could have face-to-face discussions about medical and nursing care plans, goals, and preferences. However, building a relationship between patient/family and medical/nursing staff and providing decision-making, psychological support, and risk assessment generally performed in person are still in demand. New hybrid strategies should be developed and evaluated to provide transitional care while using online systems and minimal face-to-face support during the pandemic.

Keywords COVID-19, discharge, transitional care

1. Introduction

Transitional care is indispensable to successfully guide patients from hospital to home and to prevent adverse events in this process, making it essential for efficient medical and nursing practice (*1,2*). One of the most important components of excellent transitional care is active involvement of patients and family caregivers (*1,3,4*). Previous studies show that their involvement has improved physical and mental outcomes for the person who is discharged from the hospital and improves continuity of care (*5*).

In the traditional transitional care system, family caregivers frequently visited the hospital and acquired face-to-face services, including information sharing about continuous care and treatment, medical/nursing care education, and participation in medical decision-making. Many hospitals have restricted in-person visits to minimize the spread of Coronavirus disease 2019 (COVID-19) for the safety of the patients, visitors, and staff. As a result, provision of adequate transitional care is hampered, possibly resulting in poor patient outcomes after discharge. New hybrid strategies are required for transitional care involving patients and family caregivers during the COVID-19 pandemic in Japan, and they need to be developed and evaluated.

2. Traditional transitional care system in Japan

In Japan, a new healthcare reimbursement scheme was introduced to the universal healthcare coverage system in 2008 to provide transitional care. Discharge planning nurses (DPNs) are crucial professionals of the interdisciplinary team on transitional care because they assist patients with severe conditions, including those with terminal cancer or cognitive impairment, who are highly dependent on medical and long-term care, and arrange their transfer to a local medical institution or their homes (*6*).

"Creating a plan for transitional care with patient or family caregivers' involvement" is included in requirements before processing hospital bills. Hospital staffs, including DPNs, are required to discuss patients' medical conditions and life after discharge and create a transitional care plan with associated professionals. DPNs provide transitional care strategies by combining individual care, family caregivers, and a multidisciplinary collaborative team approach.

3. Current status of patients and family caregivers' involvement in transitional care during COVID-19

During the COVID-19 pandemic, from March 2020, many hospitals prohibited inpatient visitation, even for family members or friends. As of January 2021, these restrictions continue at many hospitals. Therefore, family caregivers are unable to visit patients during hospitalization and, thus, may not fully understand their status. One frontline DPN reported that family caregivers, particularly the elderly, were confused about patients' hospital discharge and service adjustments due to limited shared decision-making or information for medical and nursing care plans after discharge, which might have increased caregivers' anxiety and resulted in discharge refusals.

Many patients with terminal illness or caregivers opted for discharge to their home to prioritize their time together. For example, some hospitals were restricted from holding face-to-face discharge conferences with patients, families, and multidisciplinary specialists. Therefore, the DPNs reported that these patients and caregivers might not have been able to make adequate decisions regarding care plans, including their goals and preferences after discharge.

4. New strategies for a smooth transition from hospital to home with COVID-19 measures

To counter the COVID-19 pandemic, new strategies should complement the traditional transitional care system.

Reducing person-to-person contact and providing services in a socially distant setting are important infection prevention measures. As an alternative, if relatives cannot visit a patient during palliative and end-of-life care, many hospitals already use Information and Communication Technology (ICT), including tablets or smartphones (*7*). However, introduction of ICT for consultation on transitional care, discharge counseling, and post-discharge follow-up is a new approach. Some hospitals have now combined infection prevention with face-to-face opportunities, *i.e*., requiring reservations for transitional care consultation, limiting the number of visiting family members, and restricting pre-discharge conferences of multidisciplinary team members. Several hospitals started a "new normal" conference using apps, such as Zoom or FaceTime (*8*), which are expected to continue, where patients/family caregivers and care teams can discuss medical and nursing care plans, goals, and preferences face-to-face.

Using the nurse-led telemonitoring system at X hospital enhanced patients/family caregivers' follow-up after discharge (*9*). This system allows nurses in the hospital and patients and caregivers to communicate through a TV screen that the older persons are familiar with, rather than a computer or smartphone. They provide the service mainly in the first one to two weeks immediately after discharge from the hospital, when the patient's condition is likely to change, and various difficulties are likely to arise. This service effectively compensates for the lack of pre-discharge medical and nursing guidance and decision support in a pandemic situation.

However, building a relationship between family caregivers and medical/nursing staff, decision-making, psychological support, and risk assessment generally performed in face-to-face communication is still demanding. The future challenge is how to promote and involve patients and caregivers in their transitional care after discharge while aiming at preventing infection because especially the time spent between patients and their families in the terminal period is extremely important. Transitional care staff, including DPNs, should not wait for the pandemic to converge. New hybrid strategies should be developed and evaluated to provide transitional care while using online systems and minimal face-to-face support during the pandemic.

Funding: This work was supported by the Ministry of Education, Culture, Sports, Science and Technology, Japan (20K23188).

Conflict of Interest: The authors have no conflicts of interest to disclose.

References

1. Coleman EA, Parry C, Chalmers S, Min SJ. The care transitions intervention: Results of a randomized trial. Arch Intern Med. 2006; 166:1822-1828.
2. Towers AM, Killett A, Handley M, Almack K, Backhouse T, Bunn D, Bunn F, Dickinson A, Mathie E, Mayrhofer A, Mikelyte R, Goodman C. Producing "Top Tips" for care home staff during COVID-19 pandemic in England: rapid reviews inform evidence-based practice but reveal major gaps. Journal of Long-Term Care. 2020; 151-166.
3. Coleman EA, Boult C; American Geriatrics Society Health Care Systems Committee. Improving the quality of transitional care for persons with complex care needs. J Am Geriatr Soc. 2003; 51:556-557.
4. Naylor MD, Shaid EC, Carpenter D, *et al*. Components of comprehensive and effective transitional care. J Am Geriatr Soc. 2017; 65:1119-1125.
5. Gibson MJ, Kelly K, Kaplan A. Family caregiving and transitional care: A critical review. *https://www.caregiver.org/sites/caregiver.org/files/pdfs/FamCGing_TransCare_CritRvw_FINAL10.31.2012.pdf* (accessed October 7, 2020).
6. Holliman D, Dziegielewski SF, Teare R. Differences and similarities between social work and nurse discharge planners. Health Soc Work. 2003; 28:224-231.
7. Association for Palliative Medicine of Great Britain and Ireland. COVID-19 and palliative, end of life and bereavement care in secondary care: Guidance to aid care, Version 6: 17 January 2021. *https://apmonline.org/wp-content/uploads/2021/02/COVID-19-Palliative-and-*

End-of-Life-Care.pdf (accessed February 1, 2021).
8. The Cancer Institute Hospital of JFCR. Come join us for an online conference. *https://www.jfcr.or.jp/hospital/conference/cancer/pdf/online.pdf* (accessed October 8, 2020) (in Japanese)
9. Yoshimasa O. Using ICT to monitor patients in their own home from the hospital. New Medical World Weekly. 2020. *https://www.igaku-shoin.co.jp/paperDetail.do?id=PA03377_03* (accessed September 24, 2020).

Received February 3, 2021; Revised February 10, 2021; Accepted February 14, 2021.

**Address correspondence to:*
Yuka Sumikawa, Department of Community Health Nursing, Division of Health Sciences and Nursing, Graduate School of Medicine, The University of Tokyo, 7-3-1 Hongo, Bunkyo-ku, Tokyo 113-0033, Japan.
E-mail: sumi0719yuka@gmail.com

Released online in J-STAGE as advance publication February 23, 2021.

Letter

DOI: 10.5582/bst.2020.03429

Zbtb7a and Zbtb7b: Opening naïve loci to reprogram ESCs

Hua Cao[1], Hong Huang[2,3,*], Huifang Tang[1,2,*]

[1] Department of Cardiology, The First Affiliated Hospital of University of South China, Hengyang, Hunan, China;
[2] Institute of Cardiovascular Disease, The First Affiliated Hospital of University of South China, Hengyang, Hunan, China;
[3] Institute of Clinical Medicine, The First Affiliated Hospital of University of South China, Hengyang, Hunan Province, China.

SUMMARY Bone morphogenetic protein 4 (BMP4) was recently reported to confer reprogramming capability to embryonic stem cells (ESCs) by reactivating naïve pluripotency genes *via* Zbtb7a and Zbtb7b. A visual reporting system was developed to first identify BMP4 as a driver for the primed-to-naïve transition (PNT). In addition, two specific inhibitors were identified as significantly improving the efficiency of PNT (~80% transition) within 8 days. The Zbtb7 family members were first introduced in the context of PNT and stem cell fate decision-making. These findings provide valuable information on acquiring naïve pluripotent stem cells for regenerative medicine.

Keywords BMP4, fate decision-making, PNT, reprogramming

The primed-to-naïve transition (PNT) between embryonic stem cells (ESCs) and epiblast stem cells (EpiSCs) is finely tuned by a set of transcription factors (TFs) and chemicals (*1*). Naïve pluripotency is defined as the self-renewal stage of ESCs, which gives rise to a whole embryo that expresses genes such as octamer-binding transcription factor 4 (Oct4), SRY-box transcription factor 2 (Sox2), Nanog homeobox (Nanog), Kruppel-like factor 4 (Klf4), and estrogen-related receptor beta (Esrrb). Primed pluripotency means that epiblast stem cells (EpiSCs) are capable of trans-lineage differentiation when genes are activated soon after implantation, such as fibroblast growth factor 4 (Fgf4), fibroblast growth factor 5 (Fgf5), and SRY-box transcription factor 17 (Sox17). PNT could serve as a good model to reveal the determination of cell fate. The process of inducing pluripotency is slow and inefficient, which are the most significant bottlenecks. A recent study by Yu *et al*. offered new insights into the relationship between chromatin remodeling and pluripotency maintained by bone morphogenetic protein 4 (BMP4) (*2*).

BMP4 is a secreted signaling molecule that belongs to the transforming growth factor-beta (TGF-β) superfamily. Previous studies indicated that Bmp4-deficient mice suffered embryonic lethality due to delayed epiblast growth as early as embryonic day 6.5 (E6.5). Despite mounting evidence suggests that BMP4 enables the exit of ESCs from pluripotency and drives their differentiation, no study has reported a need for BMP4 in reorganizing chromatin. BMP4 and retinoic acid are reported to team up with p63 to contribute to increase DNA methylation and to reduce chromatin accessibility (*3*). Gene expression is closely linked to chromatin accessibility, so whether BMP4 regulates chromatin interaction during PNT has yet to be determined.

To elucidate the mechanisms by which BMP4 determines the fate of ESCs, Yu *et al*. developed a visual reporting system to first identify BMP4 as a driver for PNT. In addition, small molecules were screened to identify those enhancing PNT. Among 606 compounds, two small molecules were identified: the enhancer of zeste 2 polycomb repressive complex 2 subunit (EZH2) inhibitor EPZ-6438 (tazemetostat) and the DOT1-like histone lysine methyltransferase (DOT1L) inhibitor EPZ-5676 (pinometostat). According to clonal analysis, which indicated the capacity for reprogramming, EPZ-6438 and EPZ-5676 induced PNT with sufficient efficiency either alone or in combination. When the two inhibitors were combined, a highly efficient induction system was created; it facilitates up to 80% transition within 8 days. Subsequently, an assay for targeting accessible-chromatin with high-throughput sequencing (ATAC-seq) provided compelling evidence that Zbtb7a and Zbtb7b were the key regulators of cell fate. These findings provide valuable information on acquiring naïve pluripotent stem cells for regenerative medicine.

A point worth noting is that a unique chromatin structure is involved in sustaining naivety. During the BMP4-induced PNT (BiPNT) of ESCs, a precise coordination of chromatin accessibility dynamics (CAD) occurs: a substantial number of loci specific

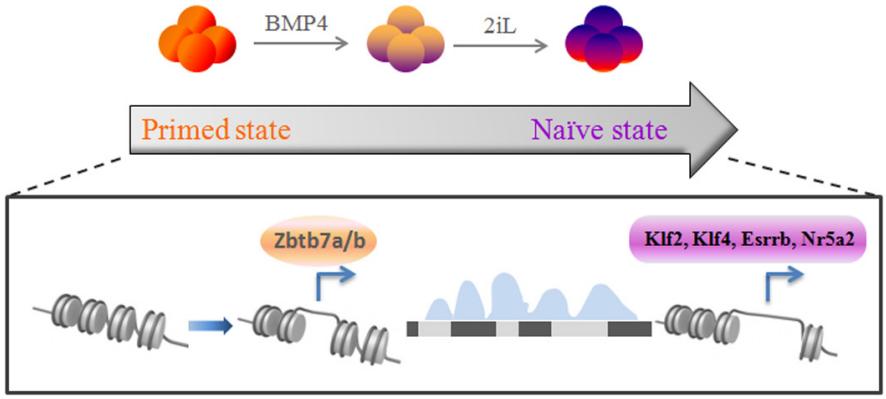

Figure 1. Rapid reprogramming of BMP4 to induce naïve stem cells allows chromatin remodeling induced by the regulation of transcription factors. Induced expression of a Zn finger/BTB domain containing protein 7a or b (Zbtb7a and Zbtb7b) is a crucial early response during BMP4-induced naive-primed pluripotent transition (PNT). Zbtb7a and Zbtb7b play a critical role in opening chromatin loci to express core pluripotent factors such as Klf2, Klf4, Esrrb, and Nr5a2.

to the primed state close over the first 3 days and then more loci related to the naïve state reopen over the next 5 days under 2 iL. In addition, the combined results of ATAC-seq, gene ontology (GO) analysis, and chromatin immunoprecipitation sequencing (ChIP-seq) suggested that *Zbtb7a*, *Zbtb7b*, and *Zbtb7c* were directly targetable genes capable of independently initiating PNT. Zbtb7a, Zbtb7b, and Zbtb7c belong to the POZ/BTB and Kruppel (POK) family of transcription factors that are capable of context-dependent regulation of cell development as well as tumorigenesis. A rescuing experiment indicated that Zbtb7a and Zbtb7b were needed to activate naïve genes such as *Nanog*, *Klf2*, *Esrrb*, and *Nr5a2*. These findings provide a comprehensive picture of Zbtb7a and Zbtb7b in altering the pluripotency gene network and determining cell fate (Figure 1). Recently, Liu *et al*. (*4*) provided a molecular roadmap of reprogramming for pluripotency at the single-cell level. They suggested that the trophectoderm-lineage-specific regulatory program was involved in reprogramming human somatic cells. Their findings suggest the existence of sub-branches as alternative pathways for determination of cell fate.

Several studies have indicated that chromatin-modifying enzymes play vital roles during the epigenetic reprogramming of pluripotency. The EZH2 inhibitor tazemetostat (EPZ-6438) and the DOT1L inhibitor pinometostat (EPZ-5676) have proven to be effective in treating a variety of solid tumors and hematological malignancies. Numerous studies have indicated that chromatin-modifying enzymes both silence domains and reactivate loci during the epigenetic reprogramming of pluripotency. Tazemetostat facilitates reprogramming mainly by preventing the acquisition of an epithelial-like phenotype. Interestingly, tazemetostat and pinometostat exhibit similar potency in reversing the mesenchymal-epithelial transition (MET) in different cancers (*5*). Generally speaking, these results indicate that selective chromatin modifiers can generate naïve stem cells in a more efficient manner with fewer exogenous transcription factors.

The differentiation of ESCs into cardiovascular lineages has provided important insights into their regulation during heart development. In embryos, the lateral/cardiac mesoderm originates from the middle of the primitive streak. Cardiac progenitor cells (CPCs) from the lateral/cardiac mesoderm differentiate into cardiomyocytes (CMs), cardiac fibroblasts (CFs), vascular smooth muscle cells (VSMCs), and vascular endothelial cells (VECs), producing the heart. The specific transitions require sequential expression of distinct transcription factors and proteins that facilitate the change in state from pluripotency to mesoderm and then to a cardiovascular fate. A recent study found that T-box transcription factor 6 (Tbx6) directs cardiovascular differentiation (*6*). Mounting evidence suggests that during the cardiovascular differentiation of ESCs, key transcription factors determine multiple cell fates. Such as, Nkx2.5, GATA-binding protein 4 (Gata4), Mef2c, Tbx2, Tbx3, Tbx5, and connexin 43 (CX43) direct the differentiation of cardiomyocytes; Gata6 and nuclear factor erythroid 2-related factor 3 (Nrf3) direct the differentiation of VSMCs; hyaluronan and proteoglycan link protein 1 (Hapln1) and high-mobility group AT-hook protein 1 (Hmga1) direct the differentiation of VECs; and CX40 and troponin I type 1 (TNNI1) direct the differentiation of CFs. In addition, growth factors such as WNT, Nodal/Activin, BMP, platelet-derived growth factor (PDGF), vascular endothelial growth factor (VEGF), and neuregulin 1 (NRG1) are involved in complex regulatory networks to determine cell fates. Moreover, epigenetic modification, such as histone acetylation and methylation, DNA methylation, ubiquitination, and N(6)-methyladenosine (m6A) modification, has been found to play a vital regulatory role in naïve pluripotency and differentiation, possibly providing a bridge between extracellular cues, chromatin remodeling, and signaling in cardiogenesis (*7-10*). Comprehensive analysis with multi-omics such

as single-cell RNA sequencing (scRNA-seq) and spatial transcriptomic profiling may help to map the landscape of temporal and spatial changes in the expression of genes specific to cardiovascular lineage commitment. All of these efforts will help to improve efficiency in deciding cell fate and to strictly control the delivery of ESCs to the heart. Comprehensive molecular and functional analysis of systems for differentiation of ESCs will provide a valuable foundation for disease modeling, regenerative medicine, and drug discovery to treat cardiovascular diseases.

In summary, a study by Pei and his colleagues has provided a new understanding and entry point for studying the chemical regulation of changes in cell fate. Their work will help to guide research on the acquisition of naïve pluripotent stem cells in human or other systems. Since a global epigenetic reorganization occurs during differentiation, more specific inhibitors need to be identified to obtain genetically stable and self-renewing naïve stem cells. Moreover, an analysis of roadmaps using multimodal single-cell assays may help to identify pluripotent subpopulations of stem cells. In addition, determining the molecular pathways that regulate stem cell renewal may provide a deeper understanding and facilitate advances in embryology.

Funding: This work was supported by the Natural Science Foundation of Hunan Province under grant No. 2019JJ50555; the Open Project Program of Guangxi Key Laboratory of Centre of Diabetic Systems Medicine, Guilin Medical University, GKLCDSM-20200101-03; the Hunan Province Technology Innovation Guidance Program-Clinical Medical Technology Innovation Guidance Project under grant No. 2018SK51603; and the Science Foundation of The Heath and Family Planning Commission in Hunan Province of China under grant No. B2019122, No. 20201920.

Conflict of Interest: The authors have no conflicts of interest to disclose.

References

1. Collier AJ, Panula SP, Schell JP, Chovanec P, Plaza Reyes A, Petropoulos S, Corcoran AE, Walker R, Douagi I, Lanner F, Rugg-Gunn PJ. Comprehensive cell surface protein profiling identifies specific markers of human naive and primed pluripotent states. Cell Stem Cell. 2017; 20:874-890 e877.
2. Yu S, Zhou C, Cao S, *et al*. BMP4 resets mouse epiblast stem cells to naive pluripotency through ZBTB7A/B-mediated chromatin remodelling. Nat Cell Biol. 2020; 22:651-662.
3. Pattison JM, Melo SP, Piekos SN, *et al*. Retinoic acid and BMP4 cooperate with p63 to alter chromatin dynamics during surface epithelial commitment. Nat Genet. 2018; 50:1658-1665.
4. Liu X, Ouyang JF, Rossello FJ, *et al*. Reprogramming roadmap reveals route to human induced trophoblast stem cells. Nature. 2020; 586:101-107.
5. Stazi G, Taglieri L, Nicolai A, *et al*. Dissecting the role of novel EZH2 inhibitors in primary glioblastoma cell cultures: effects on proliferation, epithelial-mesenchymal transition, migration, and on the pro-inflammatory phenotype. Clin Epigenetics. 2019; 11:173.
6. Sadahiro T, Isomi M, Muraoka N, *et al*. Tbx6 induces nascent mesoderm from pluripotent stem cells and temporally controls cardiac versus somite lineage diversification. Cell Stem Cell. 2018; 23:382-395 e385.
7. Geula S, Moshitch-Moshkovitz S, Dominissini D, *et al*. Stem cells. m6A mRNA methylation facilitates resolution of naive pluripotency toward differentiation. Science. 2015; 347:1002-1006.
8. Kraushaar DC, Zhao K. The epigenomics of embryonic stem cell differentiation. Int J Biol Sci. 2013; 9:1134-1144.
9. DeLaughter DM, Bick AG, Wakimoto H, McKean D, Gorham JM, Kathiriya IS, Hinson JT, Homsy J, Gray J, Pu W, Bruneau BG, Seidman JG, Seidman CE. Single-cell resolution of temporal gene expression during heart development. Dev Cell. 2016; 39:480-490.
10. Hashimoto H, Wang Z, Garry GA, Malladi VS, Botten GA, Ye W, Zhou H, Osterwalder M, Dickel DE, Visel A, Liu N, Bassel-Duby R, Olson EN. Cardiac reprogramming factors synergistically activate genome-wide cardiogenic stage-specific enhancers. Cell Stem Cell. 2019; 25:69-86 e65.

Received December 7, 2020; Revised February 6, 2020; Accepted February 9, 2021.

**Address correspondence to:*
Hong Huang and Huifang Tang, Department of Cardiology, Institute of Cardiovascular Disease, Institute of Clinical Medicine, The First Affiliated Hospital of University of South China, Hengyang 421001, Hunan Province, China.
E-mail: trave1@126.com (HH) and 1132226235@qq.com (TH)

Released online in J-STAGE as advance publication February 23, 2021.

Letter

DOI: 10.5582/bst.2020.03375

Factors affecting mode of delivery in women of advanced maternal age

Ying Dong[1,§], Lan Wang[2,3,4,§], Youhui Lu[1], Zhongxing Fu[5], Yan Du[2,3,4,*], Ling Wang[2,3,4,*]

[1] Department of Obstetrics, Shanghai Putuo Maternity & Infant Health Hospital, Shanghai, China;
[2] Laborartory for Reproductive Immunology, Obstetrics and Gynecology Hospital of Fudan University, Shanghai, China;
[3] The Academy of Integrative Medicine of Fudan University, Shanghai, China;
[4] Shanghai Key Laboratory of Female Reproductive Endocrine-Related Diseases, Shanghai, China;
[5] Ningguo Bio-Leader biotechnology Co., Ltd., Ningguo, Anhui, China.

SUMMARY With the implementation of the two-child policy in China, an increased number of women of advanced maternal age (AMA) have been giving birth. Formulating evidence-based guidance for the clinical management of this population is crucial. This retrospective study aimed to explore factors influencing the mode of delivery in women of AMA. Data on 350 women of AMA who delivered at Shanghai Putuo Maternity & Infant Health Hospital from January to June of 2016 were collected. Results indicated that most (114/134, 85%) of the multiparae chose delivery *via* cesarean section (CS) because of uterine scarring. There were significant differences in the body mass index (BMI) before pregnancy, BMI at delivery, gestational diabetes mellitus (GDM), pregnancy-induced hypertension (PIH), and placenta previa between the CS and vaginal delivery groups ($P < 0.05$ for all). The current results suggest that vaginal delivery is recommended for the first delivery whenever reasonable. Moreover, management of metabolic disorders during pregnancy is essential to effectively reduce the rate of CS among women of AMA.

Keywords advanced maternal age (AMA), cesarean section (CS), vaginal delivery, BMI, multipara

Advanced maternal age (AMA) is generally defined as pregnancy in women age 35 years or older. In recent years, the number of women of AMA in China has been increasing with the implementation of the two-child policy, changes in the concept of fertility, economic development, and the advancement of assisted reproductive technology. The rate of cesarean sections (CS) has increased with the increase in the number of women of AMA (*1*). AMA is closely associated with adverse maternal and neonatal outcomes (*2*). The risk of miscarriage, stillbirth, neonatal death, pregnancy complications, and the rate of CS are known to increase as the maternal age increases (*3*).

A retrospective study has been conducted to analyze factors associated with the delivery plan as well as maternal and neonatal outcomes in women of AMA in order to guide the clinical management of this population.

Subjects were 350 women of AMA (≥ 35 years of age) who delivered at Shanghai Putuo Maternity & Infant Health Hospital from January to June of 2016. Subjects were divided into a CS group and a vaginal delivery group. Information regarding pregnancy conditions, pregnancy complications, and neonatal outcomes was collected.

Numerical values and percentages were calculated for categorical variables. The chi-square test or Fisher's exact test was used to determine differences in categorical variables between the two groups. The mean and standard deviation (SD) or median and range were calculated for continuous variables. Continuous variables were tested for normality and equality of variances between groups. The Student's *t* test was used to compare continuous variables that were normally distributed, and nonparametric methods were used to compare non-normally distributed variables. All of the above analyses were two-sided and performed using SPSS version 22 for Windows. A P value of < 0.05 was considered statistically significant.

Among the 350 women of AMA who delivered a child, more than 70% were multiparae (249/350, 71.1%). Of the multiparae, 134 delivered *via* CS; 114 chose CS because of uterine scarring (114/134, 85%). Table 1 shows comparisons of body mass index (BMI) and pregnancy complications in women of AMA with different modes of delivery. Excluding those choosing

Table 1. Comparisons of BMI and pregnancy complications in women of AMA with different modes of delivery (excluding those choosing a caesarean section because of uterine scarring, *n* = 236)

Items	Transvaginal delivery group (*n* = 165)	Caesarean section group (*n* = 71)	*P* value
Pre-pregnancy BMI	20.96 ± 2.83	21.68 ± 3.11	0.029
BMI at the time of delivery	27.25 ± 3.65	28.23 ± 3.05	0.006
Pregnancy-induced hypertension (*n*, %)	5 (3.0%)	6 (8.5%)	0.007
Gestational diabetes mellitus (*n*, %)	28 (17.0%)	40 (56.3%)	< 0.001
Premature rupture of membranes (*n*, %)	19 (11.5%)	8 (11.3%)	1.000
Placenta previa (*n*, %)	1 (0.6%)	6 (8.5%)	0.003
Thyroid disease (*n*, %)	2 (1.2%)	3 (4.2%)	0.326

CS because of uterine scarring, a total of 236 women were included in the analysis. There were statistically significant differences in pre-pregnancy BMI (P = 0.029) and BMI at delivery (P = 0.006) between the two groups. In addition, there were significant differences in the incidence of gestational diabetes mellitus (GDM), pregnancy-induced hypertension (PIH), and placenta previa ($P < 0.05$ for all) between the two groups. However, there was no statistically significant differences in the incidence of premature rupture of membranes (PROM) or thyroid disease between the two groups.

In terms of labor complications and neonatal outcomes, there were no significant differences in postpartum hemorrhage, neonatal birth weight, neonatal asphyxia, macrosomia, or low birth weight between the two groups with different modes of delivery ($P > 0.05$ for all).

Both psychological factors and physical conditions might explain the increasing rate of CS among women of AMA. Maternal anxiety (*1*) and fear of labor pains (*4*) may affect the decision regarding the mode of delivery for both mothers and obstetricians, contributing to a CS being performed at a higher rate. A scarred uterus after a prior CS is a strong indicator of a repeat CS. A recent study reported that women with a scarred uterus preferred a CS, and that was especially true for women of AMA (*5*). However, pregnancy after a cesarean delivery was associated with an increased risk of placenta accreta, placental abruption, miscarriage, and stillbirth (*6*). Therefore, reducing the rate of CS during the first delivery is essential to reducing the rate of CS among multiparae. Pregnancy complications and chronic metabolic disorders are other possible indicators of CS in women of AMA. Recent studies have indicated that pregnant women with conditions such as hypertensive disorders, diabetes, mild renal impairment, and multiple sclerosis tended to choose a CS again, indicating that pregnancy complications affect which mode of delivery is chosen (*4*). In the current study, there were significant differences between the two groups in terms of GDM, PIH, and placenta previa. All of this evidence indicates the importance of metabolic disorder management during pregnancy to reduce the rate of CS. Women with a higher pre-pregnancy BMI or obesity were more likely to develop pregnancy complications and deliver *via* CS (*7*). Therefore, women of AMA should maintain a normal BMI through diet and exercise before and during pregnancy.

In conclusion, caution is required when choosing the mode of delivery now that the two-child policy has been implemented. Interventions must be implemented in women of AMA to reduce the rate of CS, reduce adverse pregnancy outcomes, and improve the quality of delivery. Pre-pregnancy preparation and management of metabolic disorders during pregnancy is pivotal to reducing complications and the rate of CS. Future prospective studies with an adequate sample size need to be conducted to provide more evidence.

Funding: None.

Conflict of Interest: The authors have no conflicts of interest to disclose.

References

1. Bayrampour H, Heaman M. Advanced maternal age and the risk of cesarean birth: a systematic review. Birth. 2010; 37:219-226.
2. Kahveci B, Melekoglu R, Evruke IC, Cetin C. The effect of advanced maternal age on perinatal outcomes in nulliparous singleton pregnancies. BMC Pregnancy Childbirth. 2018; 18:343.
3. Lean SC, Derricott H, Jones RL, Heazell AEP. Advanced maternal age and adverse pregnancy outcomes: A systematic review and meta-analysis. PloS One. 2017; 12:e0186287.
4. Sindiani A, Rawashdeh H, Obeidat N, Zayed F, Alhowary AAA. Factors that influenced pregnant women with one previous caesarean section regarding their mode of delivery. Ann Med Surg (Lond). 2020; 55:124-130.
5. Hua Z, El Oualja F. Indicators for mode of delivery in pregnant women with uteruses scarred by prior caesarean section: a retrospective study of 679 pregnant women. BMC Pregnancy Childbirth. 2019; 19:445.
6. Keag OE, Norman JE, Stock SJ. Long-term risks and benefits associated with cesarean delivery for mother, baby, and subsequent pregnancies: Systematic review and meta-analysis. PLoS Med. 2018; 15:e1002494.
7. Brick A, Layte R, McKeating A, Sheehan SR, Turner MJ. Does maternal obesity explain trends in caesarean section

rates? Evidence from a large Irish maternity hospital. Ir J Med Sci. 2020; 189:571-579.

Received October 22, 2020; Revised December 27, 2020; Accepted January 22, 2021.

[§]These authors contributed equally to this work.

*Address correspondence to:
Ling Wang and Yan Du, Laboratory for Reproductive Immunology, Obstetrics and Gynecology Hospital of Fudan University, 419 Fangxie Road, Shanghai 200011, P.R. China.
E-mail: Dr.wangling@fudan.edu.cn (LW), sophiedu_61@163.com (YD)

Released online in J-STAGE as advance publication January 27, 2021.

BST
BioScience Trends

Guide for Authors

1. Scope of Articles

BioScience Trends (Print ISSN 1881-7815, Online ISSN 1881-7823) is an international peer-reviewed journal. *BioScience Trends* devotes to publishing the latest and most exciting advances in scientific research. Articles cover fields of life science such as biochemistry, molecular biology, clinical research, public health, medical care system, and social science in order to encourage cooperation and exchange among scientists and clinical researchers.

2. Submission Types

Original Articles should be well-documented, novel, and significant to the field as a whole. An Original Article should be arranged into the following sections: Title page, Abstract, Introduction, Materials and Methods, Results, Discussion, Acknowledgments, and References. Original articles should not exceed 5,000 words in length (excluding references) and should be limited to a maximum of 50 references. Articles may contain a maximum of 10 figures and/or tables. Supplementary Data are permitted but should be limited to information that is not essential to the general understanding of the research presented in the main text, such as unaltered blots and source data as well as other file types.

Brief Reports definitively documenting either experimental results or informative clinical observations will be considered for publication in this category. Brief Reports are not intended for publication of incomplete or preliminary findings. Brief Reports should not exceed 3,000 words in length (excluding references) and should be limited to a maximum of 4 figures and/or tables and 30 references. A Brief Report contains the same sections as an Original Article, but the Results and Discussion sections should be combined.

Reviews should present a full and up-to-date account of recent developments within an area of research. Normally, reviews should not exceed 8,000 words in length (excluding references) and should be limited to a maximum of 10 figures and/or tables and 100 references. Mini reviews are also accepted, which should not exceed 4,000 words in length (excluding references) and should be limited to a maximum of 5 figures and/or tables and 50 references.

Policy Forum articles discuss research and policy issues in areas related to life science such as public health, the medical care system, and social science and may address governmental issues at district, national, and international levels of discourse. Policy Forum articles should not exceed 3,000 words in length (excluding references) and should be limited to a maximum of 5 figures and/or tables and 30 references.

Communications are short, timely pieces that spotlight new research findings or policy issues of interest to the field of global health and medical practice that are of immediate importance. Depending on their content, Communications will be published as "Comments" or "Correspondence". Communications should not exceed 1,500 words in length (excluding references) and should be limited to a maximum of 2 figures and/or tables and 20 references.

Editorials are short, invited opinion pieces that discuss an issue of immediate importance to the fields of global health, medical practice, and basic science oriented for clinical application. Editorials should not exceed 1,000 words in length (excluding references) and should be limited to a maximum of 10 references. Editorials may contain one figure or table.

News articles should report the latest events in health sciences and medical research from around the world. News should not exceed 500 words in length.

Letters should present considered opinions in response to articles published in *BioScience Trends* in the last 6 months or issues of general interest. Letters should not exceed 800 words in length and may contain a maximum of 10 references. Letters may contain one figure or table.

3. Editorial Policies

For publishing and ethical standards, BioScience Trends follows the Recommendations for the Conduct, Reporting, Editing, and Publication of Scholarly Work in Medical Journals (*http://www.icmje.org/recommendations*) issued by the International Committee of Medical Journal Editors (ICMJE), and the Principles of Transparency and Best Practice in Scholarly Publishing (*https://doaj.org/bestpractice*) jointly issued by the Committee on Publication Ethics (COPE), the Directory of Open Access Journals (DOAJ), the Open Access Scholarly Publishers Association (OASPA), and the World Association of Medical Editors (WAME).

BioScience Trends will perform an especially prompt review to encourage innovative work. All original research will be subjected to a rigorous standard of peer review and will be edited by experienced copy editors to the highest standards.

Ethics: *BioScience Trends* requires that authors of reports of investigations in humans or animals indicate that those studies were formally approved by a relevant ethics committee or review board. For research involving human experiments, a statement that the participants gave informed consent before taking part (or a statement that it was not required and why) should be indicated. Authors should also state that the study conformed to the provisions of the Declaration of Helsinki (as revised in 2013). When reporting experiments on animals, authors should indicate whether the institutional and national guide for the care and use of laboratory animals was followed.

Conflict of Interest: All authors are required to disclose any actual or potential conflict of interest including financial interests or relationships with other people or organizations that might raise questions of bias in the work reported. If no conflict of interest exists for each author, please state "There is no conflict of interest to disclose".

Submission Declaration: When a manuscript is considered for submission to *BioScience Trends*, the authors should confirm that 1) no part of this manuscript is currently under consideration for publication elsewhere; 2) this manuscript does not contain the same information in whole or in part as manuscripts that have been published, accepted, or are under review elsewhere, except in the form of an abstract, a letter to

the editor, or part of a published lecture or academic thesis; 3) authorization for publication has been obtained from the authors' employer or institution; and 4) all contributing authors have agreed to submit this manuscript.

Cover Letter: The manuscript must be accompanied by a cover letter prepared by the corresponding author on behalf of all authors. The letter should indicate the basic findings of the work and their significance. The letter should also include a statement affirming that all authors concur with the submission and that the material submitted for publication has not been published previously or is not under consideration for publication elsewhere. The cover letter should be submitted in PDF format. For example of Cover Letter, please visit: Download Centre (*https://ircabssagroup.com/downcentre*).

Copyright: When a manuscript is accepted for publication in *BioScience Trends*, the transfer of copyright is necessary. A JOURNAL PUBLISHING AGREEMENT (JPA) form will be e-mailed to the authors by the Editorial Office and must be returned by the authors as a scan. Only forms with a hand-written signature are accepted. This copyright will ensure the widest possible dissemination of information. Please note that your manuscript will not proceed to the next step in publication until the JPA Form is received. In addition, if excerpts from other copyrighted works are included, the author(s) must obtain written permission from the copyright owners and credit the source(s) in the article.

Peer Review: *BioScience Trends* uses single-blind peer review, which means that reviewers know the names of the authors, but the authors do not know who reviewed their manuscript. The external peer review is performed for research articles by at least two reviewers, and sometimes the opinions of more reviewers are sought. Peer reviewers are selected based on their expertise and ability to provide high quality, constructive, and fair reviews. For research manuscripts, the editors may, in addition, seek the opinion of a statistical reviewer. Consideration for publication is based on the article's originality, novelty, and scientific soundness, and the appropriateness of its analysis.

Suggested Reviewers: A list of up to 3 reviewers who are qualified to assess the scientific merit of the study is welcomed. Reviewer information including names, affiliations, addresses, and e-mail should be provided at the same time the manuscript is submitted online. Please do not suggest reviewers with known conflicts of interest, including participants or anyone with a stake in the proposed research; anyone from the same institution; former students, advisors, or research collaborators (within the last three years); or close personal contacts. Please note that the Editor-in-Chief may accept one or more of the proposed reviewers or may request a review by other qualified persons.

Language Editing: Manuscripts prepared by authors whose native language is not English should have their work proofread by a native English speaker before submission. If not, this might delay the publication of your manuscript in *BioScience Trends*.

The Editing Support Organization can provide English proofreading, Japanese-English translation, and Chinese-English translation services to authors who want to publish in *BioScience Trends* and need assistance before submitting a manuscript. Authors can visit this organization directly at *http://www.iacmhr.com/iac-eso/support.php?lang=en*. IAC-ESO was established to facilitate manuscript preparation by researchers whose native language is not English and to help edit works intended for international academic journals.

4. Manuscript Preparation

Manuscripts are suggested to be prepared in accordance with the "Recommendations for the Conduct, Reporting, Editing, and Publication of Scholarly Work in Medical Journals", as presented at *http://www.ICMJE.org*.

Manuscripts should be written in clear, grammatically correct English and submitted as a Microsoft Word file in a single-column format. Manuscripts must be paginated and typed in 12-point Times New Roman font with 24-point line spacing. Please do not embed figures in the text. Abbreviations should be used as little as possible and should be explained at first mention unless the term is a well-known abbreviation (*e.g.* DNA). Single words should not be abbreviated.

Title page: The title page must include 1) the title of the paper (Please note the title should be short, informative, and contain the major key words); 2) full name(s) and affiliation(s) of the author(s), 3) abbreviated names of the author(s), 4) full name, mailing address, telephone/fax numbers, and e-mail address of the corresponding author; and 5) conflicts of interest (if you have an actual or potential conflict of interest to disclose, it must be included as a footnote on the title page of the manuscript; if no conflict of interest exists for each author, please state "There is no conflict of interest to disclose"). Please visit Download Centre and refer to the title page of the manuscript sample.

Abstract: The abstract should briefly state the purpose of the study, methods, main findings, and conclusions. For articles that are Original Articles, Brief Reports, Reviews, or Policy Forum articles, a one-paragraph abstract consisting of no more than 250 words must be included in the manuscript. For Communications, Editorials, News, or Letters, a brief summary of main content in 150 words or fewer should be included in the manuscript. Abbreviations must be kept to a minimum and non-standard abbreviations explained in brackets at first mention. References should be avoided in the abstract. Three to six key words or phrases that do not occur in the title should be included in the Abstract page.

Introduction: The introduction should be a concise statement of the basis for the study and its scientific context.

Materials and Methods: The description should be brief but with sufficient detail to enable others to reproduce the experiments. Procedures that have been published previously should not be described in detail but appropriate references should simply be cited. Only new and significant modifications of previously published procedures require complete description. Names of products and manufacturers with their locations (city and state/country) should be given and sources of animals and cell lines should always be indicated. All clinical investigations must have been conducted in accordance with Declaration of Helsinki principles. All human and animal studies must have been approved by the appropriate institutional review board(s) and a specific declaration of approval must be made within this section.

Results: The description of the experimental results should be succinct but in sufficient detail to allow the experiments to be analyzed and interpreted by an independent reader. If necessary, subheadings may be used for an orderly presentation. All figures and tables must be referred to in the text.

Discussion: The data should be interpreted concisely without repeating material already presented in the Results section. Speculation is permissible, but it must be well-founded, and discussion of the wider implications of the findings is encouraged. Conclusions derived from the study should be included in this section.

Acknowledgments: All funding sources should be credited in the Acknowledgments section. In addition, people who contributed to the work but who do not meet the criteria for authors should be listed along with their contributions.

References: References should be numbered in the order in which they appear in the text. Citing of unpublished results, personal communications, conference abstracts, and theses in the reference list is not recommended but these sources may be mentioned in the text. In the reference list, cite the names of all authors when there are fifteen or fewer authors; if there are sixteen or more authors, list the first three followed by *et al*. Names of journals should be abbreviated in the style used in PubMed. Authors are responsible for the accuracy of the references. The EndNote Style of *BioScience Trends* could be downloaded at **EndNote** (*https://ircabssagroup.com/examples/BioScience_Trends.ens*).

Examples are given below:

Example 1 (Sample journal reference):

Inagaki Y, Tang W, Zhang L, Du GH, Xu WF, Kokudo N. Novel aminopeptidase N (APN/CD13) inhibitor 24F can suppress invasion of hepatocellular carcinoma cells as well as angiogenesis. Biosci Trends. 2010; 4:56-60.

Example 2 (Sample journal reference with more than 15 authors):

Darby S, Hill D, Auvinen A, *et al*. Radon in homes and risk of lung cancer: Collaborative analysis of individual data from 13 European case-control studies. BMJ. 2005; 330:223.

Example 3 (Sample book reference):

Shalev AY. Post-traumatic stress disorder: Diagnosis, history and life course. In: Post-traumatic Stress Disorder, Diagnosis, Management and Treatment (Nutt DJ, Davidson JR, Zohar J, eds.). Martin Dunitz, London, UK, 2000; pp. 1-15.

Example 4 (Sample web page reference):

World Health Organization. The World Health Report 2008 – primary health care: Now more than ever. *http://www.who.int/whr/2008/whr08_en.pdf* (accessed September 23, 2010).

Tables: All tables should be prepared in Microsoft Word or Excel and should be arranged at the end of the manuscript after the References section. Please note that tables should not in image format. All tables should have a concise title and should be numbered consecutively with Arabic numerals. If necessary, additional information should be given below the table.

Figure Legend: The figure legend should be typed on a separate page of the main manuscript and should include a short title and explanation. The legend should be concise but comprehensive and should be understood without referring to the text. Symbols used in figures must be explained. Any individually labeled figure parts or panels (A, B, *etc*.) should be specifically described by part name within the legend.

Figure Preparation: All figures should be clear and cited in numerical order in the text. Figures must fit a one- or two-column format on the journal page: 8.3 cm (3.3 in.) wide for a single column, 17.3 cm (6.8 in.) wide for a double column; maximum height: 24.0 cm (9.5 in.). Please make sure that the symbols and numbers appeared in the figures should be clear. Please make sure that artwork files are in an acceptable format (TIFF or JPEG) at minimum resolution (600 dpi for illustrations, graphs, and annotated artwork, and 300 dpi for micrographs and photographs). Please provide all figures as separate files. Please note that low-resolution images are one of the leading causes of article resubmission and schedule delays.

Units and Symbols: Units and symbols conforming to the International System of Units (SI) should be used for physicochemical quantities. Solidus notation (*e.g*. mg/kg, mg/mL, mol/mm^2/min) should be used. Please refer to the SI Guide *www.bipm.org/en/si/* for standard units.

Supplemental data: Supplemental data might be useful for supporting and enhancing your scientific research and *BioScience Trends* accepts the submission of these materials which will be only published online alongside the electronic version of your article. Supplemental files (figures, tables, and other text materials) should be prepared according to the above guidelines, numbered in Arabic numerals (*e.g.*, Figure S1, Figure S2, and Table S1, Table S2) and referred to in the text. All figures and tables should have titles and legends. All figure legends, tables and supplemental text materials should be placed at the end of the paper. Please note all of these supplemental data should be provided at the time of initial submission and note that the editors reserve the right to limit the size and length of Supplemental Data.

5. Submission Checklist

The Submission Checklist will be useful during the final checking of a manuscript prior to sending it to *BioScience Trends* for review. Please visit Download Centre and download the Submission Checklist file.

6. Online Submission

Manuscripts should be submitted to *BioScience Trends* online at *http://www.biosciencetrends.com*. The manuscript file should be smaller than 5 MB in size. If for any reason you are unable to submit a file online, please contact the Editorial Office by e-mail at *office@biosciencetrends.com*

7. Accepted Manuscripts

Proofs: Galley proofs in PDF format will be sent to the corresponding author *via* e-mail. Corrections must be returned

to the editor (*proof-editing@biosciencetrends.com*) within 3 working days.

Offprints: Authors will be provided with electronic offprints of their article. Paper offprints can be ordered at prices quoted on the order form that accompanies the proofs.

Page Charge: Page charges will be levied on all manuscripts accepted for publication in *BioScience Trends* ($140 per page for black white pages; $340 per page for color pages). Under exceptional circumstances, the author(s) may apply to the editorial office for a waiver of the publication charges at the time of submission.

Misconduct: *BioScience Trends* takes seriously all allegations of potential misconduct and adhere to the ICMJE Guideline (*http://www.icmje.org/recommendations*) and COPE Guideline (*http://publicationethics.org/files/Code_of_conduct_for_journal_editors.pdf*). In cases of suspected research or publication misconduct, it may be necessary for the Editor or Publisher to contact and share submission details with third parties including authors' institutions and ethics committees. The corrections, retractions, or editorial expressions of concern will be performed in line with above guidelines.

(As of June 2020)

BioScience Trends
Editorial and Head Office
Pearl City Koishikawa 603,
2-4-5 Kasuga, Bunkyo-ku,
Tokyo 112-0003, Japan.
E-mail: office@biosciencetrends.com